Computational discovery of new efflux pump inhibitors that target AcrA of the *Escherichia coli* AcrAB-TolC efflux pump

A Dissertation Presented for the
Doctor of Philosophy
Degree
The University of Tennessee, Knoxville

Adam Taylor Green
December 2019

Copyright © 2019 by Adam T. Green
All rights reserved.

DEDICATION

I dedicate this work to my son, Gavin. May you continue to be a light in my life and the rest of my family.

ACKNOWLEDGEMENTS

I would like to acknowledge my undergraduate research mentor at Wake Forest University, Dr. Samuel Cho. Without Sam, I may never have sparked an interest in scientific research and solving problems particularly in computational biophysics. Sam, with much trepidation, took an undergraduate biology student with no previous training in upper-level physics or computer science as one of his students and taught him how to use physics and computer science to understand biology. I am so grateful that he made that decision. I would also like to thank my parents for their unconditional support throughout my undergraduate and graduate education. My wife, Erin, is worthy of much acknowledgement for putting up with my stress, working late nights, and weekends to finish this degree. Thank you for your patience and understanding. My friend and colleague, Rupesh Agarwal, for being a great friend in reviewing my presentations and providing feedback on my research. Lastly, much gratitude is owed to Dr. Jerry Parks and Dr. Jeremy Smith for their patience and their willingness to always listen to my concerns and help me along the way.

ABSTRACT

Antibiotics are compounds that kill or slow the growth of bacteria to treat numerous bacterial infections. No new class of antibiotic has been identified in the past thirty years despite the increased use of current antibiotics around the world. The increased use of current antibiotics has contributed to bacterial species becoming resistant to multiple antibiotics. Bacteria possess multiple resistance mechanisms such as inactivating enzymes, mutation of the antibiotic's target, the permeability of the outer membrane, and the overexpression of efflux pumps.

Efflux pumps bind antibiotics and eject them from the bacteria. In *Escherichia coli (E. coli),* the most studied efflux pump is referred to as AcrAB-TolC. Antibiotics bind AcrB triggering a series of conformational changes that expel the drug from the cell. AcrAB-TolC is a tripartite machinery that spans the inner and outer membrane of *E. coli.* AcrA is a periplasmic adaptor that links together AcrB in the inner membrane with TolC in the outer membrane. Efflux pump inhibitors (EPIs) have been developed that interact with AcrB and thus potentiate the activity of specific antibiotics. The inhibitors act by competitive inhibition. Other mechanisms of inhibition such as blocking drug export through TolC have not been found to function in vivo.

In this work, we have identified new inhibitors that bind AcrA, inhibit efflux, and potentiate specific antibiotics. We have identified the inhibitors using multiple homology models of AcrA. For each homology model, we ran molecular dynamics (MD) simulations and extracted conformations using RMSD clustering. Ligands

were predicted to bind by using the extracted conformations from each homology model with the program AutoDock VinaMPI. For two of the inhibitors, referred to as NSC60339 (SLU-258) and clorobiocin, we used AutoDock VinaMPI and a binding site identification program called FTMap to identify and subsequently validate possible binding sites on AcrA using tryptophan fluorescence spectroscopy. Finally, we used the identified binding sites in conjunction with physico-chemical descriptors to further identify new efflux pump inhibitors that potentiate novobiocin, erythromycin, and bind AcrA with a new chemical scaffold for efflux pump inhibitors.

PREFACE

Bottom up thinkers try to start from experience and move from experience to understanding. They don't start with certain general principles they think beforehand are likely to be true; they just hope to find out what reality is like.

- John Polkinghorne

TABLE OF CONTENTS

INTRODUCTION 1
Antibiotic resistance and the discovery void 1
Structure and function of multidrug efflux pumps in *Escherichia coli* 5
Efflux pump inhibition 11
TolC as a poor drug target 16
AcrA as a good drug target 18
Approach 20

CHAPTER I IDENTIFICATION OF NOVEL EFFLUX PUMP INHIBITORS THAT INTERACT WITH ACRA BY COMPUTATIONAL METHODS 23
Overview 25
Models of ligand binding 26
Protein structure prediction 27
Molecular dynamics simulations 32
Molecular docking 41
Novel mechanism of action for NSC60339 53
Structure-activity relationship of NSC60339 56
Conclusions 67

CHAPTER II IDENTIFICATION OF BINDING SITES FOR EFFLUX PUMP INHIBITORS OF THE ACRAB-TOLC COMPONENT ACRA 69
Abstract 70
Introduction 71
Computational methods 76
Structural modeling of AcrA from MexA 84
Calculation of potential binding sites 88
Truncated AcrA lacking the MP domain binds SLU-417 and clorobiocin 93
Mutations in Site IV have the largest impacts on efflux pump function 93
Fluorescence of tryptophan residues in AcrA reports on binding of inhibitors 95
F81W and F254W, both located in Site IV, are protected from quenching when clorobiocin and SLU-258 are bound 101
SLU-258 and clorobiocin likely bind near Site IV 102
Conclusions 104

CHAPTER III DISCOVERY OF NEW EFFLUX PUMP INHIBITORS WITH A NOVEL CHEMICAL SCAFFOLD THAT INTERACT WITH THE *ESCHERICHIA COLI* EFFLUX PUMP ADAPTOR ACRA 109
Abstract 110
Introduction 111
Generation of small molecule library 118
Filtering by molecular descriptors 118
Ensemble docking 119

ELECTRON DENSITY DOCKING 120
7 COMPOUNDS POTENTIATE NOVOBIOCIN AND ERYTHROMYCIN, BIND ACRA, BUT DO NOT PERMEATE THE OUTER MEMBRANE 122
7 COMPOUNDS MAY INHIBIT EFFLUX COMPETITIVELY THROUGH INTERACTION WITH ACRB IN THE ACCESS BINDING POCKET 126
AMINOCYCLOBUTYL PYRIMIDINE SCAFFOLD IS REQUIRED FOR POTENTIATION OF NOVOBIOCIN AND ERYTHROMYCIN 131
CONCLUSIONS, SIGNIFICANCE, AND FUTURE DIRECTIONS 141
REFERENCES 147
VITA 162

LIST OF TABLES

TABLE 1. MINIMAL INHIBITORY CONCENTRATIONS AND POTENTIATING ACTIVITIES OF TOP HITS 48

TABLE 2. PERCENTAGE RANK OF TOP HITS FROM VIRTUAL SCREENING OF HINGE AND MP SITES 53

TABLE 3. SPECTRUM OF ACTIVITY FOR NSC60339 AND NSC33353 55

TABLE 4. POTENTIATION DUE TO MODIFICATION OF THE DIHYDROIMIDAZOLINE AND CENTRAL RING. 61

TABLE 5. FOUR COMPOUNDS WITH EQUAL OR IMPROVED EPI CHARACTERISTICS RELATIVE TO NSC60339. 63

TABLE 6. REMOVAL OF CENTRAL AROMATIC RING RESULTS IN LOSS OF POTENTIATION. 65

TABLE 7. STRUCTURAL DESCRIPTORS FOR NSC60339 AND 4 ANALOGS WITH IMPROVED EPI CHARACTERISTICS 66

TABLE 8. ANTIBIOTIC SUSCEPTIBILITIES OF WILD-TYPE ACRA AND SELECTED TRP MUTANTS 96

TABLE 9. FLUORESCENCE PROPERTIES OF SINGLE TRP MUTANTS OF ACRA IN THE ABSENCE AND PRESENCE OF INHIBITORS 97

TABLE 10. COMPOUND SELECTION WORKFLOW 117

TABLE 11. ELECTRON DENSITY PLACEMENT SCORES FOR ERYTHROMYCIN (ERY) AND THE SIX COMPOUNDS. 121

TABLE 12. ANTIBIOTIC SUSCEPTIBILITY AND POTENTIATION OF TOP HITS IN WT-PORE CELLS. 123

TABLE 13. POTENTIATION OF TOP HITS IN WT CELLS 123

TABLE 14. STRUCTURE-ACTIVITY RELATIONSHIP (SAR) OF COMPOUNDS THAT BIND ACRA. 133

TABLE 15. STRUCTURES WITH THE AMINOCYCLOBUTYL PYRIMIDINE SCAFFOLD THAT DO NOT BIND ACRA 135

TABLE 15. CONTINUED. 136

TABLE 16. STRUCTURES OF COMPOUNDS THAT DO NOT BIND ACRA OR POTENTIATE ANTIBIOTICS 137

TABLE 16. CONTINUED. 138

TABLE 16. CONTINUED. 139

LIST OF FIGURES

FIGURE 1. DEPICTION OF THE ACRAB-TOLC EFFLUX PUMP IN ITS NATIVE ENVIRONMENT WITH THE OUTER MEMBRANE, CELL WALL, PERIPLASM, AND INNER MEMBRANE LABELED. THE PERIPLASM IS THE SPACE BETWEEN THE OUTER AND INNER MEMBRANE. 2

FIGURE 2. MOLECULAR PICTURE OF THE K-12 GRAM-NEGATIVE OUTER MEMBRANE. POPE (ORANGE) AND POPG (GREEN) IS IN THE INNER LEAFLET. LIPID A (GREY) IS IN THE OUTER LEAFLET ATTACHED TO THE INNER CORE POLYSACCHARIDES (BLUE AND RED). DIVALENT CATIONS, MAGNESIUM (GREEN) AND CALCIUM (PINK), INTERACT WITH THE INNER CORE POLYSACCHARIDES. THE OUTER CORE POLYSACCHARIDES ARE SHOWN IN MAGENTA AND BLACK. 3

FIGURE 3. DISCOVERY VOID OF NEW CLASSES OF ANTIBIOTICS. FIGURE WAS MODIFIED FROM PUBLIC HEALTH ENGLAND. 4

FIGURE 4. STRUCTURE AND SUBSTRATE TRANSPORT PATHWAYS OF ACRB. (A) ACRB IN THREE CONFORMATIONAL STATES WITH TRANSMEMBRANE, PORTER, AND FUNNEL DOMAINS HIGHLIGHTED (PDB 4DX5). THE L STATE IS IN YELLOW, T STATE IN RED, AND O STATE IN GREEN. (B) THE SUBSTRATE CAN ENTER FROM A CLEFT IN THE PERIPLASM (BROWN SPHERE; R307), TRAVERSE THROUGH THE ACCESS BINDING POCKET (YELLOW SPHERES), THE G-LOOP (MAGENTA RIBBON), AND DISTAL BINDING POCKET (BLUE SPHERE) TO THE EXIT GATE (CYAN SPHERES; Y758, K770) WHICH PASSES THE SUBSTRATE INTO THE FUNNEL DOMAIN AND TOWARDS TOLC. (C) ALTERNATIVELY, SUBSTRATE CAN CENTER FROM THE SURFACE OF THE INNER MEMBRANE (BLACK SPHERES; D566, T678). (D) SUBSTRATE CAN ENTER FROM THE CENTRAL CAVITY (ORANGE SPHERES; T37, A100) AND TRAVERSE DIRECTLY TO THE DISTAL BINDING POCKET AND THEN ONWARDS TO THE EXIT GATE AND OUT OF THE CELL. 7

FIGURE 5. DRUG TRANSPORT MECHANISM OF ACRB. (A) FUNCTIONAL ROTATION MECHANISM OF ACRB. AN EFFLUX PUMP SUBSTRATE SUCH AS ACRIDINE (SHOWN) ENTERS ACRB IN THE L STATE TRIGGERING CONFORMATIONAL CHANGES THAT EXPAND THE DISTAL BINDING POCKET IN THE T STATE. A PROTON RELAY MECHANISM TRIGGERS A SUBSEQUENT CONFORMATIONAL CHANGE THAT COLLAPSES THE DISTAL POCKET AND EXPELS THE SUBSTRATE TOWARDS TOLC FOR EFFLUX IN THE O STATE. (B) IN THE ABSENCE OF SUBSTRATE, GAPS EXIST BETWEEN ACRA DIMERS IN THE HEXAMERIC FUNNEL. (C) THE GAPS ARE SEALED UPON SUBSTRATE BINDING AND FUNCTIONAL ROTATION IN ACRB TO PROPAGATE EFFLUX OUT OF THE CELL. THE SEALING OF THE GAPS IN ACRA SWITCHES TOLC INTO AN OPEN STATE. 9

FIGURE 6. (A) THE ATOMIC STRUCTURE OF TOLC (PDB ITQQ). THE CLOSED (B) AND OPEN STATES (C) OF TOLC FROM THE APO (CLOSED) AND INHIBITOR-BOUND (OPEN) CRYO-EM STRUCTURES (PDB 5V5S AND 5NG5). EACH STATE IS DIFFERENTIATED

BY TWO ASPARTIC ACID RESIDUES, ASP371 AND ASP374, IN EACH MONOMER OF TOLC. 10

FIGURE 7. CHEMICAL STRUCTURE OF CURRENT EFFLUX PUMP INHIBITORS MC-207,110 (A) AND MBX2319 (B) 13

FIGURE 8. MBX2319 (CYAN) IS SURROUNDED BY SIX PHENYLALANINE RESIDUES (PURPLE) IN THE HYDROPHOBIC TRAP OF THE DISTAL BINDING POCKET OF ACRB. THE SIX PHENYLALANINE RESIDUES ARE F136, F178, F610, F615, F617, AND F628. 16

FIGURE 9. HEXAMMINECOBALT (CENTER) BOUND TO THE ASPARTATE RING IN THE CLOSED STATE OF THE TOLC CRYSTAL STRUCTURE (PDB 1TQQ). CARBON ATOMS FOR ASPARTATE ARE IN CYAN. 17

FIGURE 10. THE PROTEIN INHIBITOR DARPIN (GREEN) OVERLAPS AND INTERFERES WITH THE BINDING OF THE ACRA DIMER (BLUE AND RED) TO ACRB IN THE ASSEMBLED COMPLEX. 19

FIGURE 11. FUNNEL FREE ENERGY LANDSCAPE. THE LOWEST ENERGY STATE IS DENOTED BY THE LETTER N WHICH STANDS FOR NATIVE STATE. LANDSCAPE WAS CREATED BY THE KEN DILL GROUP UNDER A CREATIVE COMMONS ATTRIBUTION 4.0 INTERNATIONAL LICENSE. 27

FIGURE 12. MULTIPLE SEQUENCE ALIGNMENT OF THE ACRA SEQUENCE (NP_414996, K-12 MG1655) WITH THE SEQUENCES FROM THE X-RAY CRYSTAL STRUCTURES OF CUSB (PDB 3NE5) AND ZNEB (PDB 3LNN). THE SEQUENCE IDENTITY BETWEEN ACRA AND CUSB AND ZNEB IS 20% AND 27%, RESPECTIVELY. 31

FIGURE 13. (A) X-RAY CRYSTAL STRUCTURE OF ACRA (PDB 2F1M) WITH THE MISSING MP DOMAIN. (B) HOMOLOGY MODEL (MODEL A) BUILT FROM CUSB AND ACRA TEMPLATES WITH MODELLER. (C) HOMOLOGY MODEL (MODEL B) BUILT FROM ZNEB TEMPLATE WITH MOE. 31

FIGURE 14. MULTIPLE SEQUENCE ALIGNMENT OF THE FULL-LENGTH ACRA SEQUENCE WITH THE SEQUENCES EXTRACTED FROM THE MP DOMAINS OF THE X-RAY CRYSTAL STRUCTURES OF CUSB AND ZNEB. THE SEQUENCE IDENTITY BETWEEN THE MP DOMAINS BETWEEN ACRA AND CUSB ARE 21%. THE SEQUENCE IDENTITY BETWEEN ACRA AND ZNEB IS 27%. THE SEQUENCE FOR THE MP DOMAIN OF ACRA WAS OBTAINED FROM A LATER HOMOLOGY MODEL BUILT USING A SEPARATE TEMPLATE. 31

FIGURE 15. RAMACHANDRAN PLOTS OF MODEL A BUILT WITH A MULTI-TEMPLATE APPROACH USING ACRA AND CUSB CRYSTAL STRUCTURES AND MODEL B BUILT USING A SINGLE-TEMPLATE APPROACH USING THE ZNEB CRYSTAL STRUCTURE. MODEL B CONTAINS NUMEROUS STRUCTURAL OUTLIERS OUTSIDE OF THE ALLOWED REGIONS; THUS, MULTIPLE STERIC CLASHES EXIST. FIVE NANOSECONDS OF MD SIMULATIONS RESOLVE SOME OF THE CLASHES, BUT SOME REMAIN. 33

FIGURE 17. BONDED POTENTIAL ENERGY PROFILES (A) REPRESENTATIVE HARMONIC POTENTIAL BOND WHICH HAS A BOND LENGTH OF 1.54 A. (B) POTENTIAL ENERGY PROFILE OF A DIHEDRAL ANGLE REPRESENTED BY MOLECULAR MECHANICS. THE TERM N REPRESENTS THE NUMBER OF MINIMA IN THE PROFILE THAT CAN BE USED TO FIT QM TARGET DATA. 36

FIGURE 18. NONBONDED ENERGY PROFILES IN AN MD SIMULATION (A) LENNARD-JONES 6-12 POTENTIAL WITH AN ATTRACTIVE ENERGY WELL AND A REPULSIVE COMPONENT. (B) COULOMBIC POTENTIAL WHICH DECAYS AT A RATE OF 1/R. 39

FIGURE 19. BACKBONE RMSD OF ACRA MODELS AND THEIR INDIVIDUAL DOMAINS OVER MD TRAJECTORIES MEASURED RELATIVE TO THE INITIAL COORDINATES OF MODEL A (LEFT) AND MODEL B (RIGHT). 40

FIGURE 20. (A) DOCKING SEARCH SPACE WITH DIMENSIONS 25 Å X 25 Å X 25 Å FOR THE HINGE SITE. THE CENTER OF THE BOX IS SHOWN AS RED SPHERES AND REPRESENTS THE C_α ATOM OF SER138. (B) DOCKING SEARCH SPACE WITH DIMENSIONS 45 Å X 45 Å X 45 Å FOR THE MP SITE. THE CENTER OF THE BOX IS SHOWN AS RED SPHERES AND REPRESENTS THE C_α ATOM OF GLN270. THE α-HELICAL HAIRPIN, LIPOYL, β-BARREL, AND MP DOMAINS ARE SHOWN IN RED, BLUE, ORANGE, AND GREEN, RESPECTIVELY. 46

FIGURE 21. (A) CONFORMATIONS EXTRACTED FROM MD SIMULATION OF MODEL A AND OVERLAID WITH THE X-RAY CRYSTAL STRUCTURE (RED) OF ACRA TO REVEAL A HINGE-BENDING MOTION AT THE LIPOYL-HAIRPIN INTERFACE. (B) RESIDUES LOCATED AT THE HINGE SITE. (C) SUSCEPTIBILITY ASSAY TO NOVOBIOCIN WITH WT ACRA AND MUTANTS AT THE HINGE SITE REVEAL THE FUNCTIONAL RELEVANCE OF THE SITE. 47

FIGURE 22. ENRICHMENT PROFILE FOR ENSEMBLE-BASED VIRTUAL SCREENING AT THE HINGE SITE TO ACRA CRYSTAL STRUCTURE (RED), HOMOLOGY MODELS (BLACK), AND EACH CONFIGURATION FROM MD SIMULATION (DOTTED). 49

FIGURE 23. ENRICHMENT PROFILE FOR ENSEMBLE-BASED VIRTUAL SCREENING AT THE MP SITE TO THE HOMOLOGY MODELS (BLACK) AND EACH CONFIGURATION FROM MD SIMULATION (DOTTED)..... 50

FIGURE 24. SEVEN COMPOUNDS THAT BIND ACRA WITH EPI-LIKE CHARACTERISTICS.. 50

FIGURE 25. HOECHST H33342 FLUORESCENCE ACCUMULATION AND EFFLUX INHIBITION ASSAYS FOR NSC60339, NSC33353, AND NSC305798 IN WT-PORE AND ΔTOLC CELLS. 54

FIGURE 26. IN VIVO PROTEOLYSIS WITH TRYPSIN FOR MBX2319 (A), MC-207,110 (B), NSC305798 (C), NSC33353 (D), NSC60339 (E), AND NSC227186 (F) REVEALED THAT NSC60339 HAS A NOVEL MECHANISM OF ACTION. 57

FIGURE 27. BEST-SCORING DOCKING POSE OF NSC60339 TO ACRA AT THE HINGE SITE. 59

FIGURE 28. PREDICTED AND EXPERIMENTAL pK_A VALUES FOR 1,2,4 TRIAZOLE AND 4-METHYL-1,2,4 TRIAZOLE. PREDICTED pK_A VALUES FOR THE DIHYDROIMIDIAZOLINE RINGS OF NSC60339. ALL PREDICTIONS WERE CARRIED OUT WITH CHEMAXON MARVIN 16.7.11. 59

FIGURE 29. LOWER SCORING DOCKING POSE OF NSC60339 AT THE HINGE SITE WITH ONLY ONE DIHYDROIMIDAZOLIUM RING INTERACTING WITH ACRA. 63

FIGURE 30. FOUR ANALOGS WITH IMPROVED OM PERMEABILITY, HOECHST H33342 UPTAKE, AND EQUAL OR IMPROVED POTENTIATION OF NOVOBIOCIN COMPARED TO NSC60339 WAS OBSERVED (**TABLE 4**). 64

FIGURE 31. NSC60339 (1), 17H, AND 17O DO NOT DISRUPT THE TRANSMEMBRANE POTENTIAL THAT MIMICS THE PROTON RELAY ACROSS THE INNER MEMBRANE. VALINOMYCIN WAS USED AS A CONTROL. 66

FIGURE 32. (A) INHIBITOR BINDING SITES PREDICTED FROM BLIND ENSEMBLE DOCKING OF SLU-258, CLOROBIOCIN AND NOVOBIOCIN (SITES I-III) AND ADDITIONAL SITES PREDICTED BY FTMAP (SITES IV-VI). SITES I, II, AND III ARE LOCATED BETWEEN THE α-HAIRPIN AND LIPOYL DOMAINS, IN THE β-BARREL DOMAIN, AND BETWEEN THE β-BARREL AND MP DOMAIN, RESPECTIVELY. SITE IV IS LOCATED BETWEEN THE β-BARREL AND LIPOYL DOMAIN, AND SITES V AND VI ARE LOCATED IN THE MP DOMAIN. FOR CLARITY, ONLY SLU-258 IS SHOWN. (B) RESIDUES MUTATED INDIVIDUALLY TO TRP FOR FLUORESCENCE QUENCHING EXPERIMENTS ARE LABELED AND SHOWN AS CYAN SPHERES. THE INTRINSIC TRP IN WILD-TYPE ACRA, W347, WAS MUTATED TO PHE. 73

FIGURE 33. SEQUENCE ALIGNMENT OF FULL-LENGTH ACRA, MEXA (CHAIN F FROM PDB 2V4D) AND CUSB (CHAIN B FROM PDB 3NE5). THE ORANGE BOXES INDICATE THE EXTENT OF THE ACRA HOMOLOGY BUILT FROM MEXA. 77

FIGURE 34. CHEMICAL STRUCTURES OF (A) CLOROBIOCIN, (B) NOVOBIOCIN, (C) SLU-258, AND (D) SLU-417. 82

FIGURE 35. SEARCH SPACE USED FOR DOCKING. THE DIMENSIONS OF THE BOX ARE 50 Å X 126 Å X 126 Å. 83

FIGURE 37. (A) SUPERPOSITION OF THE HOMOLOGY MODEL OF WT ACRA MONOMER ONTO AN ACRA PROTOMER FROM THE CRYO-EM STRUCTURE OF THE ASSEMBLED ACRAB-TOLC COMPLEX. *COLORS*: HAIRPIN (RED), LIPOYL (BLUE), BARREL (ORANGE), AND MP DOMAIN (GREEN), CHAIN D FROM PDB ENTRY 5V5S (GRAY). THE LINKERS ARE SHOWN IN MAGENTA AND WERE NOT INCLUDED IN THE RMSD CALCULATION OF EACH DOMAIN. (B) Cα RMSD OF ACRA FOR THE WHOLE PROTEIN AND FOR EACH INDIVIDUAL DOMAIN WITH RESPECT TO THE CRYO-EM MODEL OVER THE COURSE OF THE MD SIMULATION. 86

FIGURE 39. DOPE SCORE FOR ALL 100 MODELS USING THE ACRA CRYSTAL STRUCTURE (PDB 2F1M) AND THE MP DOMAIN FROM CUSB (RED) OR MEXA (BLACK). 87

FIGURE 40. THREE PREDICTED SITES FROM RMSD CLUSTERING OF BLIND ENSEMBLE DOCKING FOR (A) CLOROBIOCIN AND (B) NOVOBIOCIN REFERRED TO AS SITE I, II, AND III. RESIDUES MUTATED TO TRYPTOPHAN ARE E67, F81, I252, K241, F254, AND I343. W347 WAS MUTATED TO PHE. EACH LIGAND COMES FROM A SEPARATE CONFORMATION, BUT ONLY ONE CONFORMATION IS SHOWN FOR SIMPLICITY. 89

FIGURE 41. SLU-258 RESULTS IN A STERIC CLASH WHEN DOCKED AT SITE I (HINGE SITE) OF ACRA THAT COULD PREVENT OLIGOMERIZATION. 89

FIGURE 42. NUMBER OF OCCURRENCES OF DOCKED POSES IN EACH CLUSTER DETERMINED FROM RMSD-BASED CLUSTERING OF (A) SLU-258, (B) NOVOBIOCIN, AND (C) CLOROBIOCIN FROM BLIND ENSEMBLE DOCKING. THE RMSD CUTOFF WAS 2.5 Å. 91

FIGURE 43. BINDING OF SLU-258 AT SITE III BETWEEN THE Β-BARREL AND MP DOMAIN EXISTS BETWEEN TWO PROTEOLYTIC FRAGMENTS, K46-R296 AND K46-K346, DETERMINED IN THE PREVIOUS CHAPTER. 92

FIGURE 44. BIOLAYER INTERFEROMETRY (BLI) SPECTRA FOR (A) SLU-417, AN ANALOG OF SLU-258, BINDING TO FULL-LENGTH ACRA, (B) SLU-417 BINDING TO A TRUNCATED VARIANT OF ACRA LACKING THE MP DOMAIN (ACRA (45-312), AND (C) CLOROBIOCIN BINDING TO ACRA (45-312). 93

FIGURE 45. FLUORESCENCE OF ACRA MUTANTS CARRYING A SINGLE TRP SUBSTITUTION IN THE ABSENCE OF INHIBITORS (A) AND QUENCHING IN THE PRESENCE OF INCREASING CONCENTRATIONS OF SLU-258 (B), CLOROBIOCIN (C), AND NOVOBIOCIN (D). 99

FIGURE 46. FLUORESCENCE OF CLOROBIOCIN, SLU-258, AND NOVOBIOCIN WITHOUT ACRA. 101

FIGURE 47. TRP FLUORESCENCE IN THE ABSENCE (APO) AND PRESENCE OF CLOROBIOCIN (CLO) OR SLU-258 (SLU) WITH INCREASING CONCENTRATIONS OF POTASSIUM IODIDE (KI). 103

FIGURE 48. TRP FLUORESCENCE OF E67W, K241W AND I252W ACRA VARIANTS IN THE ABSENCE (APO) AND PRESENCE OF CLOROBIOCIN (CLO) OR SLU-258 (SLU) WITH INCREASING CONCENTRATIONS OF POTASSIUM IODIDE (KI). 103

FIGURE 49. DOCKED MODELS OF CLOROBIOCIN AND SLU-258 (MAGENTA) BOUND AT SITE IV BETWEEN THE LIPOYL AND β-BARREL DOMAINS, FLANKED BY F81 AND F254 (GREEN SPHERES). (A-B) RESIDUES WITHIN 5 Å OF EACH LIGAND ARE SHOWN IN GREEN MESH. (C-D) RESIDUES IN CONTACT WITH EACH LIGAND ARE SHOWN IN CYAN STICKS AND THE INTERACTIONS ARE INDICATED BY BLACK DASHES. 105

FIGURE 50. (A) CHEMICAL STRUCTURE OF MC-207,110 WITH AMINES SHOWN IN RED. (B) MOLECULAR DESCRIPTORS FOR MC-207,110 CALCULATED WITH MOE 2016. 115

FIGURE 51. ALIGNMENT OF THE MODELED STRUCTURES FROM ZINC15 FOR 65071797 (BLUE) AND 11839473 (RED). 121

FIGURE 52. SPR CURVES FOR THE SIX COMPOUNDS THAT BIND ACRA. COMPOUND 11839473 IS IDENTICAL TO 65071797**.** 125

FIGURE 53. LACK OF ACCUMULATION OF THE FLUORESCENT PROBE HOECHST H33342 FOR THE SIX COMPOUNDS THAT BIND ACRA. COMPOUND 11839473 IS IDENTICAL TO 65071797 127

FIGURE 54. ALIGNMENT OF THE CRYSTALLOGRAPHIC POSE OF ERYTHROMYCIN (PINK) WITH THE BEST-SCORING DOCKED POSE (BLUE). THE RMSD OF THE ALIGNMENT WAS 1.6 Å. 129

FIGURE 56. CHEMICAL STRUCTURES OF COMPOUNDS THAT POTENTIATE NOVOBIOCIN AND ERYTHROMYCIN AND BIND ACRA. 132

FIGURE 57. BEST-SCORING DOCKING POSES FOR 56871955 BOUND TO ACRA AT SITE I, II, III, AND IV 140

FIGURE 58. CONTACTS BETWEEN 56871955 AND ACRB ARE EXTENSIVE FOR THE AMINOCYCLOBUTYL PYRIMIDINE SCAFFOLD. THE FLUORINE GROUP ATTACHED TO THE PHENYL RING APPEARS TO BE UNIMPORTANT FOR BINDING TO ACRB. 140

INTRODUCTION

Antibiotic resistance and the discovery void

Antibiotic resistance is a global public health concern that can impact every person on the planet.[1] Antibiotics are drugs, typically small organic molecules, that kill or slow down the growth of bacteria during an infection.[2] Antibiotics are grouped into different classes depending on their intended target and mechanism of action.[3] For example, β-lactams such as penicillin inhibit the synthesis of the bacterial cell wall while aminoglycosides inhibit protein synthesis by interacting with the bacterial ribosome.[3] Ever since the first antibiotic, penicillin, was discovered by Alexander Fleming in 1928,[4] medical professionals have been prescribing antibiotics for the prevention and treatment of bacterial infections.[3] In addition, we have also applied the use of antibiotics in agriculture.[5] The cumulative result of different antibiotics use has provoked a multipronged response from bacteria referred to as resistance.

In 1859, Charles Darwin published his book entitled *On the Origin of Species*.[6] In this book, Darwin laid out his theory of natural selection.[6] Natural selection in the context of antibiotic resistance states that when individual bacteria are exposed to certain environmental conditions that threaten their survival (such as the use of antibiotics), certain individuals in the species will adapt to resist these conditions.[7] The individuals that adapt are then selectively favored to pass on their genes to the next generation.

The mechanism(s) of resistance obtained by the selectively favored bacteria are wide and diverse. Bacteria can develop mutations in DNA gyrase, a

key enzyme responsible for DNA replication, which prevent antibiotics in the quinolone class from inhibiting the enzyme.[8] Bacteria can express β-lactamase enzymes that bind and inactivate β-lactam antibiotics preventing them from performing their mechanism of action.[9] Resistant bacteria can also modulate the influx and efflux of multiple classes of antibiotics.[10, 11] In a sub-category of bacteria referred to as Gram-negative, bacteria contain two membrane bilayers separated by a space called the periplasm.[12] The two membranes are referred to as the outer and inner membrane (**Figure 1**). Antibiotics that enter the Gram-negative bacterial cell can pass through a hydrophobic bilayer or through proteins called porins embedded in the bilayer that contain a hydrophilic channel enabling antibiotic passage.[13] Bacteria can reduce the influx of antibiotics by decreasing the

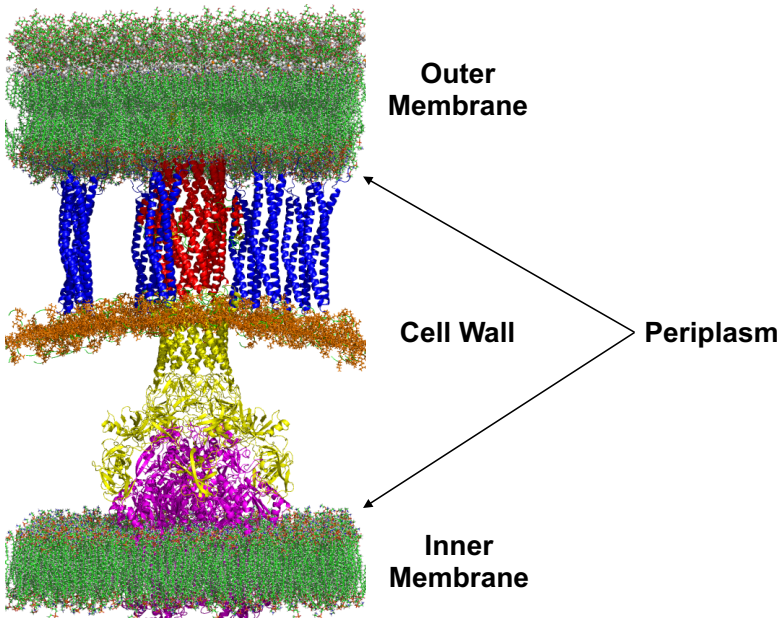


Figure 1. Depiction of the AcrAB-TolC efflux pump in its native environment with the outer membrane, cell wall, periplasm, and inner membrane labeled. The periplasm is the space between the outer and inner membrane.

expression of porins in the outer membrane.[13] Bacteria can also transport molecules known as lipopolysaccharides from the inner membrane to the outer membrane.[14] The lipopolysaccharides contain negatively charged sugar groups that are then cross-linked by divalent cations to produce a highly charged polar environment and provide a permeability barrier to antibiotics (**Figure 2**).[15-17] Antibiotics that can bypass the outer membrane are confronted by a tripartite molecular machine in the periplasm known as an efflux pump which ejects the antibiotic from the bacterial cell (**Figure 1**).[18]

The combination of mutation of the intended drug target[8], inactivating enzymes, permeability barrier,[10] and efflux are the bacterial responses to the selective pressure induced by bacteria.[12] These resistance mechanisms reduce the efficacy of currently available antibiotics. Moreover, we are living in a discovery void where a novel class of antibiotics has not been identified since the 1980s (**Figure 3**).[19]

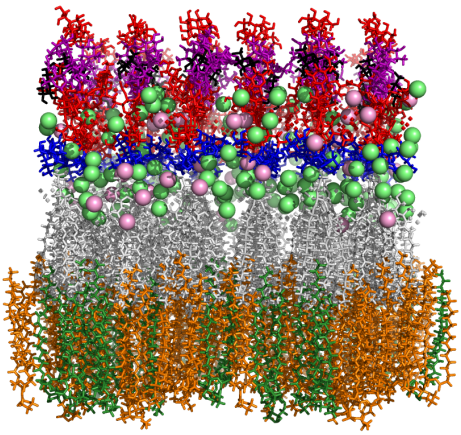


Figure 2. Molecular picture of the K-12 Gram-negative outer membrane. POPE (orange) and POPG (green) is in the inner leaflet. Lipid A (grey) is in the outer leaflet attached to the inner core polysaccharides (blue and red). Divalent cations, magnesium (green) and calcium (pink), interact with the inner core polysaccharides. The outer core polysaccharides are shown in magenta and black.

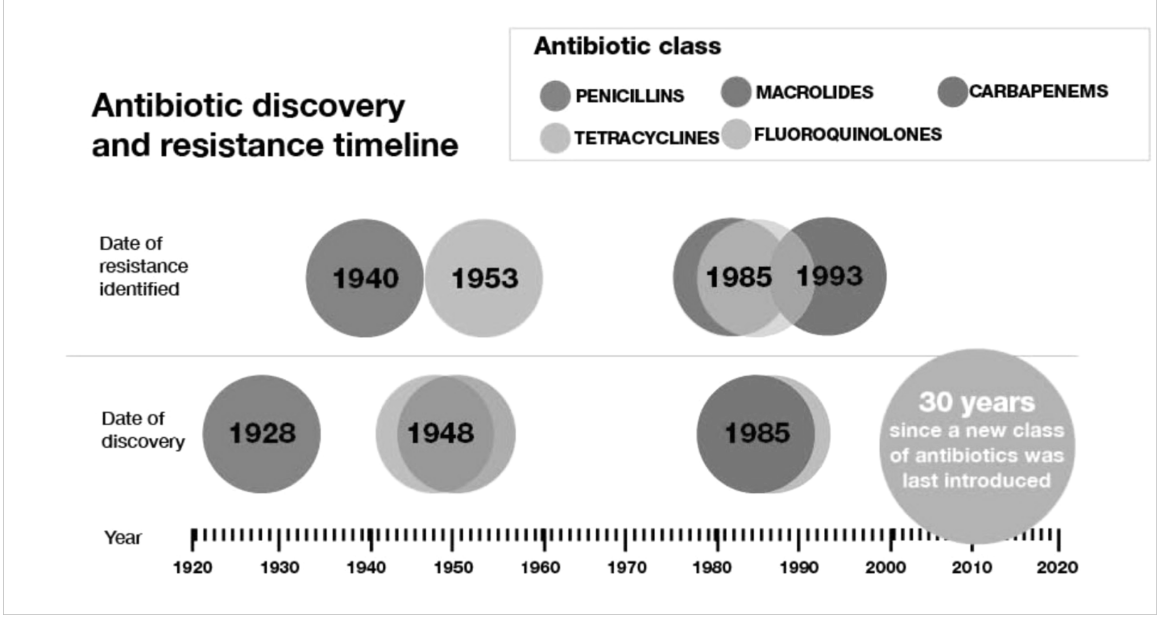


Figure 3. Discovery void of new classes of antibiotics. Figure was modified from Public Health England.

Structure and function of multidrug efflux pumps in *Escherichia coli*

About 80% of bacterial infections diagnosed in a hospital setting have been attributed to a multidrug Gram-negative species such as *Escherichia coli* (*E. coli).*[20-22] *E. coli* infections are the leading cause of urinary tract infections (UTIs) and are often related to food-born infections such as in beef and romaine lettuce.[23-25] During growth, *E. coli* produce metabolites that are toxic to the cell and need to be removed for proper cell development.[26] *E. coli* utilize efflux pumps such as AcrAB-TolC that span both membranes and the entire periplasm to extrude these metabolites (**Figure 1**). In the case of a food-born infection from undercooked beef or romaine lettuce, *E. coli* travels through the small intestine where bile acids are released and negatively harm the DNA of *E. coli.*[27] The presence of bile acids induces the expression of AcrAB-TolC which expel the bile from the periplasm and prevent it from reaching the DNA in the bacterial cell.[28] AcrAB-TolC is a complex machinery composed of three proteins from different families: Resistance-Nodulation-Division (RND), Membrane fusion proteins (MFP), and outer membrane factors (OMF).[26, 29]

AcrB is a homotrimer of the RND family composed of 1049 amino acids with a transmembrane, periplasmic (porter), and funnel domain.[30] AcrB is expressed as a functional unit with AcrA. AcrB can bind and extrude a range of compounds from bile acids, dyes (acraflavine), detergents (sodium dodecyl sulfate (SDS), solvents, and antibiotics.[18, 26, 31] Antibiotics include novobiocin, erythromycin, penicillin, and levofloxacin.[31] These antibiotics are from four different classes of

antibiotics such as aminocoumarin[32], macrolide[33], β-lactam[4, 34], and fluoroquinolones[35]; thus, AcrB exhibits a polyspecific character that contributes to multidrug resistance.

AcrB as a trimer can exist in three different conformational states referred to as loose (L), tight (T), and open (O).[30, 36] A molecule, substrate, enters AcrB in the L state through 3 possible open channels: a lower periplasmic cleft, a cleft on the surface of the inner membrane, or through a central cavity in the transmembrane domain (**Figure 4**).[37] Transport through the central cavity is involved in transport of substrates directly from the interior of the cell.[37] When a substrate enters one of the three channels in the L state, the distal pocket expands to facilitate binding in the T state after binding or bypassing another pocket referred to as the access pocket.[38, 39] The two pockets are separated a by loop referred to as a switch-loop or G-loop.[40] Substrates with a high molecular weight such as erythromycin bind at the access pocket while lighter substrates bypass the switch-loop and bind the distal pocket.[38] Substrates that enter through the central cavity can bypass the access pocket and directly bind the distal pocket.[37] A proton gradient between aspartic acid residues in the transmembrane domain triggers conformational changes that closes the open channels, shrinks the distal binding

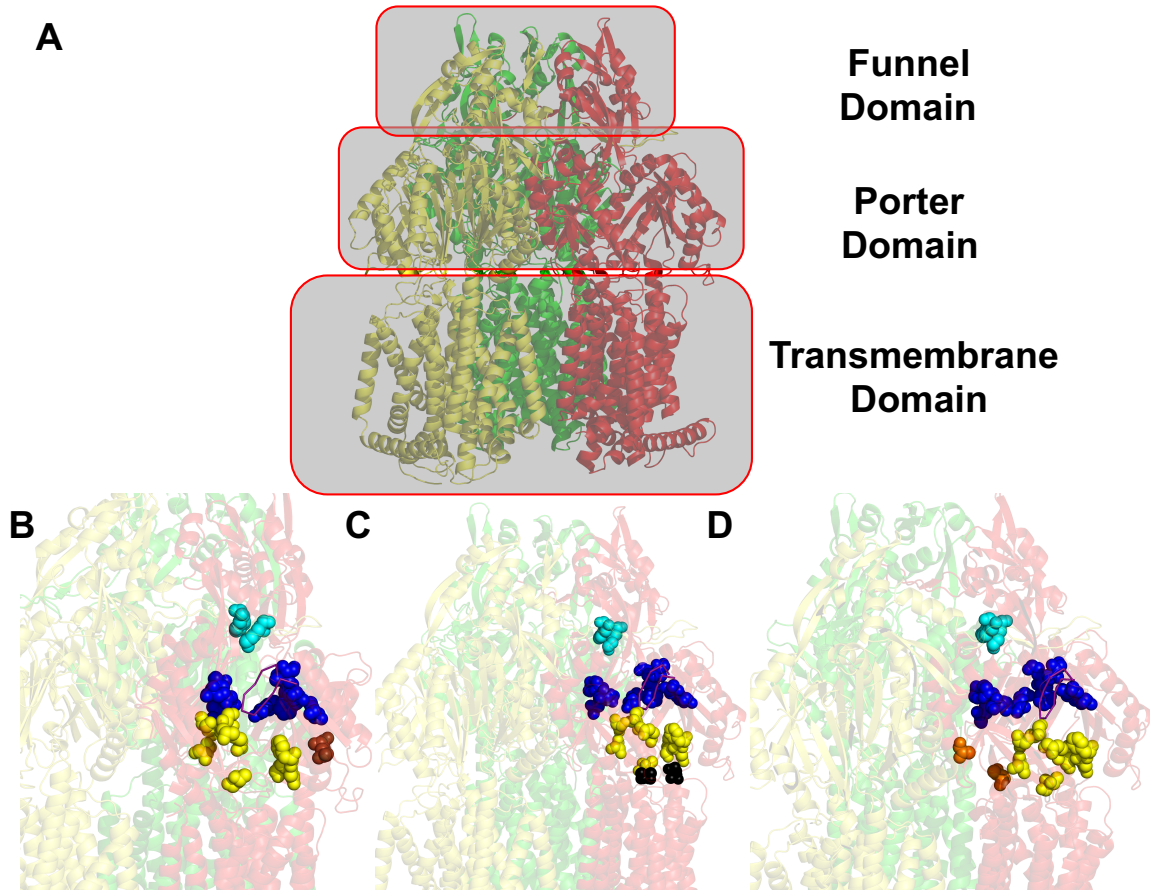


Figure 4. Structure and substrate transport pathways of AcrB. (A) AcrB in three conformational states with transmembrane, porter, and funnel domains highlighted (PDB 4DX5). The L state is in yellow, T state in red, and O state in green. (B) The substrate can enter from a cleft in the periplasm (brown sphere; R307), traverse through the access binding pocket (yellow spheres), the G-loop (magenta ribbon), and distal binding pocket (blue sphere) to the exit gate (cyan spheres; Y758, K770) which passes the substrate into the funnel domain and towards TolC. (C) Alternatively, substrate can center from the surface of the inner membrane (black spheres; D566, T678). (D) Substrate can enter from the central cavity (orange spheres; T37, A100) and traverse directly to the distal binding pocket and then onwards to the exit gate and out of the cell.

pocket, and opens a gate into the central funnel towards TolC.[39, 41] The substrate is pushed out of the cell by a peristaltic motion resulting in a functional rotation mechanism (**Figure 5**).[36]

AcrB assembles with two other proteins, AcrA and TolC, to expel substrates from the cell.[42] AcrA is a periplasmic adaptor from the MFP family.[43] It consists of four domains referred to as the α-hairpin, lipoyl, β-barrel, and membrane-proximal (MP).[44] The lipoyl, β-barrel, and MP domain interact with AcrB while the α-hairpin interacts with TolC.[44, 45] TolC is a trimer from the OMF family and consists of a 12 stranded β-barrel protein embedded in the outer membrane that is constitutively open to the environment.[26, 39, 46] In addition, TolC consists of 12 α-helices that extend into the periplasm (**Figure 6**).[46] The periplasmic tip contains a ring of aspartate residues that keep the pore in a closed state preventing substrate access (**Figure 6**). [39]

Until the determination of near-atomic resolution cryo-EM structures, the oligomeric state of AcrA and the structure of the assembled complex remained unclear.[29, 44, 47] The first model of the assembled complex used in vivo crosslinking with protein-protein docking to build a model with 3:3:3 stoichiometry.[44] AcrB, AcrA, and TolC assemble as trimers.[30, 46, 47] The model asserted that AcrA binds AcrB as a monomer, but gel filtration chromatography combined with surface plasmon resonance (SPR) concluded that the binding affinity of AcrA to AcrB is an order of magnitude higher when the N-terminus of AcrA is lipid-modified and acts as a dimer.[42, 44] In vivo, AcrA is known to be anchored to the inner membrane by a

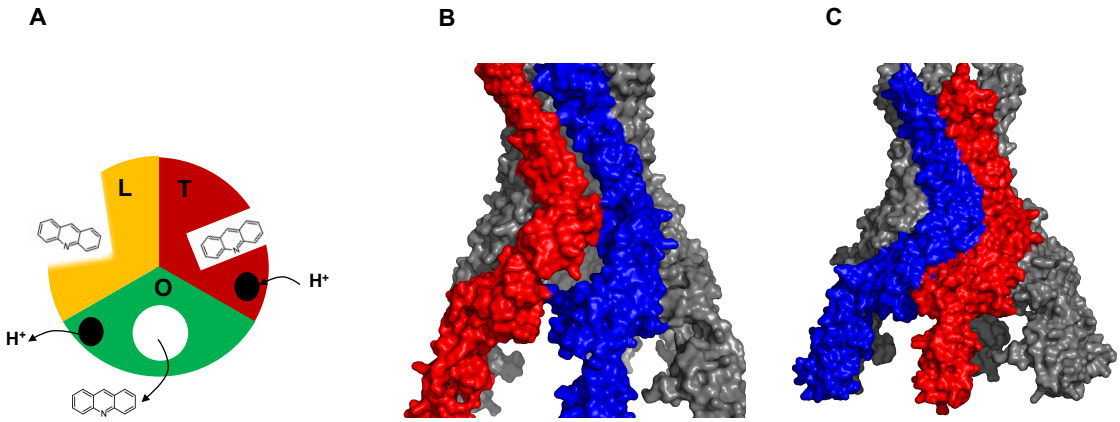


Figure 5. Drug transport mechanism of AcrB. (A) Functional rotation mechanism of AcrB. An efflux pump substrate such as acridine (shown) enters AcrB in the L state triggering conformational changes that expand the distal binding pocket in the T state. A proton relay mechanism triggers a subsequent conformational change that collapses the distal pocket and expels the substrate towards TolC for efflux in the O state. (B) In the absence of substrate, gaps exist between AcrA dimers in the hexameric funnel. (C) The gaps are sealed upon substrate binding and functional rotation in AcrB to propagate efflux out of the cell. The sealing of the gaps in AcrA switches TolC into an open state.

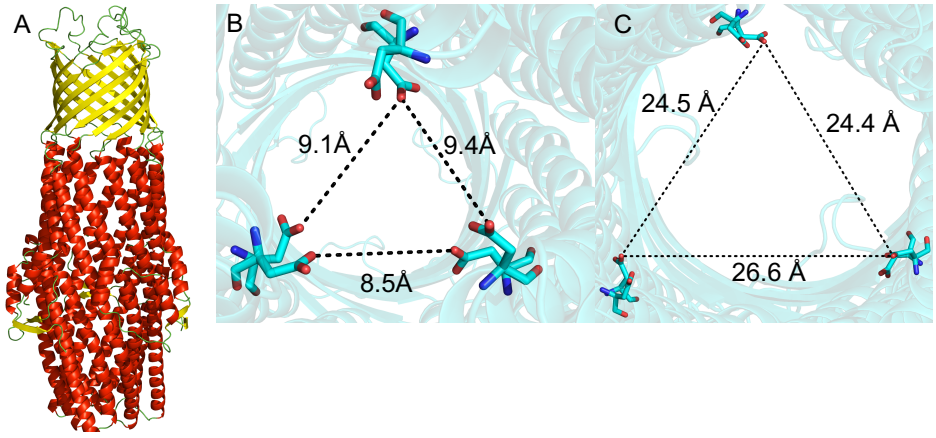


Figure 6. (A) The atomic structure of TolC (PDB ITQQ). The closed (B) and open states (C) of TolC from the apo (closed) and inhibitor-bound (open) cryo-EM structures (PDB 5V5S and 5NG5). Each state is differentiated by two aspartic acid residues, Asp371 and Asp374, in each monomer of TolC.

lipid.[48] The binding of an AcrA dimer to a trimeric AcrB results in AcrA assembling as a hexmeric funnel around AcrB (**Figure 1**).[49] The hexameric structure of AcrA has also been confirmed in the cellular environment in situ using cryo-EM imaging.[50] The question though of how AcrA connects AcrB and TolC was still in question.

Two models were proposed for how AcrA functions as an adaptor between AcrB and TolC. The first is referred to as the adaptor wrapping model.[26] In this model, AcrB and TolC directly interact and hexameric AcrA interacts with TolC and AcrB to wrap around the two proteins. AcrB was found to directly interact with TolC by disulfide crosslinking and bind with nanomolar affinity using SPR.[42, 51]The binding affinity between AcrB and TolC was comparable to AcrA and AcrB.[42] In contrast, cryo-electron microscopy (EM) found that AcrA functions as a trimer of dimers to form a hexameric funnel that bridges AcrB and TolC.[29, 39, 45, 49] There is

no direct interaction between AcrB and TolC. This is called the adaptor bridging model[26] and cryo-EM has found that the model agrees with structures from other efflux transporters such as MexAB-OprM in *Pseudomonas aeruginosa*, CusABC, and MacAB-TolC in *Escherichia coli*.[52-54]

In cryo-EM structures of AcrAB-TolC with and without a ligand bound, the complete mechanism of substrate transport from AcrB to TolC was elucidated. AcrAB-TolC transports substrates by a long-range allosteric transport mechanism.[39] In the absence of substrate, the periplasmic tip of TolC is constricted resulting in a closed state (**Figure 6**). AcrA acts a trimer of dimers to bridge AcrB with TolC and contains small gaps in between each dimer (**Figure 5B**). Upon substrate binding AcrB in the L state, the gaps in AcrA are sealed to prevent substrate leakage (**Figure 5C**) and TolC transitions to an open state to allow substrate passage (**Figure 6**).[39] Forced partial opening of TolC by mutants at the periplasmic tip lead to a decrease in TolC's affinity for AcrA.[42, 55] This indicates that the open state of TolC is less stable, which could lead to disassembly upon substrate transport.[55] TolC is an outer membrane protein that is involved in other transporters in *E. coli* such as AcrDA-TolC, AcrEF-TolC, and MacAB-TolC.[26] This disassembly of AcrAB-TolC is necessary for TolC to interact with other transporters.

Efflux pump inhibition

To overcome resistance, the long-range allosteric mechanism by which multidrug efflux pumps function must be inhibited.[56, 57] A plausible solution is

combination therapy.[58, 59] Combination therapy is interim until a new class of antibiotics can be discovered for treatment of bacterial infections, but could also be used to restore the activity of existing antibiotics from resistance.[57] The co-administration of an antibiotic with an efflux pump inhibitor (EPI) prevents the emergence of new mutant strains reducing the frequency of resistance to a specific target.[56] Overexpression of AcrAB-TolC is correlated with a reduction of DNA mismatch repair proteins resulting in a higher frequency of spontaneous mutation; thus, inhibition of efflux with EPIs helps to prevent the early stages of antibiotic resistance by hindering the ability of the bacteria to mutate the intended target of the antibiotic.[60, 61]

An EPI that targets multidrug efflux pumps such as AcrAB-TolC in Gram-negative bacteria should ideally have seven qualities. An EPI for a specific efflux pump such as AcrAB-TolC should be able to bypass the permeability barrier of the OM (i), potentiate the activity of antibiotics that are efflux pump substrates (ii), don't potentiate antibiotics in efflux-deficient cells (iii), increase the accumulation of substrates inside the cell (iv), not affect the proton relay across the inner membrane (v), have no antibacterial activity (vi), and not potentiate antibiotics that are non-substrates (vii). [35, 61, 62] An EPI that possesses these qualities would likely have a mechanism of action for AcrAB-TolC.

The first discovered EPI was PAβN (MC-207,110) (**Figure 7A**).[35] MC-207,110 was discovered through a high-throughput experimental screen of 200,000 compounds that potentiated the antibiotic levofloxacin, a fluoroquinolone

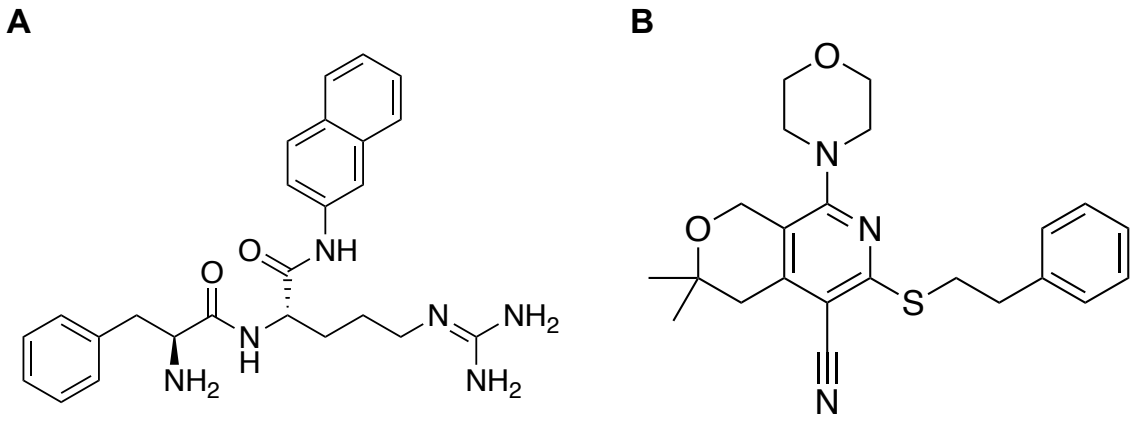


Figure 7. Chemical structure of current efflux pump inhibitors MC-207,110 (A) and MBX2319 (B).

and efflux pump substrate, in *Pseudomonas aeruginosa (P. aeruginosa) and E. coli*.[35, 62] The compound also inhibited AcrAB-TolC in *E. coli*, but with less potentiation of levofloxacin than *P. aeruginosa*.[62] Inhibition of efflux by MC-207,110 in *E. coli* was observed by the increased fluorescence and accumulation of a fluorescent dye referred to as Hoechst H33342.[62] Hoechst H33342 is a known efflux pump substrate that intercalates with DNA inside the cell.[62, 63] When an efflux pump such as AcrAB-TolC is functional, Hoechst H33342 is ejected resulting in lower fluorescence compared to efflux-deficient cells.[63] The co-administration of an EPI such as MC-207,110 increases the fluorescence of the dye compared to wild-type cells.[62] Additionally, MC-207,110 exhibited two more the qualities of an EPI by having no intrinsic antibacterial activity and not disturbing the proton gradient across the inner membrane.[35, 57]

Although, MC-207,110 is no longer in drug development because it lacks two of the qualities for an EPI: it potentiates antibiotics that are non-substrates,

specifically gentamicin, in WT and efflux-deficient cells.[62] Efflux-deficient cells are mutants where either the TolC or AcrB genes have been deleted by site-directed mutagenesis.[62] In efflux-deficient cells, MC-207,110 was found to possess an additional mode of action.[62] MC-207,110 disrupted the integrity of the outer membrane and thus increased the influx and susceptibility of antibiotics.[57] The additional mode of action indicates that MC-207,110 can bypass the outer membrane permeability barrier of Gram-negative bacteria typical of an EPI, but the ability to do so in efflux-deficient cells indicates that the compound contains toxicity issues limiting development.[64] Toxicity can be defined as eliciting a drug response from an unintended target. MC-207,110 can potentiate a non-substrate of AcrAB-TolC; therefore, it is exerting unintended responses. Responses that are beyond the inhibition of AcrAB-TolC. Further development of analogs using the MC-207,110 scaffold were ended because of toxicity.[62]

A separate independent whole cell high-throughput screen of 183,400 compounds identified a compound referred to as MBX2319 that contains a pyranopyridine scaffold that has become the basis for one of the most potent types of EPIs to date (**Figure 7B**).[61, 65] MBX2319 potentiates fluoroquinolone and β-lactam antibiotics that are efflux pump substrates, doesn't potentiate non-substrates, doesn't potentiate substrates in efflux-deficient cells, contains no intrinsic antibacterial activity, increases the accumulation of Hoechst H33342, and doesn't perturb the proton gradient across the inner membrane or disrupt influx across the outer membrane like MC-207,110.[62] The permeability of MBX2319 is

unknown, but the ability to potentiate antibiotics in WT cells suggests that permeability is not an issue.

X-ray crystal structures have been determined for MBX2319 and three analogs derived from the same scaffold.[66] The structures found that all the compounds bind the hydrophobic trap of the distal binding pocket of AcrB.[66, 67] The hydrophobic trap is characterized by six phenylalanine residues; thus, the compounds interact with AcrB through van der waals and π-π stacking interactions (**Figure 8**).[66, 67] The crystallographic poses for the compounds overlap with the crystallographic pose of minocycline to AcrB, a tetracycline antibiotic and AcrB substrate.[66, 68] Kinetic assays confirmed that MBX2319 and the three analogs act as competitive inhibitors of AcrB.[62, 65] The binding of the inhibitors outcompetes the binding of the antibiotics to the pump; thus, a greater concentration of antibiotic remains inside the cell. A complete structure-activity relationship (SAR) has been devised and identified the sections of the pyranopyridine scaffold that most contribute to potency. Sixty analogs were developed for this SAR, but none of the compounds have reached clinical development. [65, 69]

While both MC-207,110 and MBX2319 have been potential lead compounds for clinical use, none of their analogs have made It into the Food and Drug Administration (FDA) clinical phase development.[61] Both MC-207,110 and MBX2319 have different proposed mechanisms of action on AcrB. MC-207,110 was proposed by computational methods to bind at the G-loop and allosterically prevent substrate access as means of inhibiting efflux while MBX2319 inhibits

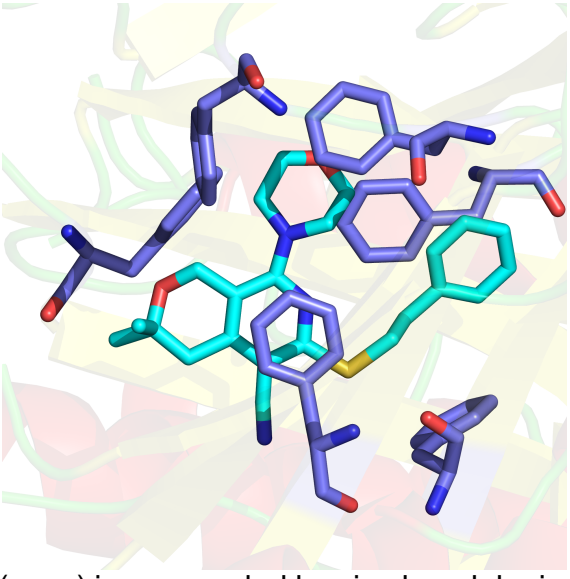


Figure 8. MBX2319 (cyan) is surrounded by six phenylalanine residues (purple) in the hydrophobic trap of the distal binding pocket of AcrB. The six phenylalanine residues are F136, F178, F610, F615, F617, and F628.

competively.[40, 62] Perhaps some new mechanisms of action are needed to discover a lead with clinical applications.

TolC as a poor drug target

To inhibit the AcrAB-TolC efflux pump through mechanisms other than AcrB, one of the possible targets is TolC. TolC is the outer membrane channel for efflux pumps in *E. coli* to expel antibiotics and other substrates from the cell.[26] If a molecule could be discovered that blocks the TolC channel, efflux should be inhibited. A molecule referred to as hexamminecobalt was co-crystallized with TolC and found to interact with the aspartate ring.[70] The aspartate ring expands and constricts to create the open and closed states of TolC (**Figure 9**).[39, 46] The binding of hexamminecobalt conceivably keeps TolC in a closed state blocking efflux of antibiotics from AcrB. Hexamminecobalt binds TolC in the sub-micromolar range,

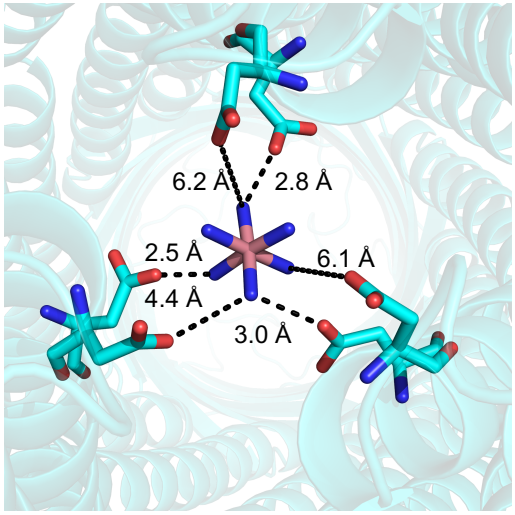


Figure 9. Hexamminecobalt (center) bound to the aspartate ring in the closed state of the TolC crystal structure (PDB 1TQQ). Carbon atoms for aspartate are in cyan.

but no antibacterial activity or potentiation of antibiotics was observed.[71] The compound has also been found to be toxic in *E. coli*.[71]

Further work sought to use computational methods combined with binding assays and single-channel electrophysiology to identify new compounds that would bind at the same site as hexamminecobalt with similar affinity.[71] Several compounds were found to bind at the same site with sub-micromolar affinity, but none of the compounds potentiated antibiotics in vivo.[71] Separate in vivo experiments carried out independently from that work concluded that the application of TolC as a target for efflux inhibition is not feasible in vivo.[55] In principle, inhibition of TolC would result in a decrease in the minimal inhibition concentration (MIC) by preventing efflux. However, antibacterial assays show that the MICs for different antibiotics are unchanged for a range of TolC concentrations 10-fold higher and lower than WT cells.[55] The results imply that AcrAB in WT cells

operates below the maximal capacity for substrate binding and extrusion; thus, TolC does not limit drug efflux.

AcrA as a good drug target

The remaining plausible drug target for efflux inhibition of AcrAB-TolC is AcrA. Unlike TolC, AcrA is expressed by the same operon as AcrB and AcrB is dependent on AcrA for efflux.[26, 72] We know from the recent cryo-EM structures that the assembly of AcrAB-TolC agrees with the *adaptor bridging model* which states that AcrB and TolC have no direct interactions and must be bridged by AcrA.[45] Inhibition of AcrA by a small molecule would conceivably disrupt the assembly of AcrAB-TolC and prevent efflux. AcrA binds AcrB with sub-micromolar affinity, but the affinity is dependent on the attachment of a lipid anchor to the N-terminus and the conformation of the MP domain.[42] The MP domain interacts with AcrB in the assembled complex.[44] A mutation, G363C, in the MP domain decreased the affinity of AcrA to AcrB.[42] The disruption of binding affinity by G363C and the lipid anchor could imply that conformational changes in the MP domain of AcrA could disrupt AcrAB-TolC assembly. A protein inhibitor referred to as DARPin binds AcrB and inhibits AcrB by displacing AcrA and thus disrupting assembly (**Figure 10**).[42] A small molecule that could bind AcrA and change the conformation of the MP domain could conceivably prevent binding to AcrB, disrupt the assembly of the pump, inhibit efflux, and ultimately potentiate the activity of antibiotics.

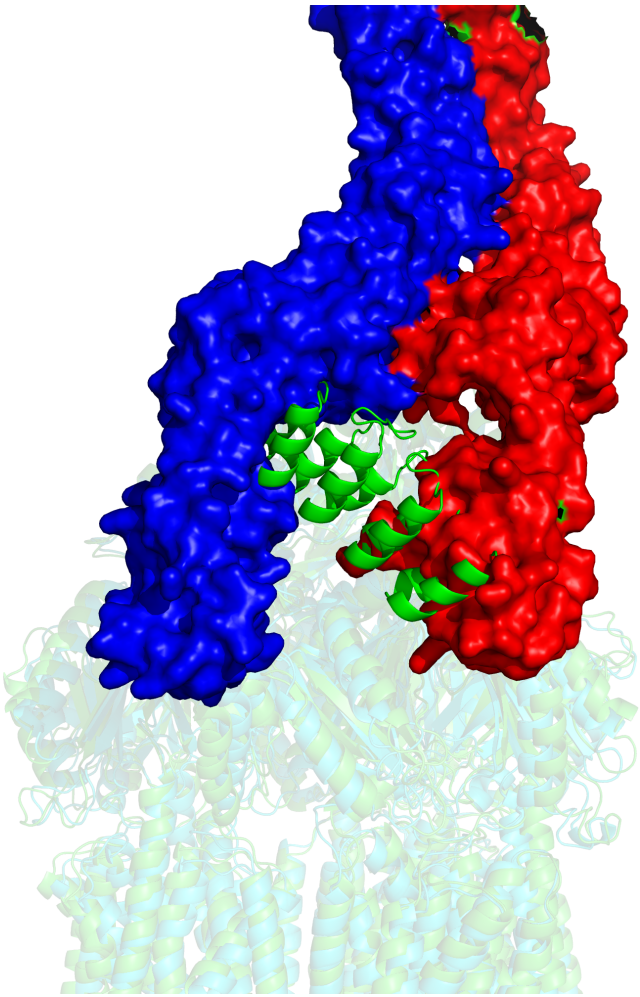


Figure 10. The protein inhibitor DARPin (green) overlaps and interferes with the binding of the AcrA dimer (blue and red) to AcrB in the assembled complex.

Approach

Antibiotics were first discovered as metabolites produced by bacteria and fungi in their natural environments that could then be used by humans to fight infection.[73] The metabolites are called natural products and were identified by a technique referred to as the Waksman platform.[73] The Waksman platform identifies natural products such as streptomycin by testing soil samples for bacteria which produce metabolites that can prevent the growth of pathogenic bacteria.[73] The discovery of natural products as antibiotics ushered in a 'golden age' of antibiotic discovery.[73]

However, since natural products were not intrinsically designed as drugs by the process of natural selection, genetic elements that contain resistance genes are prevalent in bacterial communities and can easily be transferred by horizontal gene transfer; thus, resistance is easily attained.[73] Another limitation is that natural products are often large and can be chemically intractable to produce new analogs by in vitro synthesis.[73] Synthesis of new analogs requires mutation of bacteria to produce new analogs that are subsequently purified and characterized in a labor-intensive and costly process.[73, 74] Moreover, most metabolites with antibacterial properties have already been identified.[73] On the other hand, libraries of synthetic organic compounds such as the ZINC15 database contain millions of diverse compounds that are easily amenable to in vitro synthesis.[73, 75]

Unlike natural products, synthetic organic molecules did not evolve by the process of natural selection to overcome the heterogeneous outer membrane and

efflux pumps such as AcrAB-TolC in *E. coli*.[73] Antibiotics act on multiple targets such as DNA, ribosomes, and the cell wall that are intimately connected as a mechanism of slowing down intrinsic resistance.[73] If an antibiotic only interacted with a single target, spontaneous mutation of the target would more easily render the compound inactive. Interaction of multiple connected targets also allow for the introduction of synthetic organic molecules (non-antibiotic) with proven therapeutic activity such as compounds from the National Cancer Institute (NCI).[73] The application of a non-antibiotic and antibiotic compound by combination therapy could help overcome the outer membrane and efflux in lieu of natural selection. For example, loperamide is an anti-diarrheal drug that has also been shown to destabilize the membrane potential (proton gradient) of bacteria and increase the uptake of minocycline in Gram-negative bacteria.[73] Combination therapy with a non-antibiotic also reduces the required concentration of the antibiotic which can further decrease the likelihood of resistance. [73]

Here, we have performed high-throughput virtual screening of the NCI Diversity V set containing 1,563 synthetic organic compounds and a filtered set of the ZINC15 database containing 1,427 compounds to test for their ability to bind AcrA. While experimental whole-cell screens identified previous EPIs MBX2319 and MC-207,110, neither have made it to clinical development.[35, 62] Application of multiple target-based and whole cell high-throughput experiments by GlaxoSmithKline failed to yield new antibiotics and cost $70 million over 7 years.[76]

Application of our in-silico screening attempts to identify diverse compounds faster and cheaper.

We propose that binding of a synthetic organic compound to AcrA could inhibit efflux through two possible mechanisms before assembly of AcrAB-TolC:

1) Prevention of AcrA dimerization/oligomerization
2) Prevention of the MP domain from interaction with AcrB

by binding at predicted binding sites which will be validated using tryptophan fluorescence spectroscopy and antibiotic susceptibility assays. AcrA has previously been shown to be a monomer in solution in the absence of a lipid anchor attached to the inner membrane in the assembled state.[48] Homology models of the AcrA monomer alone were built to screen the two databases of small molecules for binding AcrA. A non-antibiotic compound that could bind AcrA would disrupt the assembly. The two compounds would lead to a lower concentration of the antibiotic required to decrease bacteria growth or kill the bacteria and act on different targets helping to prevent resistance.

Finally, the database of 1,427 compounds from ZINC15 contains physico-chemical descriptors for compounds that should overcome the outer membrane; thus, computationally screened compounds that bind AcrA should conceivably increase the diversity of chemically tractable compounds for further synthesis, inhibit efflux, potentiate antibiotics, overcome the OM, and help prevent the spread of multidrug resistance with superior efficiency to natural products and high-throughput whole cell experimental screens.

CHAPTER I
IDENTIFICATION OF NOVEL EFFLUX PUMP INHIBITORS THAT INTERACT WITH ACRA BY COMPUTATIONAL METHODS

Some results from this chapter were originally published in two manuscripts of which I am a co-author. The citations for each manuscript are listed below.

- Abdali, N.; Parks, J. M.; Haynes, K. M.; Chaney, J. L.; **Green, A. T**.; Wolloscheck, D.; Walker, J. K.; Rybenkov, V. V.; Baudry, J.; Smith, J. C.; Zgurskaya, H., Reviving Antibiotics: Efflux Pump Inhibitors That Interact with AcrA, a Membrane Fusion Protein of the AcrAB-TolC Multidrug Efflux Pump *ACS Infectious Diseases* **2016,** *3*, 89-98.
- Haynes, K. M.; Abdali, N.; Jhawar, V.; Zgurskaya, H. I.; Parks, J. M.; **Green, A. T**.; Baudry, J.; Rybenkov, V. V.; Smith, J. C.; Walker, J. K., Identification and Structure-Activity Relationships of Novel Compounds that Potentiate the Activities of Antibiotics in Escherichia coli. *Journal of Medicinal Chemistry* **2017,** *60* (14), 6205-6219.

In the Abdali et al. 2016 publication, Model A of AcrA were built by Khushboo Bafna under the supervision of Jerry M. Parks (co-author) and Model B was built by Jerome Baudry. Jerry and Khushboo carried out five nanosecond MD simulations of each model. I then clustered each trajectory by their RMSD and prepared them for ensemble docking by Jerry. I then analyzed the ensemble docking and MD simulation results by calculating the enrichment profiles for each conformation of both models to observe if using structures from MD helped to improve the hit rate. I also calculated the RMSD of each domain relative to the initial structure. I docked the NCI Diversity Set V to the AcrA crystal structure and the homology models prior to MD simulation.

In the Haynes et al. 2017 publication, Figure 3 and the associated description were compiled by me and the docking of the various analogs to the hinge site of AcrA was completed by me. Analysis of the docking was completed by Jerry and calculation of molecular descriptors of NSC60339 and the analogs

was completed by Sarah Cooper. Ryne Johnston helped me with organizing the validation of the pK_a calculations with ChemAxon Marvin.

All microbiology and biochemical experiments were carried out by Helen Zgurskaya's Lab at the University of Oklahoma and John Walker's lab at St. Louis University School of Medicine.

Overview

Structure-based drug design is a part of computer-aided drug design that seeks to accelerate the discovery of new drug candidates for clinical development.[77] The concept requires knowledge of the atomic structure of the intended drug target such as AcrA. However, an experimentally determined structure of AcrA is incomplete.[78] The MP domain, which plays a key role in the assembly of AcrAB-TolC, is missing in the structure. Thus, we built comparative (homology) models of AcrA from similar proteins closely aligned in sequence, structure, and function. We then relaxed these models using MD simulation and extracted conformations by RMSD clustering of the trajectories. The conformations were then docked to compounds in the NCI Diversity V to identify new candidates that bind AcrA, inhibit efflux, and potentiate antibiotics. Multiple conformations were used to mimic a conformational selection mechanism of ligand binding. Multiple predicted inhibitors were successfully validated by experimental methods, but only one compound, NSC60339 was found to change the structure of AcrA in vivo and thus disrupt the assembly of AcrAB-TolC. A structure-activity relationship (SAR) was subsequently carried out for NSC60339. In this chapter, I not only

discuss the identification of new inhibitors that interact with AcrA and the SAR of NSC60339, but also review models of ligand binding, protein structure prediction, MD simulations, and molecular docking.

Models of ligand binding

Part of how ligands interact with their protein partners is by shape.[79, 80] A ligand that binds a protein has a complementary shape analogous to a lock and a key.[81] This 'lock-and-key' mode assumed an overly simplistic view of protein-ligand binding. The model assumes that proteins and ligands are static entities. In fact, proteins are dynamic entities that fold into their native three-dimensional structures by a free energy landscape.[82] A free energy is the probability of a specific conformation; in this case, a protein. The lower the free energy, the higher the probability.[83] In 1968, Cyrus Leventhal proposed a thought experiment that it would take a single protein longer than the age of the universe to sample all the possible conformations to find its native structure.[84, 85] The conception of a free energy landscape resolved this paradox by asserting that proteins fold by favoring conformations of lower free energy.[86] The folded, native, state is reached when a protein reaches a low energy state (**Figure 11**). A free energy landscape is dynamic and implies that a protein can change conformation when binding a ligand.[79] The binding of a ligand induces a conformational change in a protein to a lower free energy to enhance the interactions with the ligand.[87] The model is

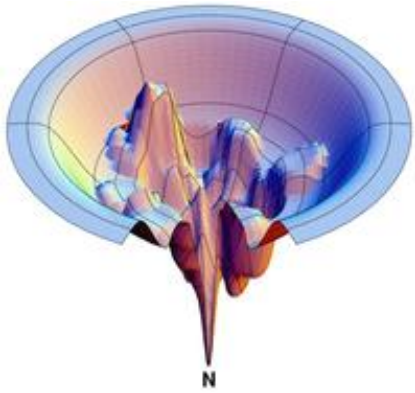


Figure 11. Funnel free energy landscape. The lowest energy state is denoted by the letter N which stands for native state. Landscape was created by the Ken Dill Group under a Creative Commons Attribution 4.0 international license.

referred to as the induced fit model of ligand binding. However, it is now known that proteins often do not exist as a single lowest energy conformation. Their free energy landscapes are far more complex; thus, they exist as an ensemble of lowest energy conformations prior to ligand binding.[82] The addition of a ligand then selects for a conformation of the protein from the ensemble prior to binding and is referred to as conformational selection.[79] All protein structure prediction and modeling algorithms such as MODELLER and MOE used here, to the best of my knowledge, utilize the assumption of a free energy landscape to find the best structures.[88] In addition, docking algorithms that predict protein-ligand binding poses that include ligand and receptor flexibility often follow the induced fit or conformational selection model of ligand binding. [89, 90]

Protein structure prediction

The number of protein sequences available is roughly 700 times the number of protein structures deposited on the Protein Data Bank (PDB).[91] Given this

information in the genomics era, accurate structural modeling could enable the identification of new drug targets, new drugs, and accelerate structure-based drug design.[91, 92] In theory, a protein structure should be able to successfully be predicted from its sequence alone and is referred as de novo modeling.[93] Protein modeling de novo requires a potential energy function to calculate the energetics of each possible conformation from a protein's sequence.[93] A potential energy function often consists of terms to estimate the van der waals (VDW) and electrostatic interactions (Coulombic), hydrogen bonding, and desolvation.[94, 95] Given proper parameters for the energy function and sampling of the possible conformations, an estimate of the energy landscape could be reconstructed and the lowest energy structure identified as the best prediction.[95] However, this approach has only been successful, to the best of our knowledge, for small single-domain proteins.[93] Larger proteins with multiple domains and/or subunits typically require the use of experimental or large-scale sequence data to construct an accurate model. [95-97]

Protein structural modeling algorithms that rely on potential energy functions and experimental data such as disulfide cross-links as restraints to guide the folding process are referred to as knowledge-based algorithms.[95] These approaches are useful when experimental data is available and when no similar protein sequences with associated structures are available. When sequence data is abundant, a commonly used method for protein structural modeling is referred to as comparative (homology) modeling. Homology modeling predicts the three-

dimensional structure of a protein sequence by threading the structure of a similar sequence that has a known protein structure.[91] This type of modeling assumes that changes in a protein structure occur much slowly than changes in a protein's sequence.[91] In other words, differences in protein sequences will still yield very similar structures.

In this work, we utilized homology modeling to construct models of AcrA that include the missing membrane-proximal domain (MP) from the crystal structure. To build a homology model, the first step is to identify a suitable template. A suitable template is a known protein structure determined from X-ray crystallography or nuclear magnetic resonance (NMR) with a sequence identity of about 25% compared to the sequence that will be modeled.[91, 92] A suitable template should also have secondary structure that agrees with the predicted secondary structure of the sequence. For one of the models (Model A), we used the HHPred web server to identify an adequate template based on sequence identity and secondary structure and then the program MODELLER to build the model.[98, 99] For the second model (Model B), we used an algorithm implemented in the commercial software MOE.[100] With MOE, we chose the crystal structure of ZneB (PDB 3LNN) as a suitable template for one of the models.[101] ZneB is part of a tripartite assembly referred to as ZneCAB that spans the bacterial envelope of *Cupriavidus metallidurans* similar to AcrAB-TolC in *E. coli*.[31, 101] It is also part of the membrane fusion protein (MFP) family like AcrA.[101] ZneCAB is an efflux transporter that is specific for the export of zinc ions.[101] The function of ZneB as

an MFP is analogous to AcrA and has a sequence identity of 27% (**Figure 12**). The structure also matches AcrA by consisting of an α-helical hairpin, lipoyl, β-barrel, and MP domain (**Figure 13**). With HHPred, ZneB was also one of the top choices for a template, but we chose CusB. CusB is also part of a tripartite complex referred to as CusCAB that is responsible for the efflux of heavy metals (silver and copper) and some hydrophilic antibiotics.[26] CusB is an MFP that forms a hexameric funnel and engages in an open-close transition.[26, 102] However, while the function of CusB is similar to AcrA, the sequence identity is only 20%; thus, we built the model with an additional template. The additional template was the partial crystal structure of AcrA that lacks the MP domain (**Figure 13**). The addition of multiple templates in homology modeling can help build more accurate models with low sequence identity.[103] Nevertheless, the sequence identity of the MP domain of CusB and AcrA was only 21% (**Figure 14**). The sequence identity between the MP domains of AcrA and ZneB were 27% (**Figure 14**). While both models contain low sequence identity, they are derived from templates that are functionally similar to AcrA. The functional similarities of CusB and ZneB may explain why the application of both models still led to identification of new efflux pump inhibitors for AcrA. Another possibility could be the incorporation of multiple conformations obtained from MD simulation that will be discussed later.

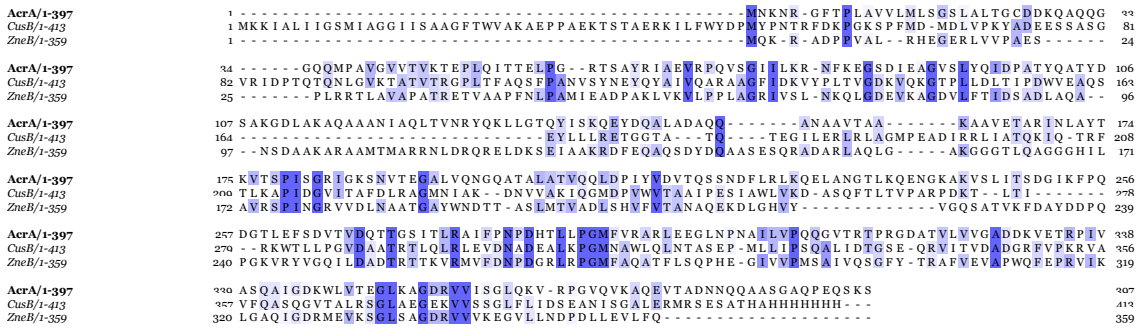


Figure 12. Multiple sequence alignment of the AcrA sequence (NP_414996, K-12 MG1655) with the sequences from the X-ray crystal structures of CusB (PDB 3NE5) and ZneB (PDB 3LNN). The sequence identity between AcrA and CusB and ZneB is 20% and 27%, respectively.

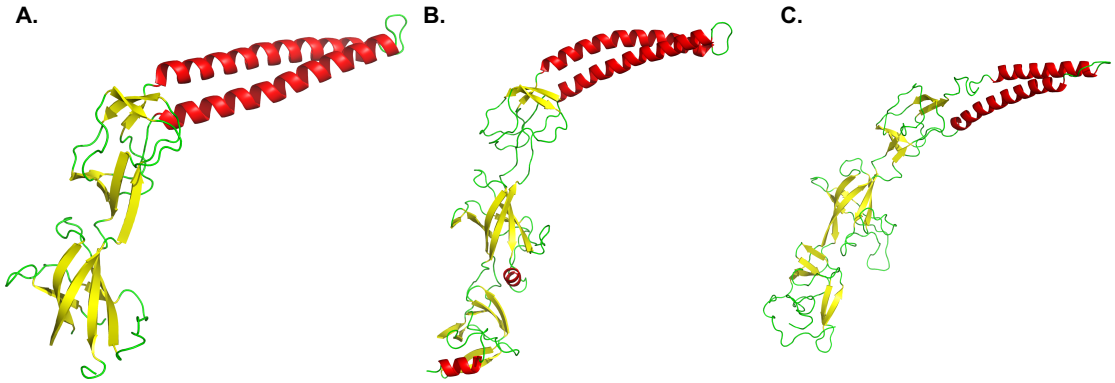


Figure 13. (A) X-ray crystal structure of AcrA (PDB 2F1M) with the missing MP domain. (B) Homology model (Model A) built from CusB and AcrA templates with MODELLER. (C) Homology model (Model B) built from ZneB template with MOE.

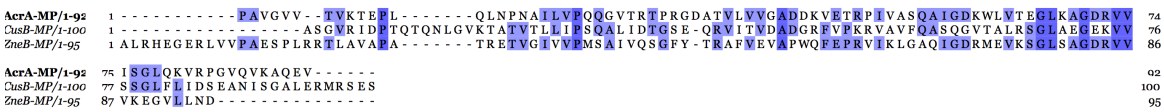


Figure 14. Multiple sequence alignment of the full-length AcrA sequence with the sequences extracted from the MP domains of the X-ray crystal structures of CusB and ZneB. The sequence identity between the MP domains between AcrA and CusB are 21%. The sequence identity between AcrA and ZneB is 27%. The sequence for the MP domain of AcrA was obtained from a later homology model built using a separate template.

Molecular dynamics simulations

Molecular dynamics (MD) simulations is a computational method that can be implemented to optimize initial homology models.[104] Loops and side chains are conformationally more variable than main chain, α-helix, and β-barrel atoms; thus, hindering the accuracy of the initial homology models.[105, 106] Ramachandran plots can be used to visually assess secondary structure elements by the ϕ,ψ angles of the protein backbone and validate the accuracy of a homology model.[91] Angles that do not correspond to a specific secondary structure may exist in disallowed regions and can indicate the presence of a steric clash in the model.[105] Ramachandran plots of the Model B mentioned above reveal a decrease in the number of ϕ,ψ angles in the disallowed regions after a short MD simulation trajectory (**Figure 15**). MD simulation refined Model B and eliminated some steric clashes between atoms. Nevertheless, some disallowed angles remain in Model B after MD simulation in contrast to Model A which revealed no disallowed angles even before MD simulation (**Figure 15**). Model A may be a structurally more reliable model of AcrA than Model B despite having a lower sequence identity. The combination of multiple templates may contribute to the improved modeling. Model B also contains an extended unstructured loop at the β-barrel domain that is absent in Model A (**Figure 13**).

MD simulation propagates the dynamics of a protein by integration of Newton ‘s second law of motion, which states that:

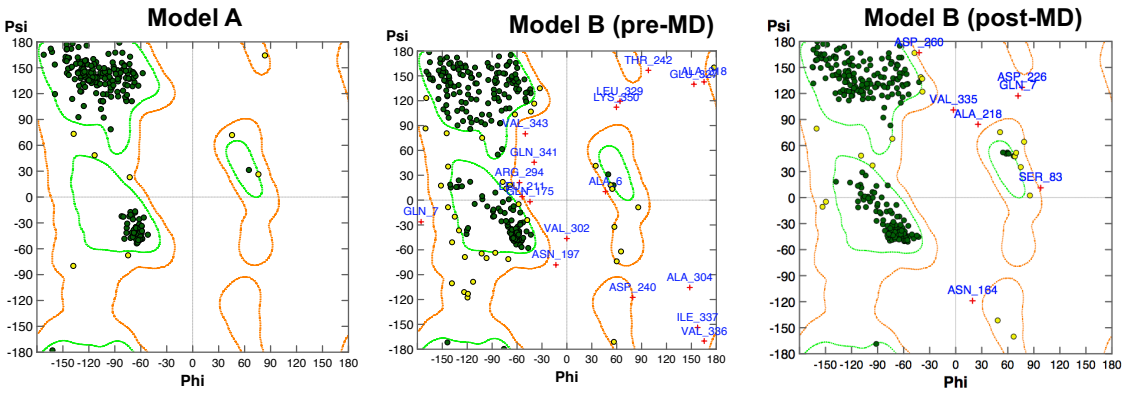


Figure 15. Ramachandran plots of Model A built with a multi-template approach using AcrA and CusB crystal structures and Model B built using a single-template approach using the ZneB crystal structure. Model B contains numerous structural outliers outside of the allowed regions; thus, multiple steric clashes exist. Five nanoseconds of MD simulations resolve some of the clashes, but some remain.

$$F_i = m_i a_i$$

where F_i, m_i, and a_i are the mass, net force, and acceleration of atom i[107] in the protein.[108] The acceleration of atom *i* can be derived by the second derivative of the position of the *i*th atom with respect to time.

$$a_i = \frac{\partial^2 r_i(t)}{\partial t^2}$$

Integration of the acceleration can then yield the positions and velocities of each atom at a defined time interval. Time in MD simulations is discretized by femtosecond units referred to as time steps. Thus, positions and velocities can be updated by various integrators such as the leapfrog algorithm reported below.[109, 110,111]

$$v\left(t + \frac{1}{2}\delta t\right) = v\left(t - \frac{1}{2}\delta t\right) + a(t)\delta t$$

$$r(t + \delta t) = r(t) + v\left(t + \frac{1}{2}\delta t\right)\delta t$$

where the velocities are calculated first from the acceleration of the atom which is taken from the net force. Initial velocities are estimated from a Maxwell-Boltzmann distribution given a target temperature of the simulation.[109] The velocities then play leapfrog to calculate the positions of each atom at a defined timestep. The net force experienced by each atom is derived by the negative gradient of the potential energy

$$F_i = -\nabla U_i$$

where U is the potential energy of the *i*th atom. The potential energy is expressed as a function that encompasses all the bonded and nonbonded components for each atom.[94, 107]

$$U = U_{bonded} + U_{nonbonded}$$

$$U_{bonded} = \sum_{bonds} K_b(b - b_o)^2 + \sum_{angles} K_\theta = (\theta - \theta_o)^2 + \sum_{dihedrals} K_\phi(1 + \cos(n_\phi - \delta)$$

$$U_{nonbonded} = \sum_{coulombic} \frac{q_i q_j}{\varepsilon r_{ij}} + \sum_{VDW} \varepsilon_{ij}[\left(\frac{R_{min,ij}}{r_{ij}}\right)^{12} - 2(\frac{R_{\min,ij}}{r_{ij}})^6]$$

The bonded and nonbonded terms encompass the essence of a molecular mechanics (MM) potential energy function or force field. MM differs from quantum mechanics (QM) by utilizing the Born-Oppenheimer approximation.[112] The Born-Oppenheimer approximates states all the degrees of freedom of the electrons of each atom are relaxed, i.e. in their lowest energy (ground) state configurations. Thus, MD simulations cannot simulate chemical reactions.[112] The bonded terms include 1-2 interactions (bonds), 1-3 interactions (angles), and 1-4 interactions (dihedrals) (**Figure 16**). The bonds and angle terms are represented by a harmonic potential (**Figure 17**) where the equilibrium values (b_0,θ_0) and force constants (K_0, K_θ) are estimated by a best-fit between ab initio quantum mechanical target data and molecular mechanics or through available experimental data (IR, X-ray diffraction, Raman).[94, 113] The dihedral term is represented by a cosine function where n represents the number of minima along the dihedral potential energy

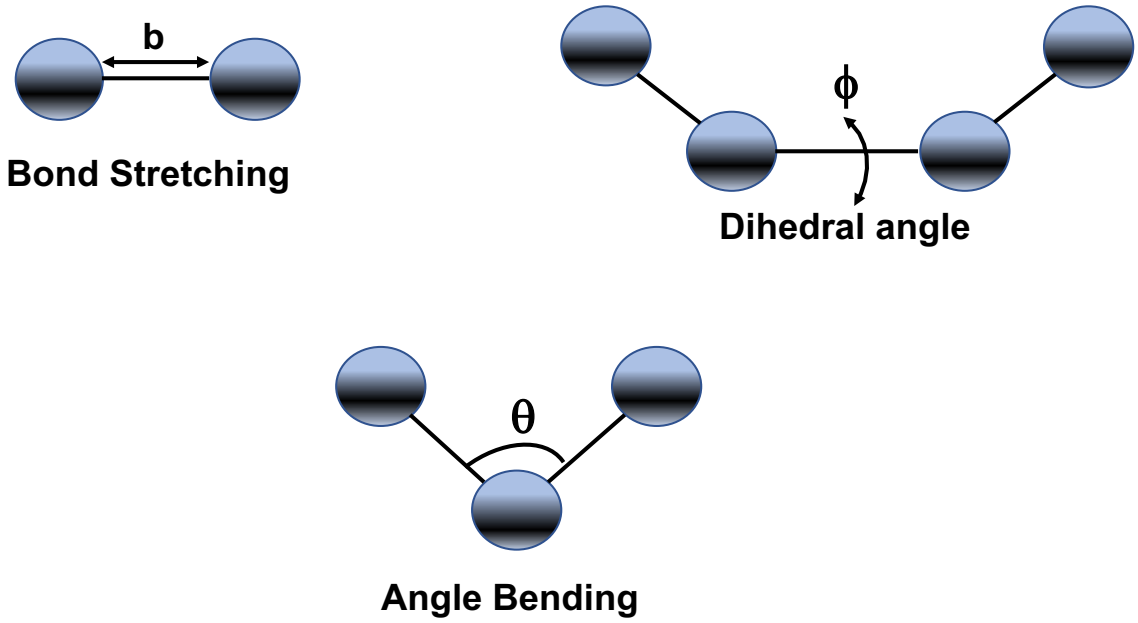


Figure 16. Bonded terms in an MD simulation: bond stretching, angle bending, and dihedral angles. Bonded terms can be characterized as 1-2, 1-3, and 1-4 interactions based on the number of atoms included.

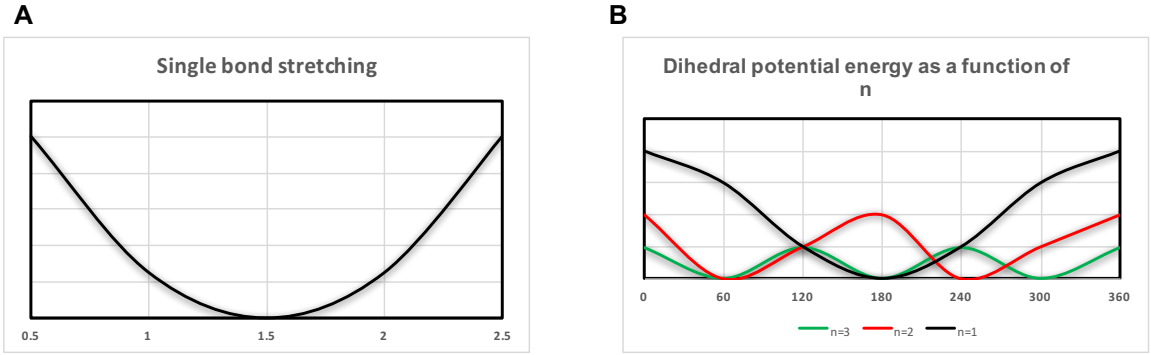


Figure 17. Bonded potential energy profiles (A) Representative harmonic potential bond which has a bond length of 1.54 A. (B) Potential energy profile of a dihedral angle represented by molecular mechanics. The term n represents the number of minima in the profile that can be used to fit QM target data.

surface (**Figure 17**). The nonbonded terms are modeled by a Coulombic and 6-12 Lennard-Jones (L-J) potential. Nonbonded interactions are divided into two subcategories: electrostatic interactions between two charged atoms and van der waals (VDW) interactions.[94] Electrostatic interactions are distance and dielectric dependent. In contrast, VDW interactions are only distance dependent.[114] The medium or solvent where two charges (q_iq_j) interact can be expressed as a constant is referred to as the dielectric constant.[94] For the MD simulations performed of our two homology models and for most proteins, water is the typical solvent and has a dielectric constant of 78.5, but a common water model used in MD simulation overestimates the dielectric constant by about 5-20% (82-96).[115]

The force field and water model used in the short MD simulation trajectories of our two homology models are referred to as CHARMM22 and TIP3P.[69] TIP3P (three-site intermolecular potential) is the most commonly used water model in MD simulation due to computational efficiency.[116] The water model only considers noncovalent interactions between the oxygen and two hydrogen atoms.[115] The interactions and hence polarizability of the lone pairs attached to the oxygen atom are ignored.[117] The negation of polarizability of the oxygen atom in water partially contributes to the incorrect dielectric constant for water in MD simulation.[115] Other reasons include the truncation of VDW and coulombic interactions and the estimation of fixed partial charges from quantum mechanical electrostatic potentials.[118, 119] VDW interactions between two atoms only favorably interact at close enough distances triggered by the effect of an induced dipole.[105] At long

enough distances, the potential energy for a VDW interaction is effectively 0 kcal/mol (**Figure 18**). Thus, MD simulation can use cut-off methods to stop calculating VDW energies past a certain distance. The standard cut-off for MD simulation with the CHARMM force field is 12 Å.[120] However, inclusion of a method referred to as Ewald summation for electrostatics and long-range corrections for VDW energies have been shown to improve the value of the dielectric constant and/or other experimental observables at a greater computational cost.[121] Ewald summation must be performed for accurate electrostatics since the potential energies decay at 1/r and thus a short cut-off produces artifacts (**Figure 18**).[122] More sophisticated water models such as TIP4P and TIP5P and polarizable force fields such as the CHARMM Drude polarizable force field have also been implemented with improved values of the dielectric constant at the expense of increased computational requirements.[117] Nevertheless, despite the systematic failure of the TIP3P water model and nonpolarizable CHARMM force field to accurately reproduce the dielectric constant, both can still reproduce other experimental observables such as heat of vaporization and solvation free energies.[114, 123] Accurate thermodynamic estimates may be due in part to error cancellation from computing energy differences, but the estimates allow us to make a successful trade-off between theoretical rigor and computational efficiency. The MD simulations with the non-polarizable force field and water model not only optimized our homology models, but also showed their interdomain flexibility.

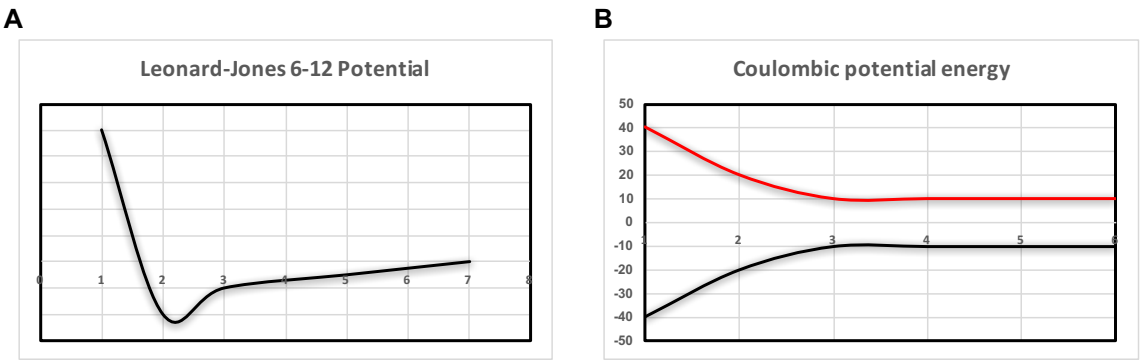


Figure 18. Nonbonded energy profiles in an MD simulation (A) Lennard-Jones 6-12 potential with an attractive energy well and a repulsive component. (B) Coulombic potential which decays at a rate of 1/r.

MD simulation can be used to assess the flexibility of the models. A model that is more flexible over short timescales may indicate less stability (greater tendency to unfold) and thus is a less suitable model for the intended sequence. The methodology is particularly important in the evaluation of potential mutants for site-directed mutagenesis.[124] A common metric used to assess flexibility in MD simulation is the root-mean-square-deviation (RMSD)

$$RMSD = \sqrt{\frac{1}{N}\sum_{i=1}^{N}(d_i)^2}$$

where d_i is the distance between a given atom in a structure and the equivalent atom in a reference structure such as the first frame of the trajectory.[125] Typically, only the backbone or C_α atoms are chosen. The greater the RMSD, the more flexible the model over the timescale of the simulation.[125] The model built with MOE referred to as Model B had a backbone RMSD of approximately 9 Å over the timescale of the simulation (**Figure 19**). The model chosen with HHPred and MODELLER referred to as Model A had a backbone RMSD of 6 Å indicating

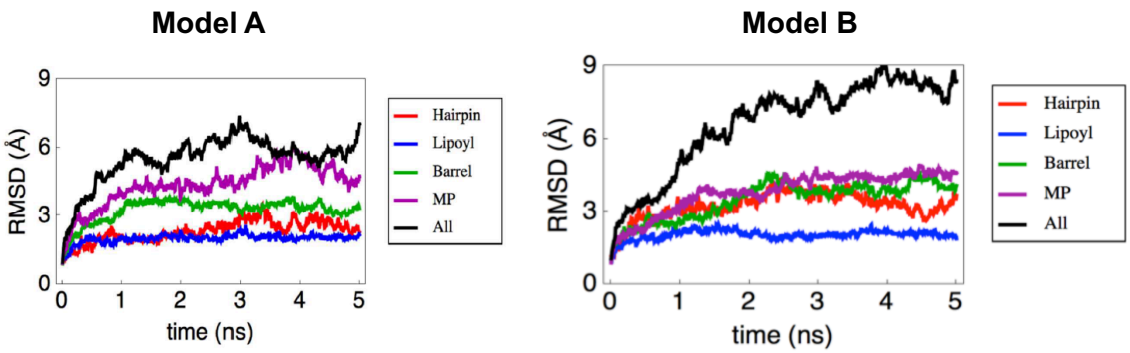


Figure 19. Backbone RMSD of AcrA models and their individual domains over MD trajectories measured relative to the initial coordinates of model A (left) and model B (right).

slightly less flexibility over the short simulation time (**Figure 19**). For both models, the interdomain flexibility was in decreasing order: MP domain, β-barrel, α-helical hairpin, and lipoyl (**Figure 19**). The decreased flexibility of Model A compared to Model B could be due to the use of a multiple templates with one of the templates being the partial crystal structure of AcrA. Greater flexibility in Model B is also in agreement with the poor structural representation observed in the Ramachandran plots (**Figure 15**). The increased flexibility of the MP domain in both models would be expected since the domain was not captured by X-ray diffraction.[78] Also, as discussed previously, conformational changes in the MP domain are known to affect the assembly and stability of the assembled complex.[42]

Backbone RMSD is not only a metric that can be used to assess flexibility, but can be also applied as a clustering algorithm that selects frames from the MD trajectory to construct an optimal ensemble of configurations for each model.[89, 126] We used the clustering tool, *g_cluster*, included with GROMACS 4.6.5 to group all the frames into specific clusters within a cutoff of 2.5 Å and then selected the

centroid structure from each cluster as a conformation in the ensemble.[127] For Model A and B, 12 and 15 conformations were selected, respectively. These conformations were then used as the basis for a form of molecular docking referred to as ensemble-based virtual screening to identify new efflux pump inhibitors for AcrA.

Molecular docking

Molecular docking is used to predict the binding poses of new ligands to specific target such as a protein.[107] Docking is useful for distinguishing between binders and non-binders; thus, helping to infer structure-activity relationships (SAR) and constructing a priority list of compounds to be tested for experimental validation.[126] A docking algorithm consists of two components: sampling and scoring.[107] The most commonly used docking software is the program AutoDock likely due to its speed, ease of use, and open-source platform.[128] Also, when multiple docking algorithms are compared to experimental data, AutoDock Vina consistently appears as one of the best algorithms.[129] AutoDock Vina was significantly optimized from previous versions of AutoDock and was found to have improved agreement with crystallographic poses and experimental binding affinities.[130]

Vina begins from a random initial conformation and position in a pre-defined grid or search space.[107, 131] The search space can be an experimentally known binding site or predicted by various algorithms.[130] A single docking run consists of a series of sequential steps that consist of a random perturbation of the ligand

position. The precise number of steps is determined on-the-fly by Vina depending on the size of the grid and the flexibility of the ligand. Larger grids and more flexible ligands will require more steps (i.e. more positions to perturb).[130] Each step is then assigned a score, an estimate of the protein-ligand binding free energy, and the gradient of the score with respect to the position is computed until no change in the gradient is detected.[107] A gradient of 0 or close to zero would indicate that the resulting pose is at a minimum on the free energy landscape.[112] The pose is accepted in a protocol analogous to a metropolis Monte Carlo (MC) algorithm.[130] If the energy of the pose is improved (lower) from the previously accepted pose, then the new pose is accepted. If not, then the pose is accepted per a probability set by the metropolis criterion. For the sake of simplicity, the original implementation of the metropolis criterion is shown below:

$$Prob \sim \exp\left[\frac{-(E_1 - E_0)}{k_B T}\right]$$

where E_1 and E_0 and the new and previous energies, respectively, k_B is the Boltzmann constant, and T is the temperature.[107] Vina uses a stochastic global optimization protocol that can be considered a variant of the metropolis criterion and MC method.[130, 132] The use of a metropolis MC algorithm helps to ensure that accepted poses are not trapped in a local minimum; thus, only global minima are accepted.[133] The resulting accepted poses are then ranked for a given ligand. The number of docking runs that Vina implements can be tuned by the user through a parameter referred to as the exhaustiveness.[134] The default exhaustiveness is 8 and was used for all docking calculations described in this chapter.[134] Larger boxes

and more flexible ligands likely require a higher exhaustiveness at the expense of more computational time providing a hindrance for screening large databases of compounds. [130]

The scores that define the estimated free energies of each pose of the ligand bound to the protein in Vina are based on empirical weights to estimate intermolecular (protein and ligand) and intramolecular (ligand and protein alone) contributions of the estimated binding free energy of the predicted pose.[130, 135] The estimated weights consist of terms that define the shape of a given pose in the binding site, hydrophobic interactions, desolvation, and hydrogen bonding.[130] Vina is thus based on the concept that a protein-ligand complex should form a complementary shape. For example, a pose that results in a steric clash with no hydrophobic or hydrogen bonding interaction may have an unfavorable score and likely not be accepted by the Vina algorithm. The empirical weights were determined using linear regression of the PDBBind training set containing 190 protein-ligand complexes with experimentally known binding affinities. [130]

In contrast to Vina, a previous implementation of AutoDock used an MM potential energy function that consisted of a Coulombic term for electrostatics, an L-J 6-12 potential for VDW interactions, a separate 6-12 potential to specifically describe hydrogen bonding, and a desolvation term.[135] The sampling algorithm was also not related to MC, but referred to as a Lamarckian genetic algorithm.[131] It is interesting to note that the introduction of a non-physics based scoring function led to improved agreement with experimental data.[130] This trend is also true for

many other empirical docking algorithms and may be indicative of a move that could pave the way for more machine learning/deep learning algorithms to predict protein-ligand binding affinities.[129]

Vina always incorporates the flexibility of the ligand, but flexibility of side chains within the chosen binding site or search space can be selected by the user.[130] It is estimated that docking algorithms predict the incorrect binding pose for approximately 50-70% of all ligands when only a single protein receptor conformation is considered.[136] Inclusion of side chain flexibility increases the computational cost which can hinder large-scale screening of chemical databases and requires knowledge of the binding site.[126] In our case for AcrA, we predicted two possible binding sites that will be discussed below to dock 1,563 compounds from the NCI Diversity Set V; thus, an alternative method to incorporate receptor flexibility was needed.

An alternative method is referred to as ensemble docking or the relaxed complex scheme.[137] The method incorporates receptor flexibility within AutoDock Vina by docking each ligand to multiple conformations obtained from RMSD clustering of a short MD simulation trajectory of the protein.[138] Conformations extracted from a 2 ns simulation have been shown to identify new ligands and a novel binding site not observed in crystal structures.[139] A quantitative metric to assess the impact of multiple conformations on docking success is called enrichment.[126] The enrichment is defined by the following equation:

$$Enrichment = \frac{\#\ of\ binders\ in\ a\ subset}{total\ \#\ of\ ligands\ in\ subset}$$

where a subset is defined as a part of the total screening database that is ranked according to the scoring function.[126] The inclusion of multiple conformations allows for a sampling of local (side chain) conformations and thus mimic a conformational selection and/induced fit model of ligand binding.[126, 140] A parallelized version of AutoDock Vina referred to as VinaMPI was constructed to parallelize the ensemble docking of multiple conformations to a database of potential ligands on petascale supercomputers.[138] We implemented VinaMPI in all docking calculations presented in this chapter.

We docked the 1,563 compounds from the NCI Diversity Set V because the compounds are freely available for experimental testing and previous work has been involved in repurposing FDA-approved drugs such as chemotherapeutics as new antibiotics.[141] We identified two potential binding sites as search spaces for docking runs referred to as the hinge and MP sites (**Figure 20**). The latter has been discussed previously to play a role in the assembly of the pump and in the interactions between AcrA and AcrB, but the functional relevance of the former, the hinge site, has been unclear.[42] Previous MD simulations of a close homolog of AcrA, MexA in *P. aeruginosa*, has revealed a hinge-bending motion between the lipoyl and α-helical hairpin domain.[125] We showed that the residue E67 when mutated to arginine and alanine decreases the MIC of novobiocin and erythromycin, substrates of AcrAB-TolC, compared to the WT indicative that the efflux of both antibiotics has been impaired (**Figure 21**). A smaller search space was used for the hinge site due to the functional relevance.

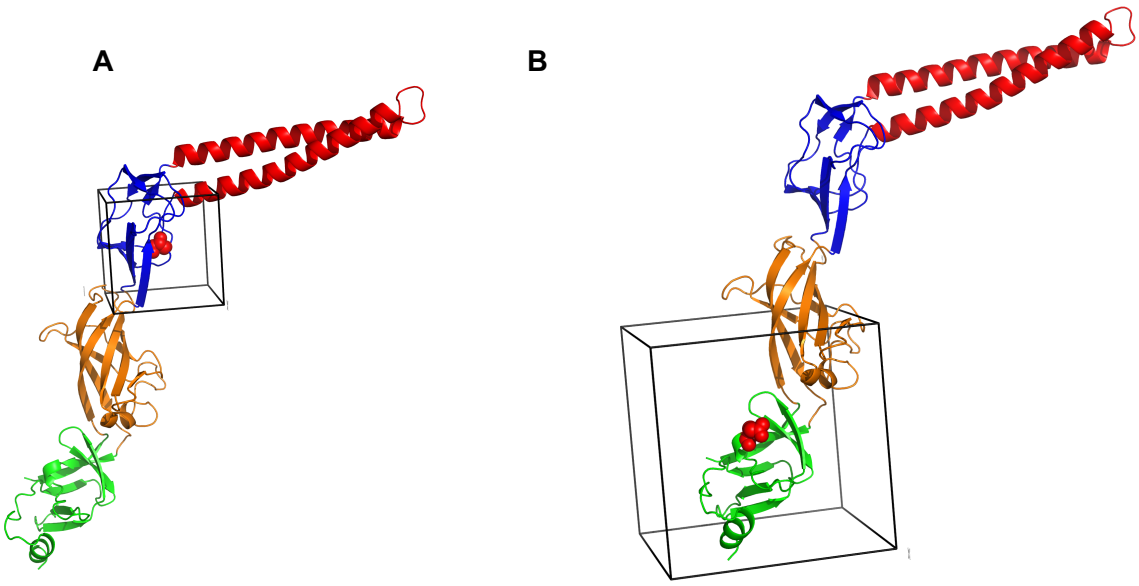


Figure 20. (A) Docking search space with dimensions 25 Å x 25 Å x 25 Å for the hinge site. The center of the box is shown as red spheres and represents the C_α atom of Ser138. (B) Docking search space with dimensions 45 Å x 45 Å x 45 Å for the MP site. The center of the box is shown as red spheres and represents the C_α atom of Gln270. The α-helical hairpin, lipoyl, β-barrel, and MP domains are shown in red, blue, orange, and green, respectively.

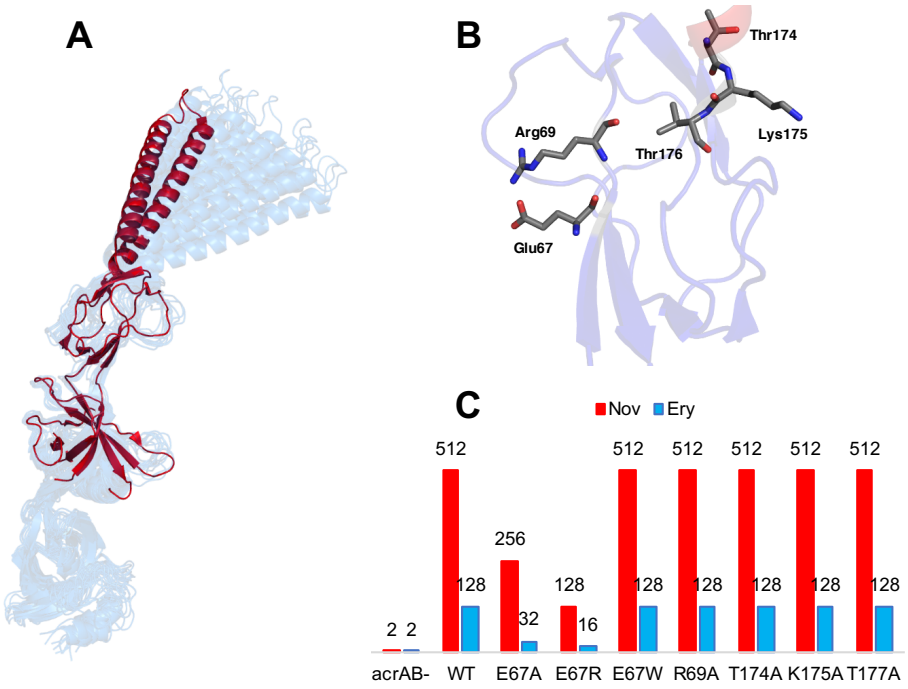


Figure 21. (A) Conformations extracted from MD simulation of Model A and overlaid with the X-ray crystal structure (red) of AcrA to reveal a hinge-bending motion at the lipoyl-hairpin interface. (B) Residues located at the hinge site. (C) Susceptibility assay to novobiocin with WT AcrA and mutants at the hinge site reveal the functional relevance of the site.

In contrast, the entire MP domain was searched centered just above the interface between the β-barrel and MP domain and covered the entire domain (**Figure 20**). The precise binding site at the MP domain will be explored in the following chapter.

Docking to both sites identified 11 compounds that potentiate novobiocin and erythromycin (**Table 1**). The application of multiple conformations in our virtual screening accelerated the identification of the 11 compounds. The top 1-2% of compounds in the ranked database have a ~10% increase, enrichment, in the identification of the 11 compounds when one or more of the conformations from MD are used for the hinge and MP sites in contrast to the initial homology models and the crystal structure (**Figure 22-23**). Enrichment reveals that ensemble-based virtual screening was helpful in the identification of new compounds with efflux pump inhibitor (EPI) characteristics.

To determine if the 11 compounds have EPI-like characteristics and interacts with AcrA, they should ideally possess the seven qualities mentioned previously and bind with AcrA. Seven out of 11 compounds were determined to bind AcrA by surface plasmon resonance (SPR) (**Figure 24**).

Table 1. Minimal Inhibitory Concentrations and Potentiating Activities of Top Hits

	MIC WT μM	MIC WT-Pore μM	MIC ΔTolC μM	MIC ΔTolC-Pore μM	MPC4 NOV μM	MPC4 ERY μM	Potentiation in ΔTolC Pore?	AcrA Binder?
NSC60339	>200	200	12.5	12.5	25	12.5	none	yes
NSC227186	>50	25	6.25	3.13	6.25	3.13	none	yes
NSC33353	200	100	12.5	12.5	1.56	3.13	none	yes
NSC305798	50	25-50	25	12.5	12.5	3.13	none	yes
NSC50651	>50	3.13	6.25	0.8	1.56	6.25	none	yes
NSC354844	>100	6.25	50	6.25	1.56	none	none	yes
NSC207895	25	6.25	25	12.5	0.78	1.56	none	yes
NSC260594	>50	3.13	0.8	0.1	0.39	3.13	yes	no
NSC325014	25	3.13	12.5	3.13	3.1	0.39	none	no
NSC56410	12.5	3.13	1.56	1.56	0.39	none	yes	no
NSC26980	3.13	3.13	0.19	0.19	0.39	0.39	yes	no

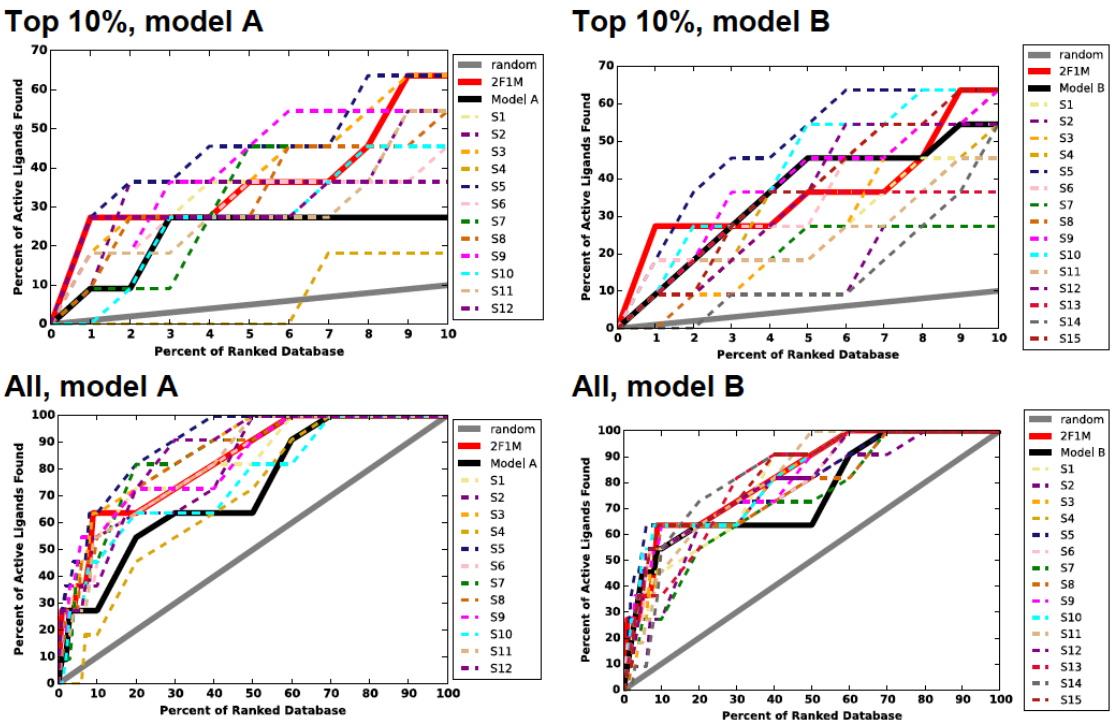


Figure 22. Enrichment profile for ensemble-based virtual screening at the hinge site to AcrA crystal structure (red), homology models (black), and each configuration from MD simulation (dotted).

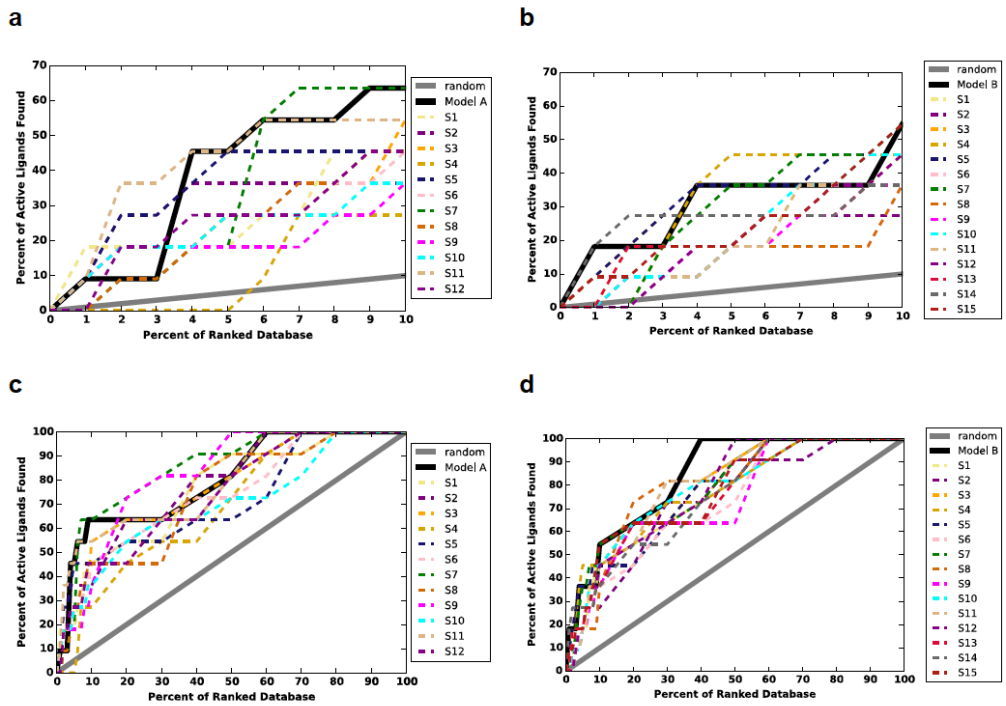


Figure 23. Enrichment profile for ensemble-based virtual screening at the MP site to the homology models (black) and each configuration from MD simulation (dotted).

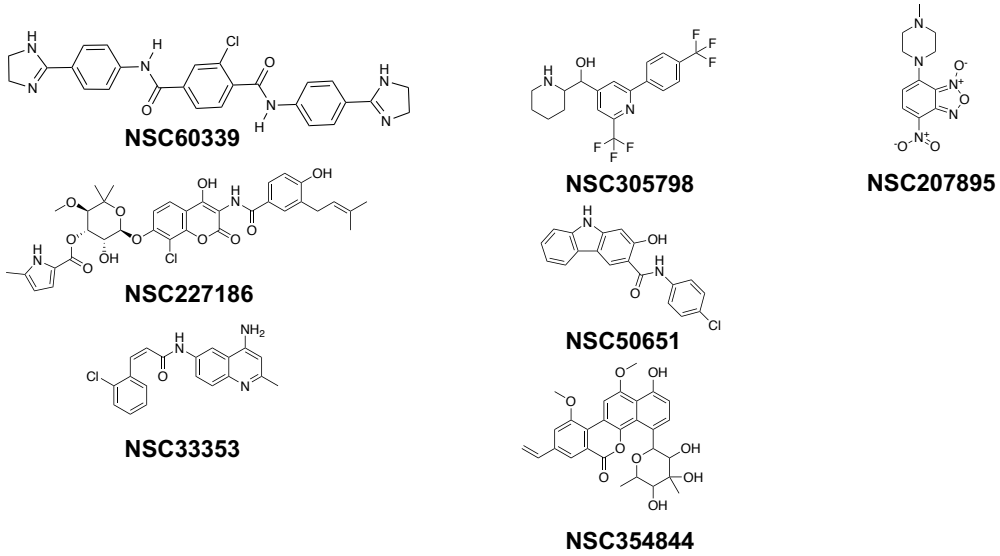


Figure 24. Seven compounds that bind AcrA with EPI-like characteristics.

As a reminder, the characteristics of an EPI are as follows.[61, 62]

i) bypass the OM permeability barrier
ii) potentiate efflux pump substrates
iii) No potentiation of substrates in ΔTolC cells
iv) Inhibits efflux and thus increases the uptake of substrates in the cell
v) No disturbance of proton gradient across the inner membrane
vi) No antibacterial activity
vii) No potentiation of non-substrates.

None of the 7 compounds can bypass the OM permeability barrier (**Table 1**). The MIC values of the remaining compound are lower in WT-Pore cells compared to WT indicating greater susceptibility in WT-pore cells (**Table 1**). WT-pore cells contain 2.4 nm pores in the OM that increase the porosity and thus allow a more diverse array of compounds to enter the OM and interact with periplasmic targets such as AcrA.[142] Once a compound is identified to potentiate and bind AcrA, analogs can later be constructed to improve accumulation in WT cells. Six of the 7 compounds potentiate both efflux pump substrates novobiocin and erythromycin and all 7 lack potentiation in efflux-deficient, ΔTolC, cells (**Table 1**). Potentiation is monitored by the minimal potentiating concentration (MPC_n) of the EPI that causes the minimal inhibitory concentration (MIC) of the antibiotic to decrease at least n-fold. In our case, n is 4. The lower the MPC_4, the greater the potency. As an example, the lowest MPC_4 value for an EPI of AcrAB-TolC is near zero at 0.05 μM.[61] NSC354844 lacks potentiation of erythromycin (**Table 1**). All the compounds contain very weak intrinsic antibacterial activity with MIC values less than 200 μM and disruption of the proton gradient was not assessed (**Table 1**). The higher the

MIC value, the weaker the antibacterial activity. A MIC value indicated as “>200” as effectively no antibacterial activity. Potentiation of non-substrates was not assessed likely because of the compounds’ intrinsic antibacterial activity. The compounds likely act on other targets to inhibit the growth of *E. coli*. All 7 compounds except NSC354844 and NSC207895 are substrates of AcrAB-TolC which implies that they also bind AcrB and are subject to efflux (**Table 1**). The MIC values decrease in WT ΔTolC-Pore cells (**Table 1**). The ability to function as substrates for 5 of the 7 compounds may indicate that these compounds interact with other transporters in *E. coli* such as AcrDA-TolC and AcrEF-TolC. Four of the seven compounds: NSC60339, NSC227186, NSC33353, and NSC305798 were chosen for further characterization to test their ability to increase the accumulation of Hoechst H33342 probe, an AcrAB-TolC substrate, their spectrum of activity in other Gram-negative bacteria, and their mechanisms of action. The remaining three compounds were excluded because they were ranked lower in the docking calculations for at least one site (**Table 2**). However, all three compounds could be re-examined to further elucidate their mechanism of action and efflux inhibition despite being low in the ranked database for at least one of the sites. NSC207895 binds AcrA, has sub-micromolar MPC_4 values for novobiocin and erythromycin, and is not a substrate of AcrAB-TolC (**Table 1**). NSC354844 is also a non-substrate of AcrAB-TolC and could be of interest despite lacking potentiation in erythromycin (**Table 1**). NSC50651 has the same EPI-like characteristics and shortcomings as the four chosen inhibitors, but has the sub-micromolar MPC_4

Table 2. Percentage rank of top hits from virtual screening of hinge and MP sites

Ligand	Top Hinge Rank	Top MP Rank
NSC60339	1.5%	5%
NSC227186	0.5%	2%
NSC33353	10%	5.5%
NSC305798	10%	2%
NSC50651	10%	10%
NSC354844	5%	20%
NSC207895	50%	50%
NSC260594	5%	2.5%
NSC325014	40%	60%
NSC56410	20%	70%
NSC26980	40%	60%

values for novobiocin and erythromycin (**Table 1)**. Nevertheless, all three compounds have greater intrinsic antibacterial activity than the four chosen for further characterization diminishing their ability to function as unique EPIs.

Novel mechanism of action for NSC60339

Three of the four chosen inhibitors successfully satisfy criterion number 4 by increasing accumulation and thus inhibiting efflux as measured by fluorescence of the AcrAB-TolC substrate and fluorescent probe Hoechst H33342. NSC227186 also known as clorobiocin is intrinsically fluorescent and thus could not accurately be tested. Since NSC227186 is also a substrate, it may be a competitive inhibitor for AcrAB-TolC. The binding of AcrA may not be the primary mechanism of action for NSC227186. For NSC60339, the fluorescence of Hoechst H33342 increases and plateaus at 3X the initial rate of uptake in the absence of the inhibitor in WT-pore cells (**Figure 25**). WT-pore contains a functional AcrAB-TolC complex; thus, fluorescence should only slowly increase in contrast to ΔTolC cells. ΔTolC cells

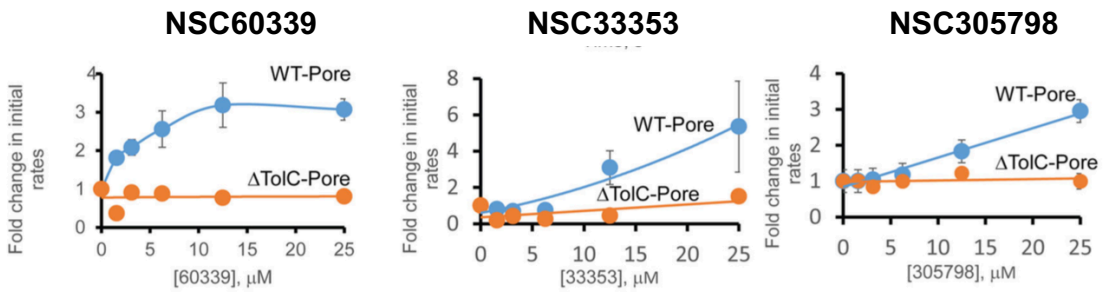


Figure 25. Hoechst H33342 fluorescence accumulation and efflux inhibition assays for NSC60339, NSC33353, and NSC305798 in WT-Pore and ΔTolC cells.

show no change in initial rate of uptake for NSC60339 and NSC305798 as fluorescence increases equally as rapid with and without the inhibitor (**Figure 25**). Both NSC33353 and NSC30598 in WT-Pore cells increase fluorescence linearly in contrast to NSC60339 and the slope of Hoechst H33342 uptake in ΔTolC cells is positive for NSC33353 (**Figure 25**). If fluorescence is increasing in the presence of NSC33353 in ΔTolC cells, it likely means that NSC33353 has additional interactions in bacteria (**Figure 25**). In fact, when we compare the spectrum of activity of NSC33353 and NSC60339 across five different bacteria: *Escherichia coli*, *Pseudomonas aeruginosa*, *Acinetobacter baumannii, Enterobacter cloacae, and Klebsiella pneumoniae*, we see that NSC33353 potentiates novobiocin and erythromycin in all of them except *Pseudomonas aeruginosa* (**Table 3**). On the other hand, inhibition by NSC60339 appears to be specific for *E. coli* (**Table 3**). The MPC_4 values for NSC60339 are higher than previously shown due to OM impermeability.

NSC60339 is also the only discovered compound to change the structure of AcrA in vivo in the assembled complex. Proteolysis by trypsin cleaves the C-

Table 3. Spectrum of activity for NSC60339 and NSC33353

	MIC, μM		MPC_4 NOV, μM		MPC_4 ERY, μM	
Bacteria	NSC60339	NSC33353	NSC60339	NSC33353	NSC60339	NSC33353
E. coli	>200	200	100	25	50	25
P. aeruginosa	>100	>100	>100	>100	>100	>100
A. baumannii	>100	>100	>100	6.25	>100	50
E. cloacae	>100	>100	>100	25	>100	25
K. pneumoniae	>100	>100	>100	12.5	>100	12.5

terminus of lysine and arginine residues when they are exposed to water. In the absence of NSC33353, NSC305798, NSC227186, and NSC60339, two proteolytic fragments are present (**Figure 26**). The two fragments are K46-K396 which represents the complete protein and K46-R296 which represents the α-helical hairpin, lipoyl, and β-barrel domains. In the presence of NSC60339, a new fragment, K46-K346, is present. K346 is in the MP domain (**Figure 26**). The binding of NSC60339 to AcrA changes the structure of the MP domain that exposes K346 to water for cleavage by trypsin. Previous EPIs MC-207,110 and MBX2319 do not change the structure of AcrA (**Figure 26**).

NSC60339 is also the only discovered compound to change the structure of AcrA in vivo in the assembled complex. Proteolysis by trypsin cleaves the C-terminus of lysine and arginine residues when they are exposed to water. In the absence of NSC33353, NSC305798, NSC227186, and NSC60339, two proteolytic fragments are present (**Figure 26**). The two fragments are K46-K396 which represents the complete protein and K46-R296 which represents the α-helical hairpin, lipoyl, and β-barrel domains. In the presence of NSC60339, a new fragment, K46-K346, is present. K346 is in the MP domain (**Figure 26**). The binding of NSC60339 to AcrA changes the structure of the MP domain. Previous EPIs MC-207,110 and MBX2319 do not change the structure of AcrA (**Figure 26**).

Structure-activity relationship of NSC60339

To improve the potentiation of AcrAB-TolC substrates such as novobiocin by an

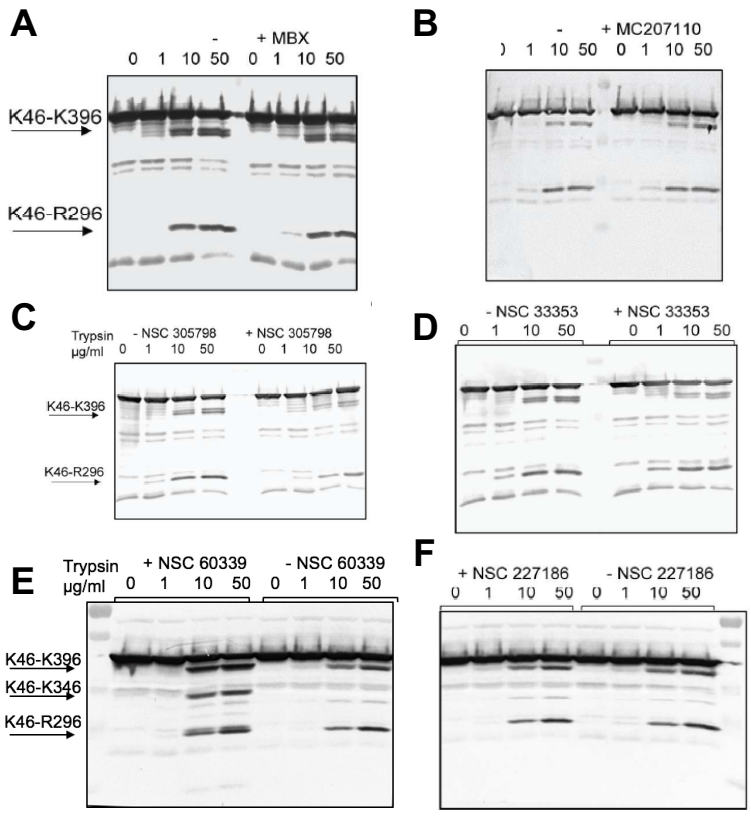


Figure 26. In vivo proteolysis with trypsin for MBX2319 (A), MC-207,110 (B), NSC305798 (C), NSC33353 (D), NSC60339 (E), and NSC227186 (F) revealed that NSC60339 has a novel mechanism of action.

EPI, a structure-activity relationship (SAR) needs to be derived. A SAR is the identification of correlations between different parts of a drug's structure with biological activity.[65] For NSC60339, we compared the modification of the structure with MPC_4 values for novobiocin to assess the impact of the structure on the potentiation of substrates. We began our SAR by examining the best-scoring docking pose for NSC60339 to the hinge site of AcrA. Docking suggested that the dihydroimidazoline ring could form interactions with the backbone carbonyls of A172 and I65 (**Figure 27**). The chloro group was also found to oriented towards V176, a hydrophobic residue; thus, modification of this group may impact potentiation (**Figure 27**). Moreover, we predicted the pK_a of the sp^2 nitrogen to be 9.84 for the dihydroimidazoline ring acting as a meta substituent to the central ring and 9.24 for the same nitrogen as the ortho substituent to the central ring with the software ChemAxon Marvin 16.7.11 (**Figure 28**).[143] The pK_a is estimated from the acid dissociation constant, shown below, and is a measure of a functional group's tendency to donate or accept a proton.[105]

$$\mathrm{pK_a} = -\log(K_a)$$

$$K_a = \frac{[H^+][A^-]}{[HA]}$$

A^- is the concentration of the conjugate base of the dissociated species in solution. The Henderson-Hasselbach equation states,

$$pH = pK_a + \log\left(\frac{[A^-]}{[HA]}\right)$$

that when the pH of the solution is less than the pK_a of the ionizable atom, the atom

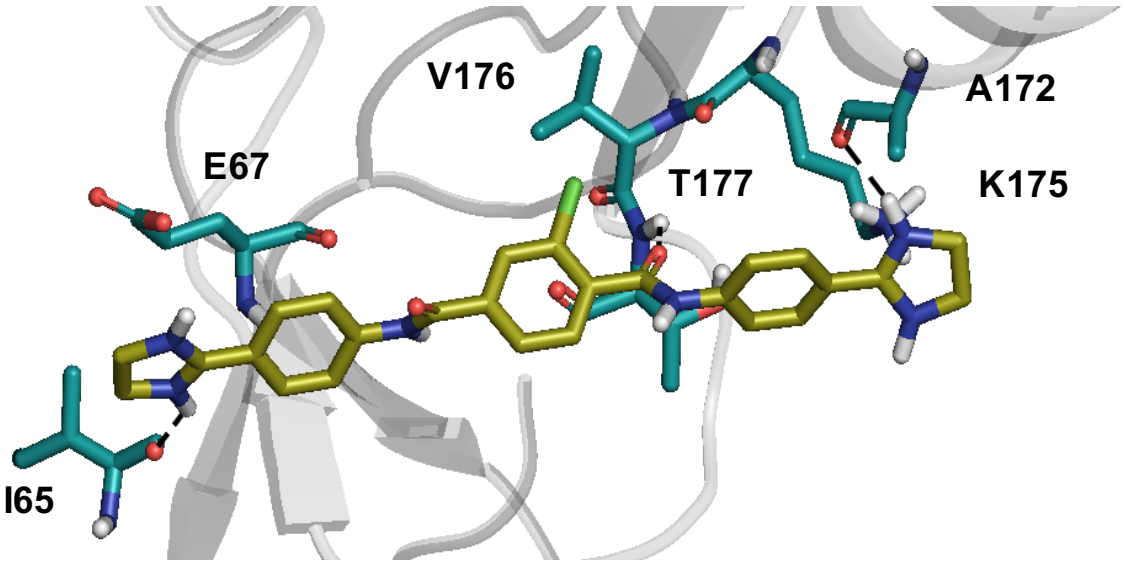


Figure 27. Best-scoring docking pose of NSC60339 to AcrA at the hinge site.

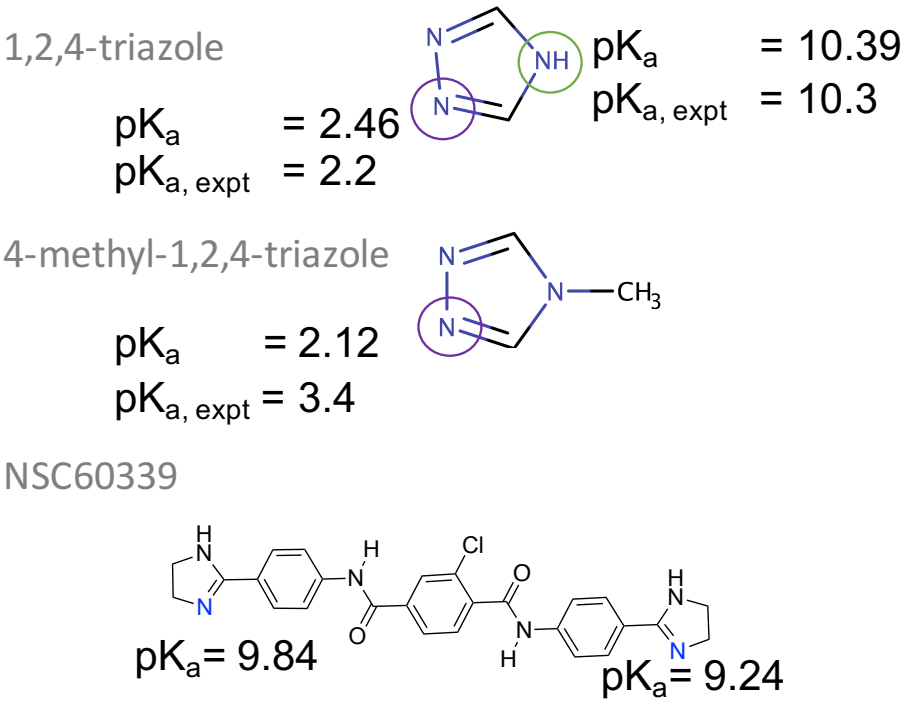


Figure 28. Predicted and experimental pK_a values for 1,2,4 triazole and 4-methyl-1,2,4 triazole. Predicted pK_a values for the dihydroimidiazoline rings of NSC60339. All predictions were carried out with ChemAxon Marvin 16.7.11.

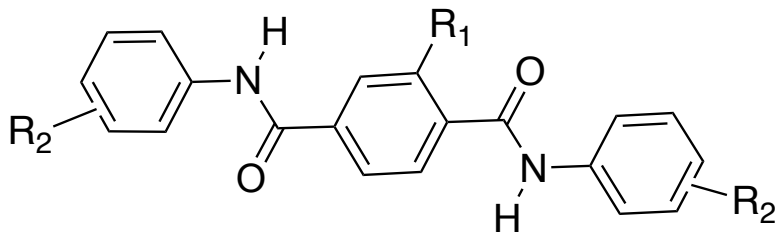
will be protonated.[105] Conversely, when the pH is greater than the pK_a, the atom will be deprotonated. The pH is a measure of the concentration of dissociated protons in solution:

$$pH = -\log(H^+)$$

thus, a solution with a low pH is more effective at donating protons to molecules such as NSC60339.[105] The predicted pK_a values for the dihydroimidazoline are greater than a standard pH solution of 7; thus, the dominant chemical species of NSC60339 should be di-cationic and be identified as dihydroimidazolium rings. To validate our predictions, we predicted the pK_a of two similar rings with known experimental pK_a values: 1,2,4 triazole and 4-methyl-1,2,4 triazole (**Figure 28**). 1,2,4 triazole has an experimental pK_a values of the nitrogens of 2.2 and 10.3(**Figure 28**).[144] The predicted pK_a values by ChemAxon Marvin are 2.46 and 10.39, respectively. 4-methyl-1,2,4 triazole has an experimental pK_a of 3.4 and a predicted pK_a of 2.12 (**Figure 28**).[144] The predicted values are close to the known experimental values; thus, we should be able to trust with reasonable accuracy that NSC60339 is di-cationic in solution.

As mentioned previously, the docking pose of NSC60339 at the hinge site reveals hydrogen bonding interactions with the dihydroimidazolium rings (**Figure 27**). Complete replacement of the dihydroimidazolium rings with groups such as hydoxymethyl, cyano, and sulfonic acid resulted in a loss of potentiation as measured by a higher MPC_4 value compared to NSC60339 (**Table 4**). Sulfonic acid is negatively charged which would result in electrostatic repulsion with E67 if

Table 4. Potentiation due to modification of the dihydroimidazoline and central ring.



Compound	R_1	R_2	MPC_4 NOV
NSC60339	-Cl	4, 	25
4a	-Cl	4, -CN	>400
4b	-Cl	3, -CN	>400
4c	-Cl	4, $-CH_2OH$	>200
4d	-H	4, $-SO_3H$	>100
9a	-H	3, 	50
9b	-H	4, 	50
9c	-F	4, 	100
9d	-Br	4, 	50
9e	$-NO_2$	4, 	25
9f	$-CH_3$	4, 	25

binding occurs at the hinge site. The basic nitrogen in the dihydroimidazolium ring acting as a hydrogen bond donor appears to be required for potentiation. When the dihydroimidazolium ring was shifted from a para (1,4) to a meta (1,3) position, only a 2-fold increase in MPC_4 was observed (**Table 4**). We then speculated that only a single dihydroimidazolium ring is needed for potentiation. We identified a lower scoring pose of NSC60339 at the hinge site in which only one dihydroimidazolium ring is interacting at the hinge site (**Figure 29**). The lower-scoring pose has a score of -5.8 kcal/mol while the best-scoring pose has a score of -7.8 kcal/mol, a difference of 2 kcal/mol. The training set of AutoDock Vina has a standard error of 2.85 kcal/mol compared to the experimental binding affinities; thus, a difference of 2 kcal/mol is insignificant in terms of docking calculations.[130]

Four compounds with one dihydroimidazolium ring were found to exhibit improved permeability, accumulation of Hoechst H33342, and equal or improved potentiation of novobiocin (**Table 5**). Two of the compounds (17h and 17i) contain halo substituents, chlorine and bromine, on a benzene ring ortho (1,2) to the dihydroimidazolium ring (**Figure 30**). The other two compounds (17o and 17p) contain hydrophobic alkyl groups para (1,4) to the dihydroimidazolium ring (**Figure 30**). Further SAR analysis revealed that replacement of the central ring in NSC60339 with an additional chloro, a nitro, methyl, and a bromo had similar MPC_4 values (**Table 4**). It was only when a fluorine was used that a loss of potentiation

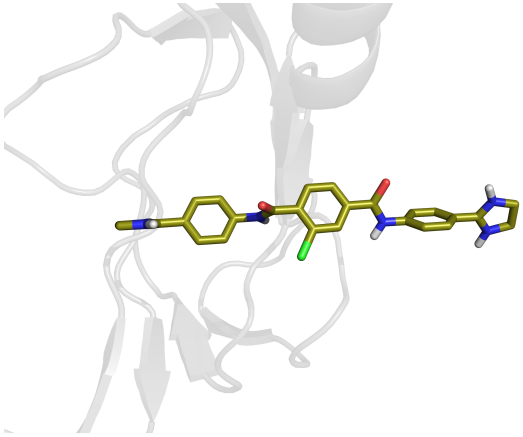


Figure 29. Lower scoring docking pose of NSC60339 at the hinge site with only one dihydroimidazolium ring interacting with AcrA.

Table 5. Four compounds with equal or improved EPI characteristics relative to NSC60339.

Compound	MPC_4 NOV μM	WT MIC / WT-Pore MIC	WT-Pore MIC / WT-Pore ΔTolC MIC	Hoechst H33343 uptake rate	WT-Pore MIC / WT-Pore + NOV MIC	WT-Pore MIC / WT-Pore + ERY MIC
NSC60339	25	4	8	3.2	16	8
17h	25	1	4	9.7	32	8
17i	50	1	8	11.6	32	32
17o	50	2	2	6.3	8	8
17p	12.5	1	2	2.6	2	2

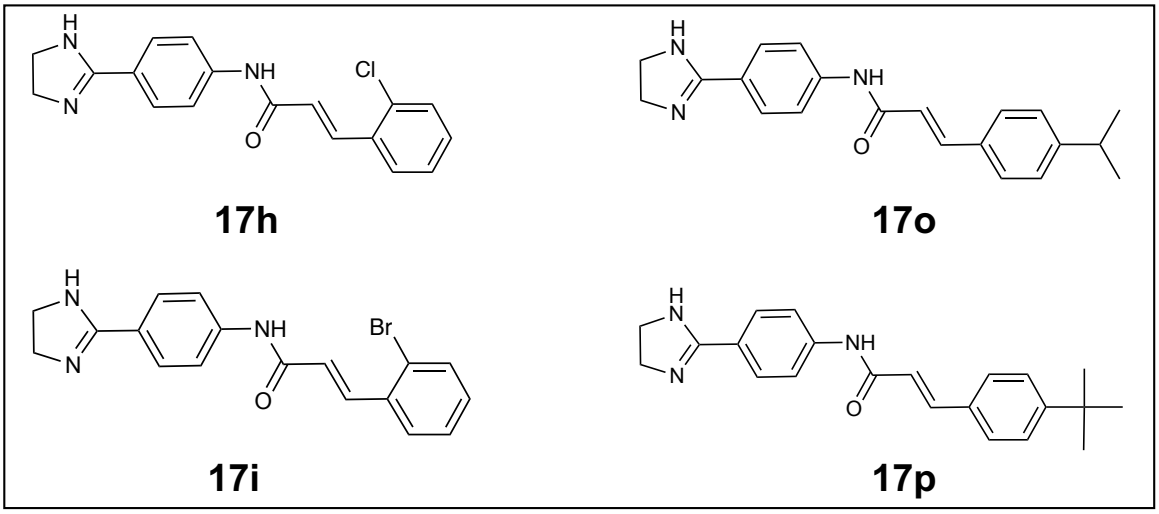


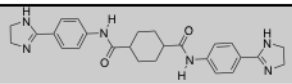
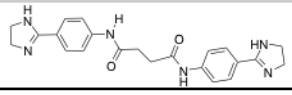
Figure 30. Four analogs with improved OM permeability, Hoechst H33342 uptake, and equal or improved potentiation of novobiocin compared to NSC60339 was observed (**Table 4**).

was observed (**Table 4**). In addition, removal of the central phenyl ring for a more conformationally flexible cyclohexyl ring or an acyclic core resulted in a loss of potentiation (**Table 6**).

Compounds 17h,17i, 17o, and 17p had lower WT MIC / WT-Pore MIC ratios than NSC60339 resulting in improved permeability (**Table 5**). Three of the compounds also had lower ratios of MIC WT-Pore / MIC WT-Pore-ΔTolC cells indicating that the compounds were less susceptible to efflux as an AcrAB-TolC substrate and possessed less antibacterial activity (**Table 5**). Three of the 4 compounds also had improved uptake or accumulation of Hoechst H33342 and equal or greater potentiation of novobiocin or erythromycin (**Table 5**). NSC60339 in addition to 17h and 17o were also found not disrupt the proton gradient across the inner membrane (**Figure 31**). This was previously not assessed at the time Table 1 was compiled. Valinomycin is an antibiotic that is known to disrupt electrochemical gradients; thus, it served as a useful control to assess disruption of the proton gradient across a membrane. [145]

The four new compounds have an increased rigidity (fewer rotatable bonds), more amphiphilic (hydrophobic and hydrophilic groups), and possess low globularity (long, planar) (**Table 7**). These properties correlate with compounds

Table 6. Removal of central aromatic ring results in loss of potentiation.

Compound	Structure	MPC_4 NOV μM
11		>400
13		>400

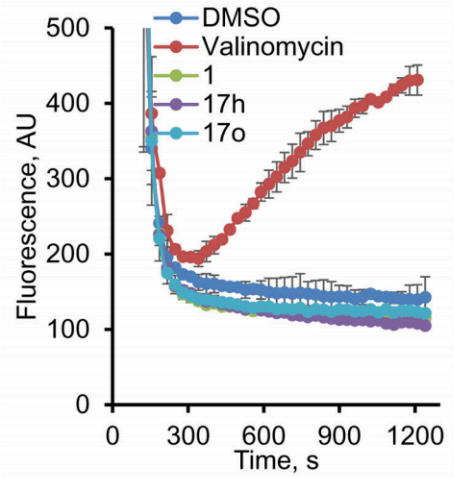


Figure 31. NSC60339 (1), 17h, and 17o do not disrupt the transmembrane potential that mimics the proton relay across the inner membrane. Valinomycin was used as a control.

Table 7. Structural Descriptors for NSC60339 and 4 analogs with improved EPI characteristics

Compound	# primary amines	# secondary amines	# tertiary amines	globularity	# single rotatable bonds	Amphiphilic moment
1	0	4	0	0.14	6	2.3
17h	0	2	0	0.16	4	3.4
17i	0	2	0	0.16	4	3.3
17o	0	2	0	0.17	5	4.0
17p	0	2	0	0.16	4	4.1

that can accumulate across the OM in *E. coli*.[146] Although, the compounds only contain 2 secondary amines and no primary amines or ammonium groups. The addition of an ammonium group has been shown to provide a Gram-positive antibiotic with broad-spectrum activity.[146]

Conclusions

The application of homology modeling using templates from the CusB and ZneB crystal structures and the extraction of multiple conformations from each model using MD simulation led to the identification of 4 new compounds with several EPI-like characteristics. One of those compounds, NSC60339, is specific for *E. coli* and changes the structure of AcrA *in vivo*; thus, the compound possesses a novel mechanism of action not seen in the other inhibitors or MC-207,110 and MBX2319. However, none of the compounds that bind AcrA can permeate the outer membrane. Lead optimization of NSC60339 to 4 new analogs helped to overcome the OM permeability barrier with improved EPI characteristics. Thus, the application of artificial WT-pore cells is a novel innovation to identify new diverse compounds that could later be optimized to improve their permeability.

Our next step is to continue to identify more potent diverse compounds that bind AcrA and accumulate across the OM. To fulfill this step, we first need to experimentally confirm the ligand binding site(s) on AcrA. In this study, we proposed two possible sites, the hinge and MP, but others may exist. We chose to use a combination of site-directed mutagenesis, tryptophan fluorescence

spectroscopy, blind docking, and MD simulation to indirectly infer probable binding site(s) on AcrA for two of the four compounds.

CHAPTER II
IDENTIFICATION OF BINDING SITES FOR EFFLUX PUMP INHIBITORS OF THE ACRAB-TOLC COMPONENT ACRA

Some results from this chapter were originally published in a manuscript from which I am a co-first author. The citations for the manuscript are listed below.

- Darzynkiewicz, Z. M.*; **Green, A. T***.; Abdali, N.; Hazel, A.; Fulton, R. L.; Kimball, J.; Gryczynski, Z.; Gumbart, J. C.; Parks, J. M.; Smith, J. C.; Zgurskaya, H. I., Identification of Binding Sites for Efflux Pump Inhibitors of the AcrAB-TolC Component AcrA. *Biophysical journal* **2019,** *116* (4), 648-658.
- co-first author

In this work, I built a new homology model of the AcrA MP domain using a different template from the previous chapter. The template represents a closer homolog of AcrA that was missed when the previous models were made. I also carried out MD simulation and RMSD-clustering to extract 29 conformations from the model. I conducted blind ensemble docking and subsequent clustering of the poses to identify the most common binding sites explored by NSC60339, NSC227186, and novobiocin. I also carried out FTMap calculations to examine additional possible binding sites missed by blind ensemble docking. Lastly, I wrote and designed the logic of the manuscript that reconciled the computational and experimental results. The experiments were carried out by members of Helen Zgurskaya's lab at the University of Oklahoma.

Abstract

The overexpression of multidrug efflux pumps is an important mechanism of clinical resistance in Gram-negative bacteria. Recently, four small molecules

were discovered that inhibit efflux in *Escherichia coli* and interact with the AcrAB-TolC efflux pump component AcrA. However, the binding site(s) for these molecules is not known. Here, we combine ensemble docking with tryptophan fluorescence spectroscopy, site-directed mutagenesis, and antibiotic susceptibility assays to probe binding sites and effects of binding of for two of these molecules. We conclude that clorobiocin (NSC227186) and SLU-258 (NSC60339) likely bind at a site located between the lipoyl and β-barrel domains.

Introduction

According to a report from the Center for Disease Control and Prevention (CDC), approximately two million illnesses and 23,000 deaths are caused by antibiotic resistance each year in the United States alone.[147] Some strains of *Escherichia coli* are now resistant to at least six different classes of antibiotics and strains of *Pseudomonas aeruginosa* are now resistant to all classes of antibiotics.[1]

One of the primary mechanisms for multidrug resistance in Gram-negative bacteria such as *E. coli* and *P. aeruginosa* is the overexpression of multidrug efflux pumps, which expel antibiotics taken up by the bacteria.[1] In *E. coli*, the multidrug efflux pump is AcrAB-TolC and its counterpart in *P. aeruginosa* is MexAB-OprM. AcrAB-TolC consists of three proteins, AcrA, AcrB, and TolC, which upon assembly span both membranes and the periplasm.[12] A cryo-EM structure of the assembled pump in the apo state was resolved at 16 Å resolution.[29] Cryo-EM structures of both the apo state and inhibitor (MBX2931)-bound state were both recently resolved at 6.5 Å.[39] In agreement with biochemical and genetic studies,

these structural analyses showed that the complex has a stoichiometry of 3:6:3 for AcrB, AcrA, and TolC, respectively.[42, 49] Each protomer of the AcrB homotrimer consists of both a transmembrane and a periplasmic domain, while each protomer of the TolC homotrimer consists of a β-barrel domain and a mostly α-helical periplasmic domain. The complex is assembled by the membrane fusion protein AcrA. Six AcrA protomers interact as a trimer of dimers in the assembled pump, connecting the inner membrane transporter, AcrB, to the outer membrane component, TolC (**Figure 1**). [39]

AcrA consists of four domains connected by flexible linkers: the α-helical hairpin, lipoyl, β-barrel, and membrane-proximal (MP) domains (**Figure 32**).[78] The α-helical hairpin domain interacts with the coiled-coil domains of TolC. The lipoyl and β-barrel domains are the most conserved features of diverse MFP proteins.[43] The MP domain is contained primarily within the C-terminal region of the AcrA sequence, but also includes an N-terminal β sheet. This highly flexible domain binds directly to one monomer of the inner membrane transporter AcrB.[39] The 6.5 Å cryo-EM structure of the apo complex revealed spacious gaps between each AcrA dimer through which antibiotics might be inadvertently expelled into the periplasm. However, in cryo-EM models with the inhibitor MBX2931 bound to AcrB the gaps between AcrA dimers are absent and the channel in TolC is open, thus allowing antibiotics and other efflux pump substrates to exit the cell (**Figure 5**).[39]

Whereas most efflux pump inhibitors target the transporter, AcrB, the

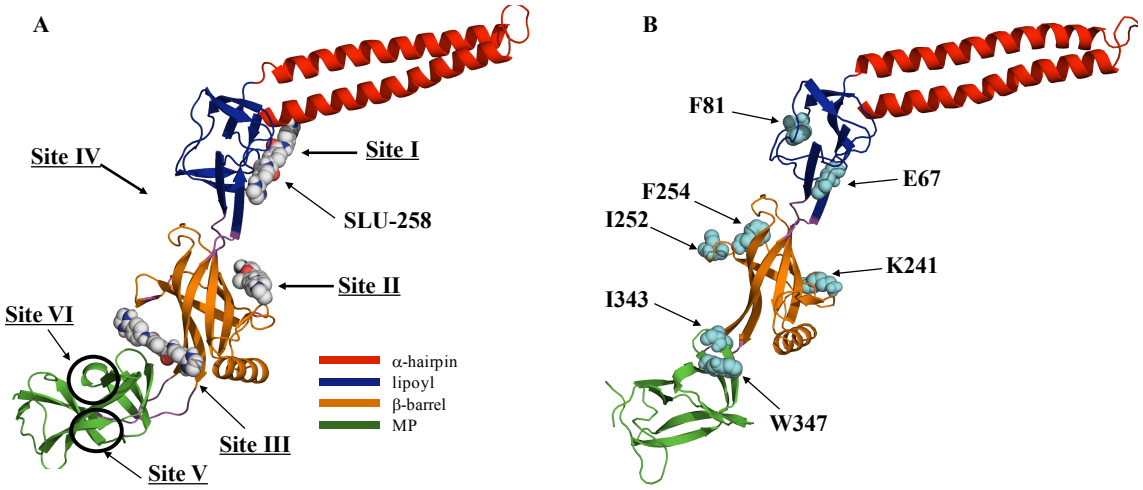


Figure 32. (A) Inhibitor binding sites predicted from blind ensemble docking of SLU-258, clorobiocin and novobiocin (Sites I-III) and additional sites predicted by FTMap (Sites IV-VI). Sites I, II, and III are located between the α-hairpin and lipoyl domains, in the β-barrel domain, and between the β-barrel and MP domain, respectively. Site IV is located between the β-barrel and lipoyl domain, and Sites V and VI are located in the MP domain. For clarity, only SLU-258 is shown. (B) Residues mutated individually to Trp for fluorescence quenching experiments are labeled and shown as cyan spheres. The intrinsic Trp in wild-type AcrA, W347, was mutated to Phe.

assembly of the pump has been targeted by searching for molecules that bind to AcrA as shown in the previous chapter. A combination of virtual screening, antibiotic potentiation assays and surface plasmon resonance (SPR) led to the discovery of four molecules that inhibit efflux in *E. coli* and interact with AcrA. Each molecule potentiated the activity, i.e., decreased the minimal inhibitory concentration (MIC), of the antibiotics novobiocin and erythromycin and bound AcrA in vitro (**Table 1**). Using an in vivo proteolysis approach, it was also found that the inhibitor NSC60339 (SLU-258) altered the structure of AcrA (**Figure 26**). In the absence of SLU-258, cleavage by trypsin occurred at two sites, R296 and K396, whereas addition of this inhibitor also resulted in cleavage at K346, indicating that SLU-258 likely alters the structure of AcrA in a manner that increases the accessibility of K346 (**Figure 26**). Subsequently, structure-activity relationships inferred from a docked pose of SLU-258 to AcrA helped guide the modification of the chemical scaffold of SLU-258 to develop second-generation EPIs targeting AcrA (**Figure 27**). A further four synthesized analogs were identified that demonstrated improved EPI characteristics (**Table 5)**.

Despite possible interactions between inhibitors and AcrA, the binding site(s) for these inhibitors remain to be definitively determined. Further development of improved efflux pump inhibitors that target AcrA would benefit from better binding site characterization and from a knowledge of allosteric communication that might be inhibited by binding and disrupting pump assembly.

Several methods are available for the determination of binding site(s) to a

protein. One method would be to determine an atomic-level structure of the protein-ligand complex using X-ray crystallography.[66] However, AcrA is conformationally flexible and currently only one crystal structure exists that lacks the MP domain.[78] Determination of a co-crystal structure could thus be impractical if binding occurs at the MP domain. Another approach could be nuclear magnetic resonance (NMR) spectroscopy, but AcrA is quite large with a molecular weight of 41 kDa. The large size and flexibility of AcrA could make resonance assignments of individual residues difficult making NMR a potentially impractical approach.[47, 148] While X-ray crystallography and NMR would identify the binding site and mode for a given inhibitor, another method would only provide information about the binding site. This method couples site-directed mutagenesis with a binding assay such as surface plasmon resonance (SPR) by mutating predicted binding site residues and testing if the affinity decreases.[149] However, the AcrA inhibitors bind with affinity in the low to mid micromolar range and possibly in more than one binding site (**Figure 20**).[69] Originally, two predicted binding sites were used to identify the inhibitors as discussed in the previous chapter. The low affinity, possibility of more than one binding site, and flexibility of AcrA may indicate that binding to AcrA is more driven by conformational changes than direct contacts. In vivo proteolysis has already shown that NSC60339 changes the structure of AcrA (**Figure 26**). The binding of the inhibitors may be entropically, not enthalpically driven. Here we combine structural modeling of AcrA and computational ensemble docking with tryptophan (Trp) fluorescence spectroscopy, site-directed mutagenesis, and antibiotic

susceptibility assays to examine potential binding sites and effects of binding of efflux pump inhibitors by conformational changes.

Computational methods

A structural model of the AcrA monomer was generated from a partially complete X-ray crystal structure of AcrA (PDB entry 2F1M)[78] and a full-length structure of MexA (PDB entry 2V4D)[44] using MODELLER 9.17.[99] The sequences of full-length wild-type AcrA and MexA were aligned with the SALIGN algorithm in MODELLER (**Figure 33**).[150] The sequence of wild-type AcrA was then threaded onto the 2F1M and 2V4D templates. One hundred models were generated and the model with the lowest DOPE score was used for molecular dynamics (MD) simulation.

The program MODELLER aims to construct three-dimensional models of proteins by a method referred to as the satisfaction of spatial restraints.[99] The sequence to be modeled is first aligned to the sequences of the template structures through a function such as SALIGN embedded within MODELLER.[91, 151] In our case, the template structures are AcrA and MexA. The alignment of the template structures to the modeled sequence allow MODELLER to derive distance and dihedral restraints from the template structures that will be used to build the structural model of the sequence.[151] Additional restraints such as preferences for bond lengths and bond angles are taken from the CHARMM22 force field.[151]

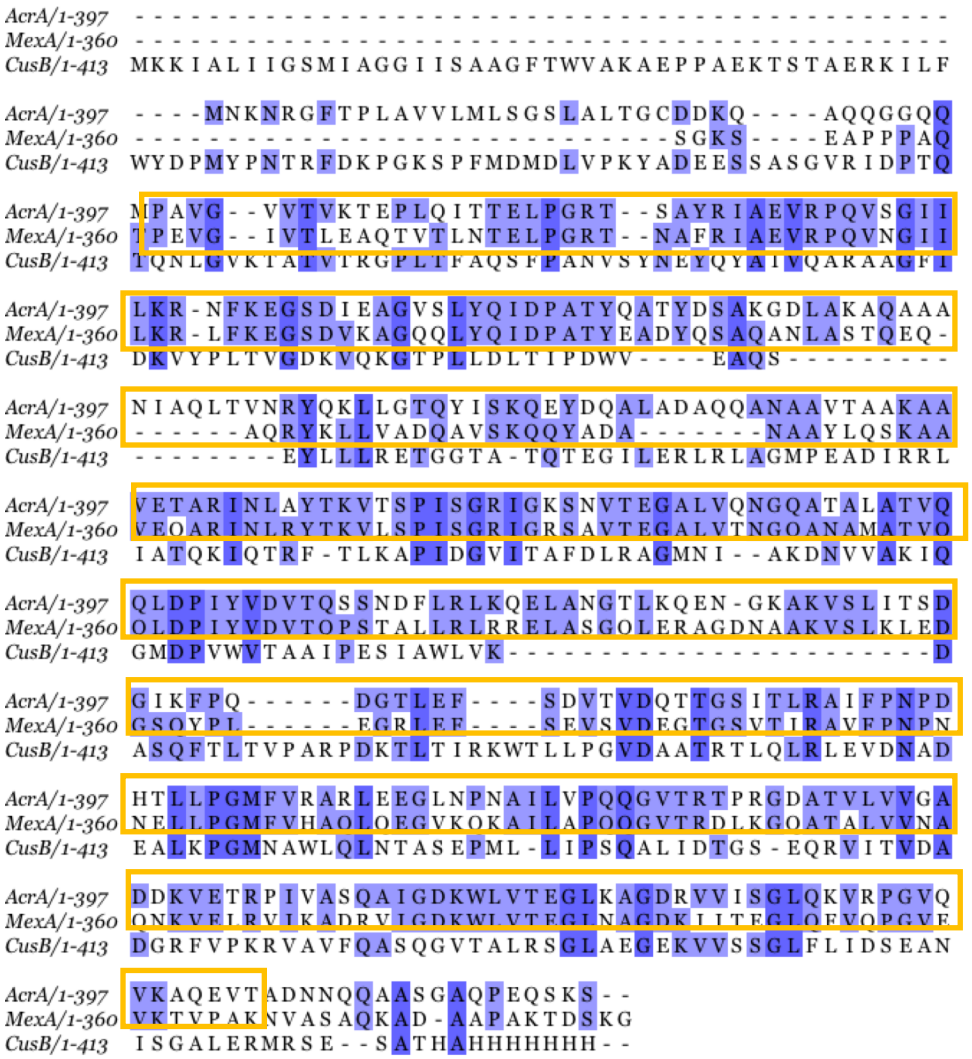


Figure 33. Sequence alignment of full-length AcrA, MexA (chain F from PDB 2V4D) and CusB (chain B from PDB 3NE5). The orange boxes indicate the extent of the AcrA homology built from MexA.

Restraints that encompass statistical preferences for dihedral angles and inter-atomic distances based on analysis of a representative set of known proteins structures are also assigned by MODELLER.[151] Additional restraints from various experimental sources such as disulfide cross-linking, NMR NOESY restraints, or cryo-EM density maps can also be added to help improve the accuracy of the models.[151] No experimental restraints were available at the time of our modeling. All the restraints are then combined into an objective function, a function that is designed to be minimized, by a combination of energy minimization and MD simulation with simulated annealing.[151] Energy minimization through a method referred to as conjugate gradients allows MODELLER to identify a model that is located at some minima of the objective function.[151] Further sampling by MD simulation with simulated annealing enhances the sampling and allows MODELLER to more likely identify the model with the lowest objective function i.e. the global minimum that is akin to the native state on a free energy landscape (**Figure 11**). The lowest value of the objective function is the one that best satisfies the spatial restraints assigned by the sequence-structure alignment.[151] The sampling of the objective function by MD simulation with simulated annealing is based on a random search to identify the global minimum; thus, changes in the initial conditions will lead to different models.[151] Thus, we built 100 models that claimed to satisfy the spatial restraints and each model was subject to further evaluation by the DOPE score.

DOPE, discrete optimized protein energy, is a knowledge-based or statistical potential that estimates the free energy or potential of mean force by the probability or likelihood that a given model approximates a representative set of 1472 crystallographic structures from the protein data bank (PDB).[152] DOPE estimates the probability of distances between all atoms types from all the amino acids in the model in reference to the probabilities for the same distances obtained from 1472 representative diverse structures from the PDB.[152] The representatives have a resolution of less than or equal to 1.8 Å and share a sequence identity of less than 30% with each other. The DOPE score is then the negative logarithm of the sum of the products of the probability distributions from all atom pairs for the model ($P_{i,j\ model}$) and the selected experimental structures in the PDB ($P_{i,j,exp}$).[152]

$$DOPE = -k_B T \ln \left(\frac{P_{i,j,model}(r)}{P_{i,j,exp}(r)}\right)$$

which is the definition of the potential of mean force in statistical mechanics and the units are in kT. The terms i and j represent the atom types that define their distance. Based on this statistical mechanical definition of the DOPE score, the lower the score, the greater the accuracy of the model given the probabilities of distances from the structures in the PDB. The DOPE score can be evaluated after the modeling is complete; thus, it is independent of the objective function and can be used to evaluate the best model prior to further calculations such as MD simulation.[152]

MD simulation was performed on the model with the lowest DOPE score to explore the flexibility of the protein and discover potential binding sites. A 50 ns MD simulation of the best-scoring model was carried out using the AMBER99SB force field and TIP3P water model to describe the protein and solvent, respectively.[153, 154] Periodic boundary conditions were applied and a cutoff of 1.4 nm was used for real-space nonbonded interactions. The Particle Mesh Ewald (PME) method with a grid spacing of 0.16 nm and the Verlet cutoff scheme were used to describe long-range electrostatics.[122] A long-range dispersion correction was applied to the energy and pressure to account for truncation of the Lennard-Jones interactions.[119] All bonds were constrained with the LINCS algorithm, which enabled the use of a 2-fs time step with the leapfrog integrator.[111, 155] The model was solvated in a triclinic box with a minimum of 3.0 nm between the protein and the nearest face of the box. The charge of the system was neutralized with 3 Cl^- ions and the energy was minimized with a tolerance of 1000 kJ mol^{-1} nm^{-1} and a step size of 0.01 nm. A two-step equilibration was carried out prior to data collection. In the first equilibration step, the temperature was adjusted over 1 ns to 298 K in an NVT ensemble using a V-rescale thermostat with a time constant of 0.1 ps.[156] In the second step, the pressure was adjusted over 1 ns to 1 bar using a Parrinello-Rahman barostat with a time constant of 2 ps.[157] During both equilibration steps, harmonic restraints were applied to all heavy atoms of the protein with a force constant of 1000 kJ mol^{-1} nm^{-2}. Production MD simulations for

data collection were carried out in the NPT ensemble without harmonic restraints. All MD simulations were performed with GROMACS 5.1.2.[109]

All-atom RMSD clustering of the MD trajectory was performed with *gmx cluster* to select conformations for ensemble docking.[109, 127] Using an RMSD cutoff of 0.4 nm, 29 conformations were selected. The inhibitors SLU-258, clorobiocin, and novobiocin (**Figure 34**) were docked to each conformation with VinaMPI, a massively parallel implementation of AutoDock Vina.[138] The initial structures for clorobiocin and novobiocin were obtained from the ZINC15 database and SLU-258 was obtained from NCI Diversity Set V.[75] The protonation state for each inhibitor was taken as the major predicted state at pH 7 from the ZINC15 database.[75] Clorobiocin and novobiocin were assigned a charge of -1 and SLU-258 a charge of +2 (**Figure 34**). Hydrogen atoms were added to SLU-258 with MOE 2016.[100]

The docking search space was centered at the center of mass of each conformation and included the entire protein except for the tip of the α-hairpin domain (**Figure 35**), which was excluded due to limits on the size of the search space in AutoDock Tools.[134] Each docking run was performed three times with an exhaustiveness of 1000 and a maximum number of poses for ligand and protein conformations of 25. The poses from all docking runs for each ligand were

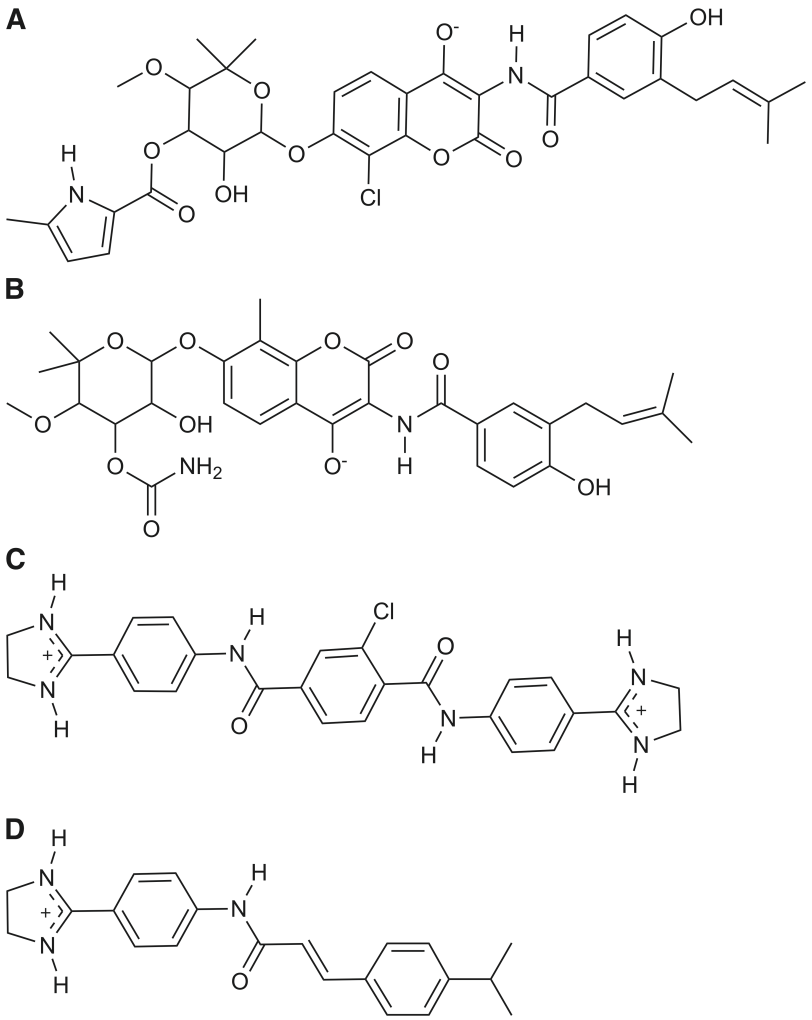


Figure 34. Chemical structures of (A) clorobiocin, (B) novobiocin, (C) SLU-258, and (D) SLU-417.

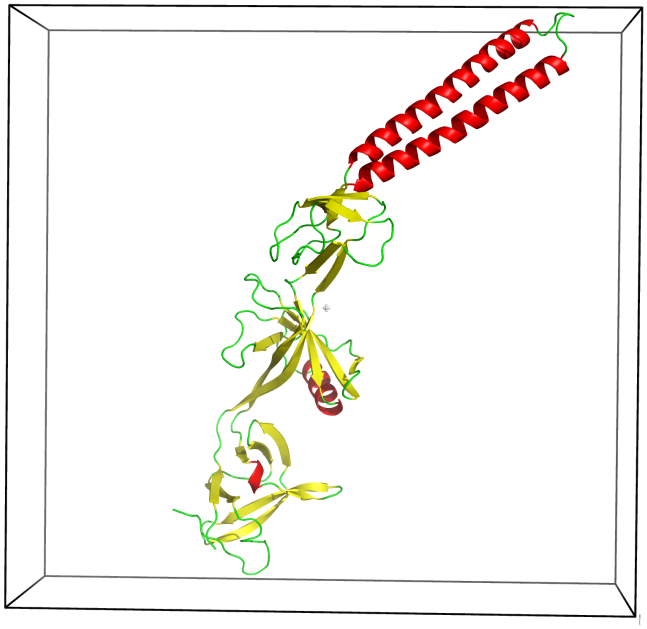


Figure 35. Search space used for docking. The dimensions of the box are 50 Å x 126 Å x 126 Å.

combined and clustered based on the RMSD of all ligand atoms with a cutoff of 0.25 nm. The centroid poses from two of the largest clusters were selected as the predicted binding sites. A third site referred to as Site I was also known as the hinge site described previously (**Figure 20A**).

A single representative conformation obtained from RMSD clustering of the 50 ns MD simulation trajectory of the WT AcrA monomer was submitted to the FTMap (http://ftmap.bu.edu/home.php) web server with default options.[158]

Clorobiocin and SLU-258 were docked separately to 29 conformations of AcrA near Site IV, which is located between F81 and F254 since Site IV was not identified by the blind ensemble docking. The same conformations of AcrA and each inhibitor as the blind docking were used. The center of the docking search space was the center of mass of F81 and F254 for each conformation with grid dimensions 25 Å x 25 Å x 25 Å. The exhaustiveness was set to 10 and the maximum number of binding poses for each conformation was 25. The center of mass was calculated using the MDAnalysis Python package.[159]

Structural modeling of AcrA from MexA

We first generated a structural model of WT AcrA using the X-ray structures of truncated AcrA and full-length MexA as templates. Residues 1-37 at the N-terminus and 380-397 at the C-terminus were excluded from the model because neither template covered these regions (**Figure 33**). The sequence identity between the MP domain of AcrA and MexA is 56% (**Figure 36**). In the 6.5 Å cryo-



Figure 36. Sequence alignment and identity between the MP domain of the AcrA homology model and the MP domain of MexA from PDB 2V4D. The sequence identity is 56%.

EM structure of apo AcrAB-TolC, AcrA was also modeled using X-ray structures of AcrA and MexA as templates.[39] Alignment and Cα superposition of snapshots from the 50 ns MD simulation of the WT model onto a single chain of AcrA from the assembled complex revealed an overall RMSD for the whole protein of around 6 Å (**Figure 37**). However, the individual domain RMSDs were ~3 Å for the β-barrel and MP domains and ~2 Å or lower for the hairpin and lipoyl domains (**Figure 37**). Thus, most the motion of the protein occurs at the interfaces between the domains.

Ramachandran plots that depict the orientation of the backbone dihedral angles and define the secondary structure of a protein reveal 3 outliers[105]: Gln372, Asn232, and Asn239 (**Figure 38**). All three residues are located in the MP domain and/or at the α-helix of the β-barrel domain. The α-helix of the β-barrel domain and the MP domain was not determined in the X-ray crystal structure of AcrA[78]; thus, these outliers may be steric clashes from poor side chain packing during model construction. The outliers were absent after the energy minimization with the steepest descent algorithm in GROMACS 5.1.2.[109, 110] The Ramachandran plot agrees with the plot for Model A with β-sheet being the dominant secondary structure for AcrA. In addition, the DOPE scores for all the models was estimated to be 1000 kT lower than Model A built with the CusB template (**Figure 39**). The

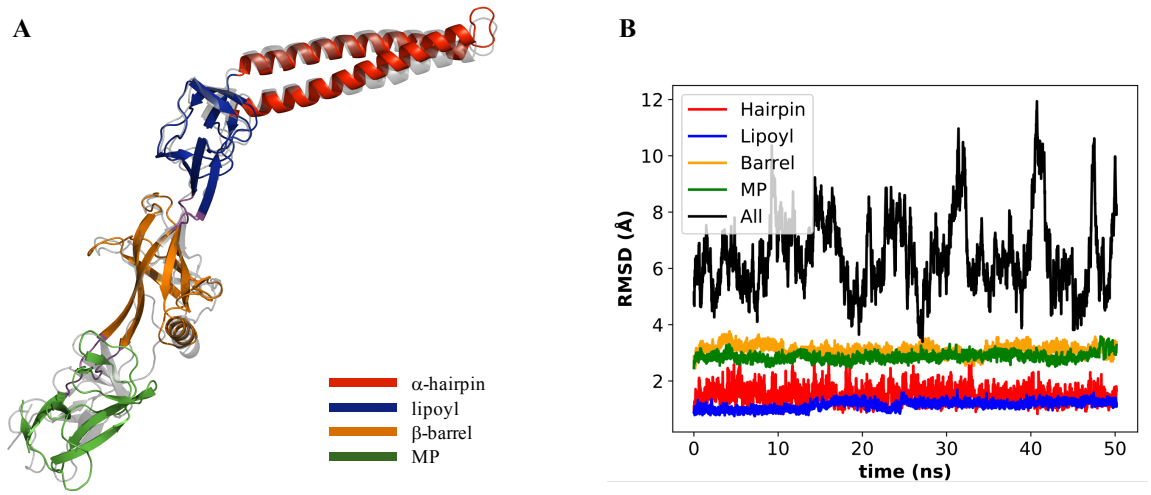


Figure 37. (A) Superposition of the homology model of WT AcrA monomer onto an AcrA protomer from the cryo-EM structure of the assembled AcrAB-TolC complex. *Colors*: hairpin (red), lipoyl (blue), barrel (orange), and MP domain (green), chain D from PDB entry 5V5S (gray). The linkers are shown in magenta and were not included in the RMSD calculation of each domain. (B) Cα RMSD of AcrA for the whole protein and for each individual domain with respect to the cryo-EM model over the course of the MD simulation.

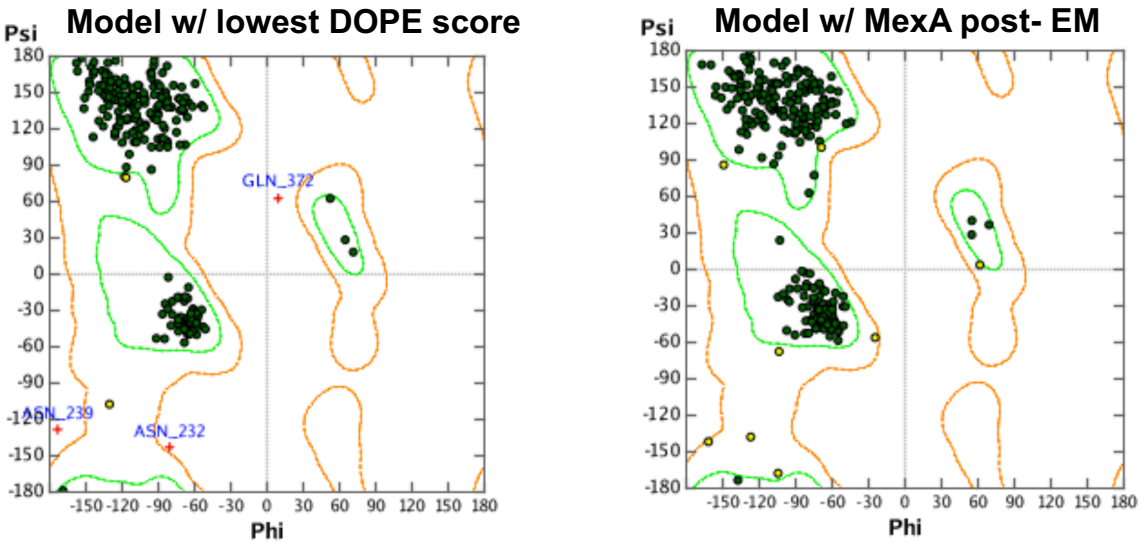


Figure 38. Ramachandran plots with the lowest DOPE score before and after energy minimization. Energy minimization included the full solvated and ionized system. Plots were rendered using MOE 2016.

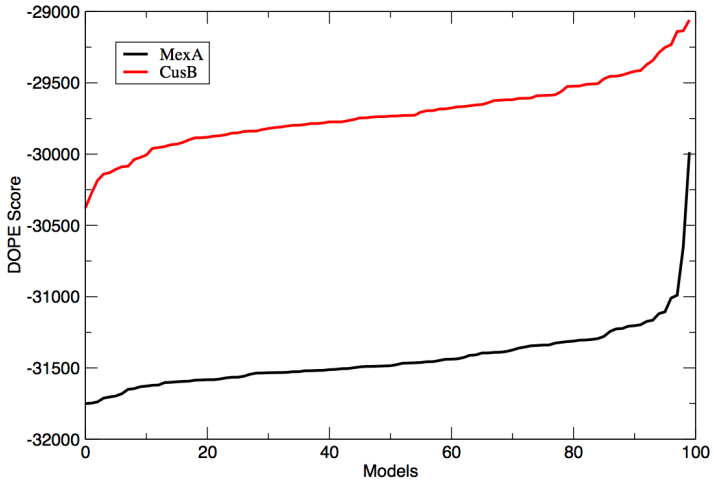


Figure 39. DOPE score for all 100 models using the AcrA crystal structure (PDB 2F1M) and the MP domain from CusB (red) or MexA (black).

lower scores indicate a greater probability of agreement with known experimental structures. The lower score is likely due to the higher sequence identity of MexA than CusB resulting in a better sequence-structure alignment and spatial restraints used to derive the model.

Calculation of potential binding sites

Using the structural model of AcrA, a combination of computational methods was used to locate potential binding sites. Twenty-nine conformations of WT AcrA were extracted from an MD simulation trajectory using RMSD clustering for use in blind ensemble docking of the efflux pump inhibitors SLU-258 and clorobiocin (**Figure 32 & 40**). The efflux pump substrate, novobiocin, was also assessed (**Figure 40**).

Three sites were selected by clustering of the docked poses by RMSD, which we refer to as Sites I, II, and III (**Figure 32A & 40**). Site I is located at the interface of the α-hairpin and lipoyl domains and has been found by site-directed mutagenesis to be functionally important (**Figure 21**). When residues at Site I, such as E67, were mutated to Ala, the minimal inhibitory concentration (MIC) of the antibiotics novobiocin and erythromycin decreased, indicating that the mutations impair efflux function and make the bacteria more susceptible to the antibiotics (**Figure 21**). We found that binding of SLU-258 at Site I could result in a steric clash that would inhibit AcrA oligomerization, which would presumably disrupt the assembly of the full complex (**Figure 41**).

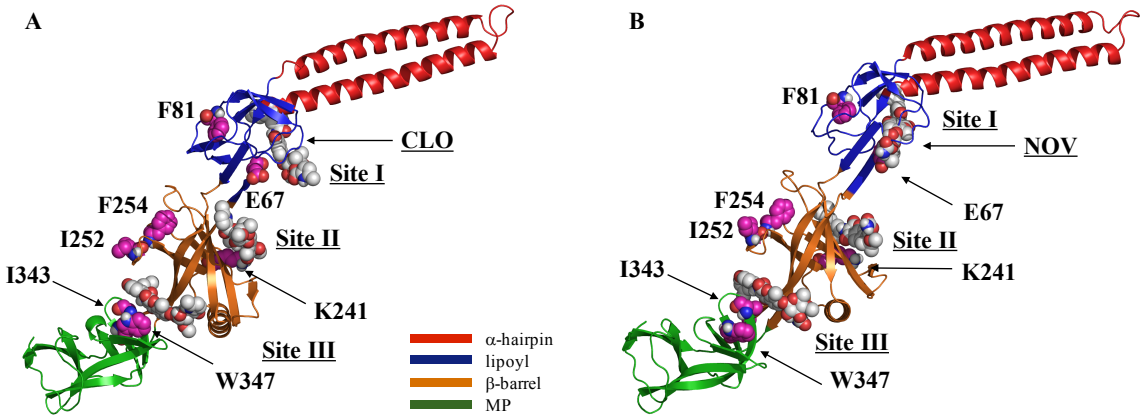


Figure 40. Three predicted sites from RMSD clustering of blind ensemble docking for (A) clorobiocin and (B) novobiocin referred to as Site I, II, and III. Residues mutated to tryptophan are E67, F81, I252, K241, F254, and I343. W347 was mutated to Phe. Each ligand comes from a separate conformation, but only one conformation is shown for simplicity.

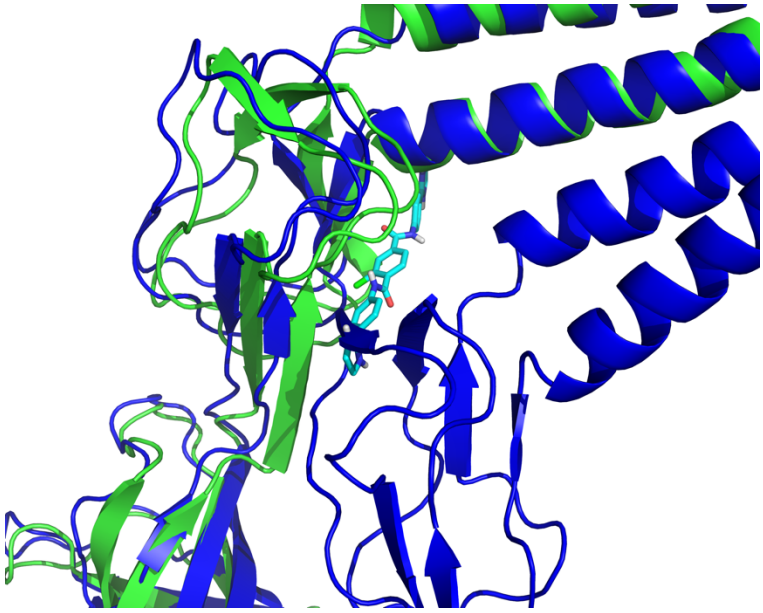


Figure 41. SLU-258 results in a steric clash when docked at Site I (hinge site) of AcrA that could prevent oligomerization.

Sites II and III were the most highly populated sites in the ensemble docking of each inhibitor (**Figure 42**). Site II is located in the β-barrel domain and Site III is located between the β-barrel and MP domains (**Figure 33A**). Previously, it was found that in vivo proteolysis of the assembled AcrAB-TolC pump with trypsin resulted in a major fragment of AcrA (K46−R294/R296) (**Figure 26**). Upon addition of SLU-258, a fragment corresponding to residues K46−K346 of AcrA was also observed (**Figure 26**). These findings indicate that the inhibitor alters the structure of AcrA, presumably making K346 more accessible to trypsin. K346 is located in the MP domain near Site III (**Figure 43**). One possibility would be that inhibitor binding at Site III changes the structure of AcrA. In the assembled complex, the MP domain interacts with AcrB (**Figure 10**). If an inhibitor binds at Site III, it could prevent the MP domain of AcrA from interacting properly with AcrB and thus prevent assembly of the pump. Alternatively, the change in structure may result by propagation from binding at another site to Site III allosterically.

To search for additional binding sites that may have been overlooked by blind ensemble docking, we used the binding site identification program FTMap. FTMap works in an analogous manner to blind ensemble docking with the exception that small organic solvent molecules are used to map possible binding sites using a molecular mechanical energy function.[158] FTMap identified Sites I, II, and III, but also identified three more sites located in the MP domain and between the β-barrel and lipoyl domain (**Figure 32A**). One site, Site IV, is located between the β-barrel and lipoyl domain. The other two sites, V and VI, are in the MP domain.

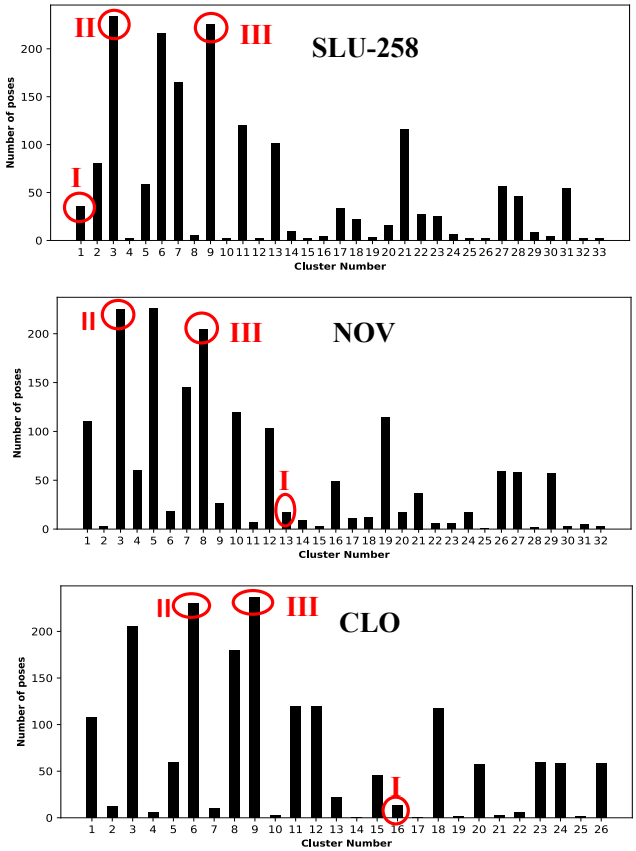


Figure 42. Number of occurrences of docked poses in each cluster determined from RMSD-based clustering of (A) SLU-258, (B) novobiocin, and (C) clorobiocin from blind ensemble docking. The RMSD cutoff was 2.5 Å.

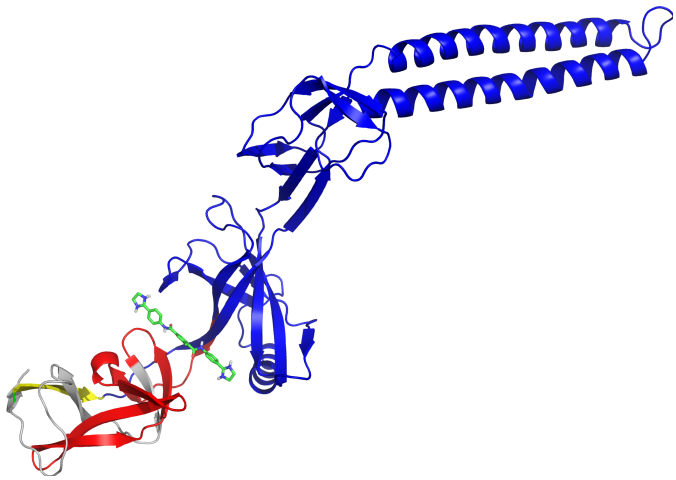


Figure 43. Binding of SLU-258 at Site III between the β-barrel and MP domain exists between two proteolytic fragments, K46-R296 and K46-K346, determined in the previous chapter.

Truncated AcrA lacking the MP domain binds SLU-417 and clorobiocin

We first assessed the binding of clorobiocin and SLU-417 (**Figure 34**), a derived analog of SLU-258, to a truncated construct of AcrA lacking the MP domain (residues 45-312) using biolayer interferometry (BLI). Binding of SLU-417 to the truncated construct was observed with responses similar to the full-length protein (**Figure 44**), diminishing the likelihood that Sites III, V, and VI are major inhibitor binding sites in AcrA. Clorobiocin was also found to bind the truncated construct.

Mutations in Site IV have the largest impacts on efflux pump function

We carried out site-directed mutagenesis of selected residues near Sites I, II, III, and IV (**Figure 32B**) and performed Trp fluorescence spectroscopy on the mutants to detect inhibitor binding. Changes in Trp fluorescence can occur by three different mechanisms: static quenching, dynamic quenching, and changes in the environment.[160] Static quenching occurs when a fluorescent molecule (such as

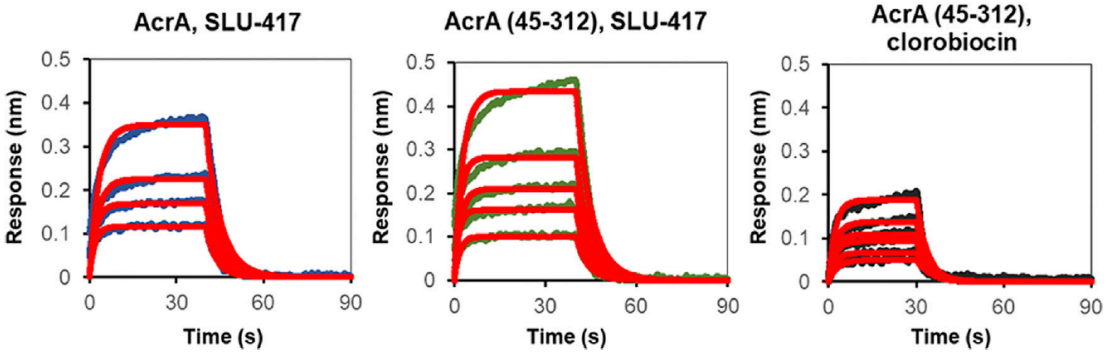


Figure 44. Biolayer interferometry (BLI) spectra for (A) SLU-417, an analog of SLU-258, binding to full-length AcrA, (B) SLU-417 binding to a truncated variant of AcrA lacking the MP domain (AcrA (45-312), and (C) clorobiocin binding to AcrA (45-312).

clorobiocin, novobiocin, and SLU-258) quenches fluorescence intensity through direct contact with the Trp residue. Dynamic quenching occurs when excitation of the fluorescent molecule transfers energy in the excited state from the Trp to the molecule without direct contact. Changes in the local environment of Trp that result in increased or decreased solvent exposure can also modify fluorescence properties.[160]

Wild-type AcrA contains only one intrinsic Trp residue, W347, which is located near Site III. Thus, W347 was mutated to Phe and the following residues were mutated individually to Trp: E67W near Site I, K241W near Site II, I252W and I343W near Site III, and F81W and F254W near Site IV (**Figure 32B**). E67, K241, and I343 were chosen because they are on the surface of AcrA and may be close enough for an inhibitor bound in each site to interact directly with each of these residues through static quenching. F81, I252, and F254 were chosen because we expect that they could interact indirectly with inhibitors through an allosteric change in the local environment of the Trp or excitation energy transfer through dynamic quenching (**Figure 32A**).

To determine whether these Trp mutations in AcrA affect functionality of the efflux pump, we measured the MICs of selected antibiotics for strains carrying the AcrA variants and compared them to the WT. We measured the MICs for novobiocin, erythromycin, and tetracycline in cells with and without pores in their outer membrane (WT and WT-Pore). All three of these antibiotics are AcrAB-TolC substrates. The presence of pores diminishes the permeability barrier of the outer

membrane, allowing antibiotic activity and the corresponding effects on efflux to be assessed directly.[142] Sodium dodecyl sulfate (SDS), which is also an AcrAB-TolC substrate, was used as a non-antibiotic control. All selected mutants were expressed and retained at least partial efflux function compared to the wild-type (**Table 8**). However, the mutant F81W (Site IV) exhibited the largest decrease in MIC for each antibiotic, as cells carrying this AcrA variant were hypersusceptible to antibiotics even with the native OM. In hyperporinated cells, which have increased influx of antibiotics into the periplasm, E67W (Site I) provided weak protection against antibiotics. All other AcrA mutants containing Trp substitutions were functionally similar to the AcrA W347F variant and were 2-4 fold less active than WT AcrA (**Table 8**). These results show that the F81W and E67W substitutions decrease the activity of the AcrAB-TolC efflux pump. Thus, these two residues are functionally important for efflux. E67 was already known to functionally important with mutations to alanine and arginine (**Figure 21**). The other residues are also functionally important, but to a lesser extent including residues I343 and W347 at the MP domain.

Fluorescence of tryptophan residues in AcrA reports on binding of inhibitors.

The fluorescence spectrum of apo WT AcrA consists of a single maximum (λ_{max} = 330 nm, **Table 9**), which indicates that the single W347 is not exposed to an aqueous environment but is buried in the protein.[161] Substitution of W347 in AcrA W347F abolished this maximum. The fluorescence emission spectra and

Table 8. Antibiotic Susceptibilities of Wild-Type AcrA and Selected Trp Mutants

	No Pore				Pore			
	NOV[a]	ERY	TET	SDS	NOV	ERY	TET	SDS
-	1	0.5	0.25	19.5	0.5	0.25	0.06	9.7
pUC18	1	1	0.25	39	0.12	0.12-0.2	0.06	9.7
WT	256	64	0.5	>10000	32	8-16	0.5	312
W347F	128	16	0.5	>10,000	8	2-4	0.25	312
W347F K241W	128	16	0.5	>10,000	4	1	0.125	156
W347F I252W	128	32	1	>10,000	4	1	0.25	156
W347F F254W	128	16	0.25-0.5	>10,000	8	1	0.125	78
I343W	256	64	0.5	>10000	8	2-4	0.125	39-78
W347F I343W	128-256	16	0.25	>10,000	8	1	0.25	156
W347F E67W	64-128	16-32	0.5	>10,000	4	1	0.25	39
W347F F81W	8	2	0.25	39.1	1	0.125	0.25	15.6

[a] NOV, novobiocin; ERY, erythromycin; TET, tetracycline; SDS, sodium dodecyl sulfate.

Table 9. Fluorescence properties of single Trp mutants of AcrA in the absence and presence of inhibitors

		WT	F81W	I252W	I343W	E67W	F254W	K241W
λ_{max}, nm[a]	apo	330	330	350	310, 340	350	330	350
	Clo[e]	338	338	350	345	350	338	350
	SLU	338	341	350	348	353	341	353
	Nov	336	341	350	343	350	340	350
τ, ns[b]	apo	3.19; 2.60	2.36; 1.68	4.66; 3.91	2.99; 2.09	6.33	2.60; 2.12	4.59; 4.03
	Clo	3.25; 2.61	1.88; 1.51	4.63; 4.0	2.83; 2.09	6.24	2.52; 2.11	4.52; 4.0
	SLU	3.18; 2.66	2.07; 1.53	4.49; 3.67	2.88; 2.13	6.22	2.53; 2.14	4.43; 3.87
	Nov	3.23; 2.62	2.0; 1.38	4.75; 4.11	2.95; 2.13	6.38	2.62; 2.12	4.54; 3.98
K_D, μM[c]	SLU	67.2±12.6	46.9±11.3	49.2±19.8	53.5±16.8	40.6±7.2	64.7± 27.8	45.9±13.4
	Clo	37.3±23.3	13.5±2.2	22.8±7.7	20.9±3.5	22.3±9.0	23.6±4.6	35.8±2.5
K_{sv}[d]	apo	1.19±0.02	1.12± 0.05	4.8 ± 0.05	1.47± 0.06	12.97±0.25	0.84 ± 0.01	2.44± 0.01
	Clo	1.39±0.05	0.65± 0.01	4.61± 0.03	1.21± 0.03	12.1±0.26	0.72 ± 0.01	2.15±0.03
	SLU	1.43±0.03	1.28± 0.03	4.59± 0.05	1.29±0.05	13.25±0.34	0.95± 0.02	1.99± 0.04

[a], the wavelength of fluorescence emission maximum
[b], averaged tau intensities and amplitudes
[c], dissociation constants calculated based on quenching of tryptophan fluorescence
[d], the Stern-Volmer quenching constant
[e], Clo, clorobiocin; SLU, SLU-258; Nov, novobiocin

maxima of the F81W and F254W variants were similar to that of the WT protein, suggesting that these Trp residues are also buried within the protein. Surprisingly, the I343W mutant exhibited two distinct fluorescence emission peaks at 310 and 340 nm, indicating that this mutant adopts two states, in which this Trp residue has different exposure to the buffer (**Figure 45**). Furthermore, these states differ from that of the WT protein. All the remaining mutants have λ_{max} values of 350 nm, indicating that their Trp residues are exposed on the surface of AcrA and different than the WT protein.

With the addition of clorobiocin or SLU-258 to the WT, λ_{max} of W347 increased to 338 nm. Similarly, for the F81W and F254W mutants, λ_{max} increased to 338 nm for clorobiocin and 341 nm for SLU-258. Therefore, the binding of these inhibitors to WT, F81W and F254W (Site IV) AcrA changed their Trp fluorescence by exposing these residues to the solvent. At the same time, the fluorescence intensity (quenching) of these AcrA variants decreased with increasing concentrations of clorobiocin and SLU-258 (**Figure 45**). The greatest Trp fluorescence quenching occurred for F81W (Site IV) and I343W (Site III) upon addition of clorobiocin and SLU-258, followed by F254W (Site IV) (**Figure 45**). F81W and I343W had quenching efficiencies of ~40-45% for SLU-258, and F81W has an efficiency of ~40% with clorobiocin. These results indicate that binding of SLU-258 and clorobiocin change the structure of AcrA. Quenching by I343W at Site III is consistent with SLU-258 changing the structure of AcrA in vivo using trypsin proteolysis (**Figure 43**). It is also possible that the inhibitor is in contact with

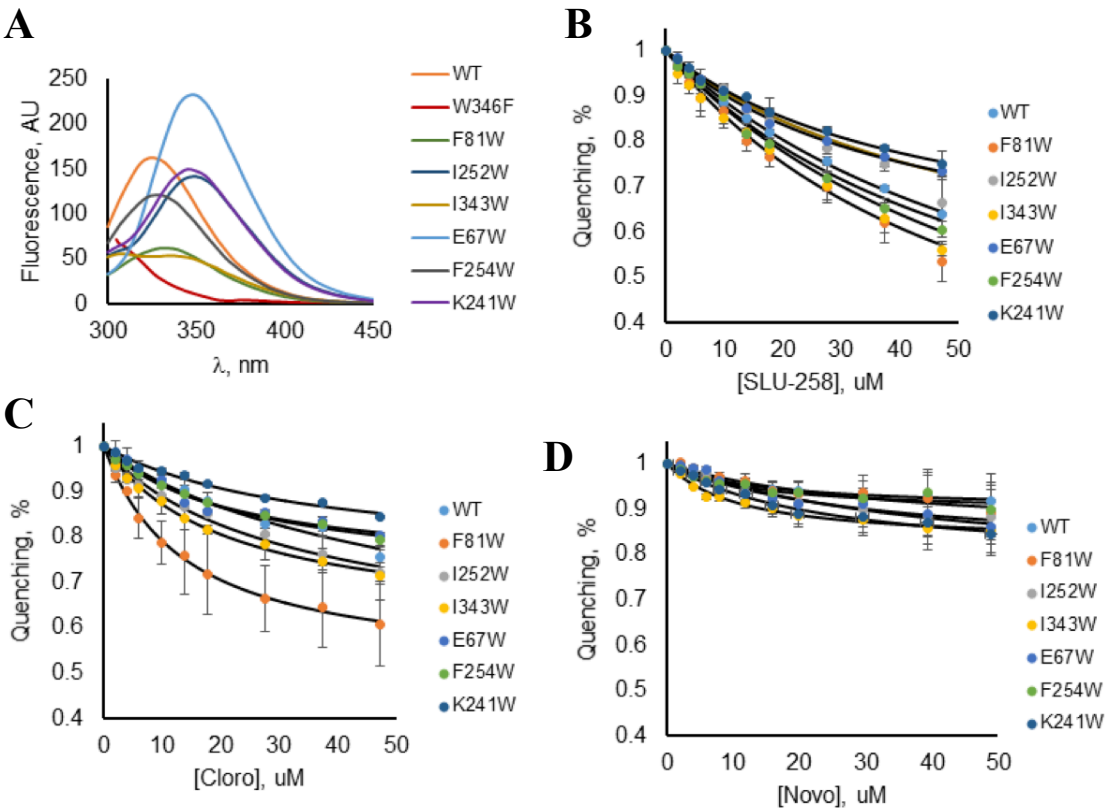


Figure 45. Fluorescence of AcrA mutants carrying a single Trp substitution in the absence of inhibitors (A) and quenching in the presence of increasing concentrations of SLU-258 (B), clorobiocin (C), and novobiocin (D).

each mutant residue concerned through a static quenching mechanism due to the intrinsic fluorescence of clorobiocin and SLU-258 without AcrA (**Figure 46**). No changes in the fluorescence maxima were detected for E67W (Site I), I252W (Site III), and K241W (Site II) for clorobiocin suggesting that these solvent-exposed Trp residues do not undergo large conformational changes in the presence of ligands (**Table 9**). Small changes of 3 nm with E67W and K241W for SLU-258 indicate that the binding poses of clorobiocin and SLU-258 may be different (**Table 9**). Quenching by novobiocin was marginal for all the mutants, likely due to the low intrinsic fluorescence of this compound (**Figure 45D & 46**).

The Trp fluorescence quenching was used to estimate the affinities of clorobiocin and SLU-258 to different AcrA variants. We found that, independent of the Trp position, both ligands have comparable micromolar affinity to the protein due to the magnitude of the error bars, with clorobiocin binding to AcrA two to three times more tightly than SLU-258 (**Table 9**). A similar affinity of SLU-258 to AcrA (78 μM) was reported previously based on surface plasmon resonance (SPR) measurements.[69] Although, it should be noted the SPR measurements also found clorobiocin to have a K_d of 213 μM.[69] Fluorescence identified clorobiocin to bind tighter than SLU-258, but the reverse was true using SPR. The experimental affinity measurements for AcrA are not reliable for the determination of inhibitor binding sites.

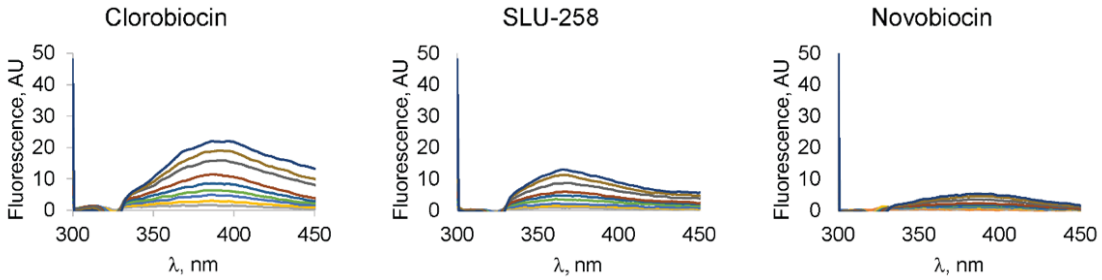


Figure 46. Fluorescence of Clorobiocin, SLU-258, and novobiocin without AcrA.

F81W, F254W, and I343W exhibited the lowest intensities, amplitudes, and lifetimes in the presence of clorobiocin and SLU-258 (**Table 9**). However, as described above, the I343W oscillates between the low and high solvent exposure which may also explain the proteolysis with trypsin (**Table 9** and **Figure 26**). I343 is located in the MP domain, which is absent in the X-ray crystal structure of AcrA and is known to be conformationally flexible.[78] The MP domain is highly flexible *in vitro* and can change conformation regardless of whether a ligand is bound.[44] In contrast, Site IV, which is flanked by F81W and F254W, was resolved in the crystal structure and is therefore expected to be more rigid. Hence, fluorescence changes near Site IV are more likely to be due to inhibitor binding.

F81W and F254W, both located in Site IV, are protected from quenching when clorobiocin and SLU-258 are bound

To further examine whether clorobiocin and SLU-258 bind near F81W or F254W (Site IV), we analyzed quenching of the Trp fluorescence by increasing concentrations of potassium iodide with and without inhibitors. If an inhibitor binds near F81W or F254W, fluorescence of the Trp concerned may be protected from

iodide quenching by the inhibitor. Indeed, F81W was significantly protected (42% reduction in quenching) from iodide by clorobiocin (**Figure 47**). Weak protection by clorobiocin (15% reduction in quenching) was also observed for F254W (**Figure 48**). No significant changes in potassium iodide quenching were found for Trp residues at any other positions for clorobiocin and SLU-258 (**Figure 47 & 48**).

In the presence of clorobiocin, Trp residues in F81W and F254W are more solvent-exposed, as indicated by red shifts in the respective fluorescence spectra (**Table 9**). Thus, it is unlikely that protection of iodide is a result of relocating these Trp residues deeper into the protein structure due to its conformational change or oligomerization. Clorobiocin is therefore likely to protect F81W directly from quenching by iodide. The effect of SLU-258 was different, as its presence resulted in somewhat enhanced quenching of F81W and F254W with iodide. Thus, clorobiocin and SLU-258 may have different binding poses or interact with different residues in AcrA that is not able to be observed in tryptophan fluorescence.

SLU-258 and clorobiocin likely bind near Site IV

The following observations all point to SLU-258 and clorobiocin binding at or near Site IV:

(i) Both inhibitors bind to an AcrA construct lacking the MP domain.

(ii) F81W impairs efflux.

(iii) Fluorescence changes upon binding the inhibitors to F81W and F254W most resemble the corresponding changes in the wild-type.

(iv) Both clorobiocin and SLU-258 interfere with the quenching of potassium

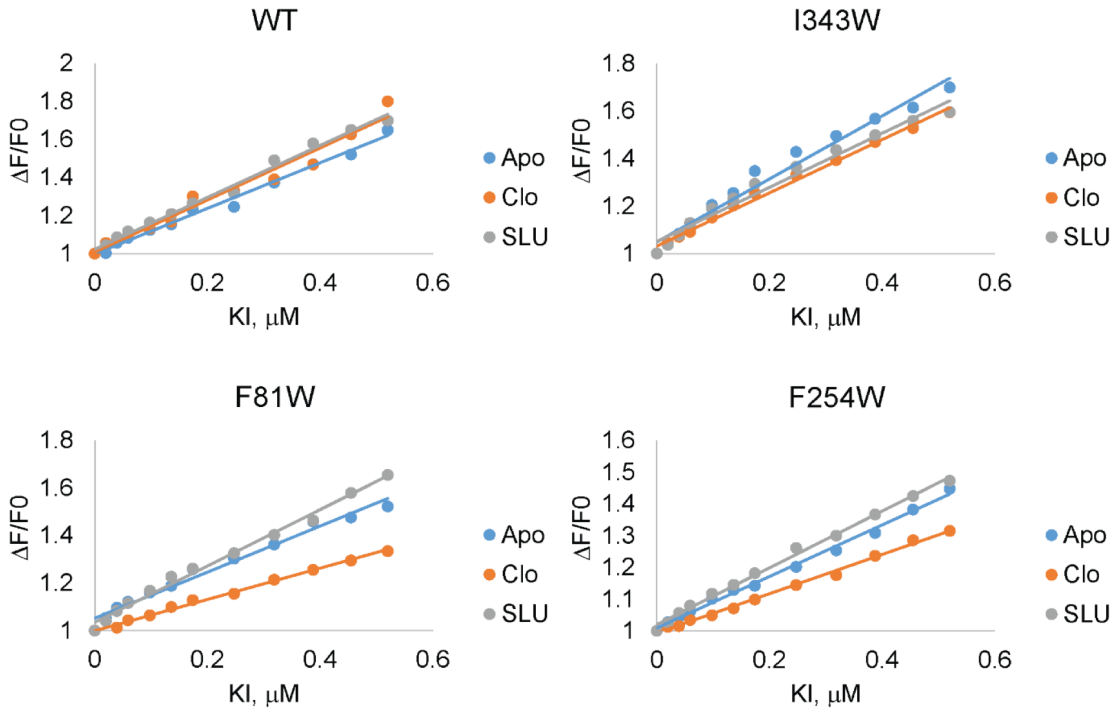


Figure 47. Trp fluorescence in the absence (Apo) and presence of clorobiocin (CLO) or SLU-258 (SLU) with increasing concentrations of potassium iodide (KI).

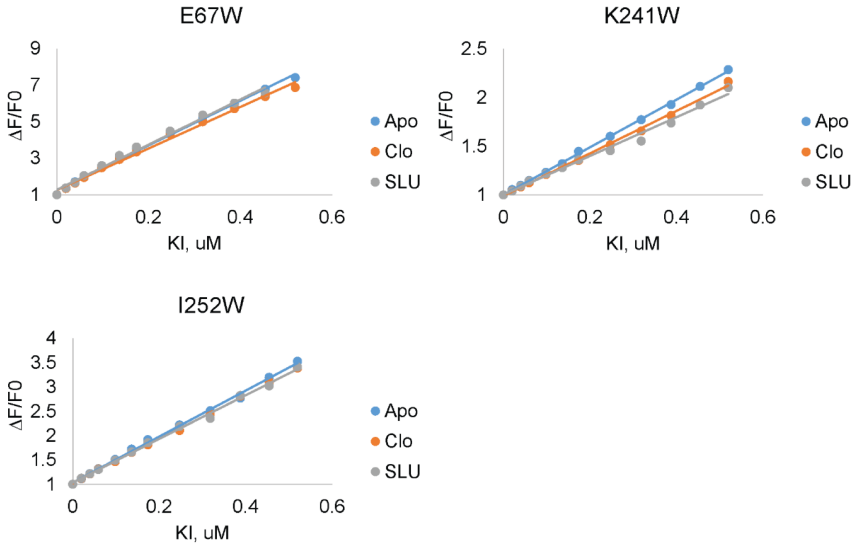


Figure 48. Trp fluorescence of E67W, K241W and I252W AcrA variants in the absence (Apo) and presence of clorobiocin (CLO) or SLU-258 (SLU) with increasing concentrations of potassium iodide (KI).

iodide with F81W and F254W in Site IV.

These results provide evidence that Site IV is associated with clorobiocin and SLU-258 binding (**Figure 49**). In the docked models the inhibitors engage in largely different interactions with the binding site. Whereas the negatively charged clorobiocin forms hydrogen bonding and electrostatic interaction with R183, in contrast the R183 side chain is pointed away from the positively charged SLU-258 inhibitor (**Figure 49**). In addition, the hydroxy group of T205 forms a hydrogen bonding interaction with clorobiocin but is oriented away from SLU-258. Nevertheless, clorobiocin and SLU-258 both form hydrogen bonding interactions with Q207, but clorobiocin also forms a hydrogen bond with the backbone of G185, while SLU-258 form a hydrogen bond with the backbone carbonyl of H285 (**Figure 49**). Thus, Site IV, which engages in different interactions for clorobiocin and SLU-258, provides the best explanation for the binding site location of SLU-258 and clorobiocin.

Conclusions

A combination of computational modeling and experimental Trp fluorescence spectroscopy has been used to identify likely binding sites of clorobiocin and SLU-258 to the membrane fusion protein AcrA of the AcrAB-TolC efflux pump in *E. coli*. Our findings point to Site IV, which is located at the interface of the β-barrel and lipoyl domain, as the most likely binding site for the two inhibitors. The F81W mutation in Site IV increased the susceptibility of antibiotics to *E. coli* and this effect is correlated with the highest quenching of fluorescence

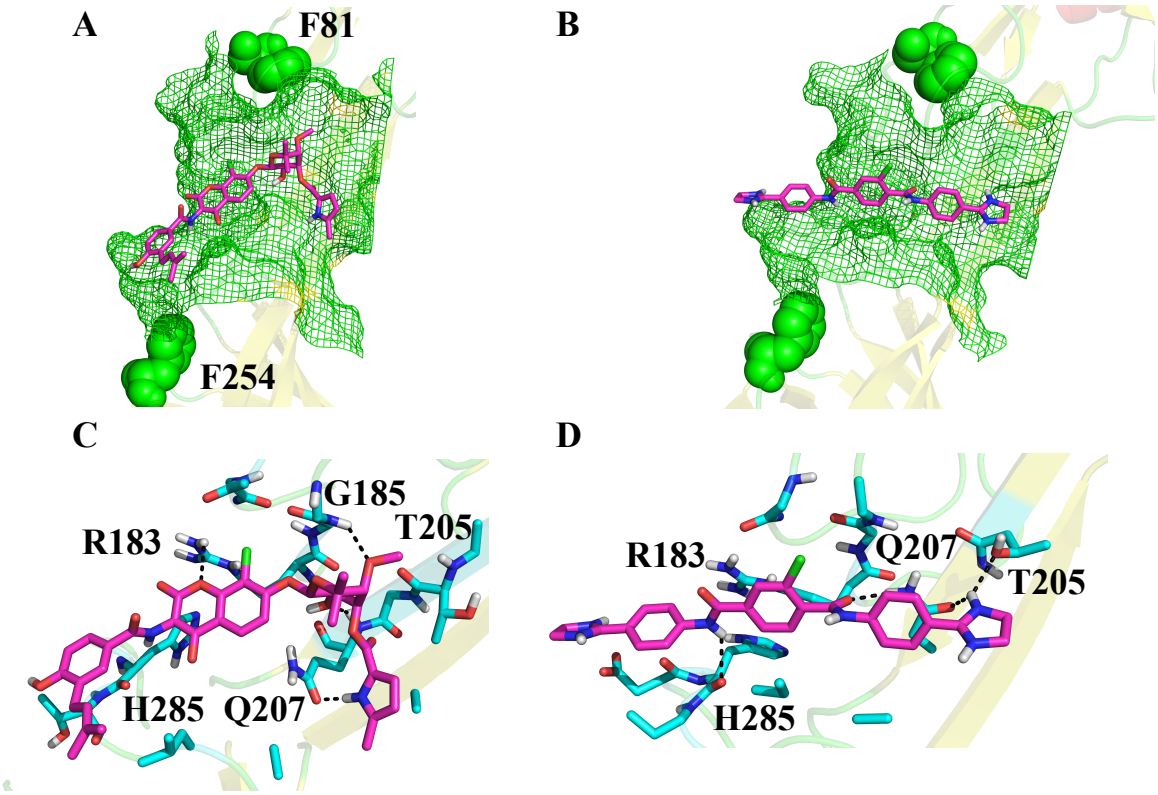


Figure 49. Docked models of clorobiocin and SLU-258 (magenta) bound at Site IV between the lipoyl and β-barrel domains, flanked by F81 and F254 (green spheres). (A-B) Residues within 5 Å of each ligand are shown in green mesh. (C-D) Residues in contact with each ligand are shown in cyan sticks and the interactions are indicated by black dashes.

intensity of all Trp mutants. Both F81W and F254W mutants that flank Site IV possessed λ_{max} values that are identical to the wild-type apo protein, with similar shifts relative to the wild-type in the presence of each inhibitor. The lifetimes for both residues were the shortest of all the mutants and they were the only two mutants that interfered with quenching by potassium iodide (**Table 9**).

The mechanism of inhibition for both inhibitors remains unknown. However, if the inhibitors indeed bind at Site IV, a conformational change might occur that causes the protein to adopt a more closed state, which could interfere with assembly of the pump. In the model of the complex, SLU-258 forms a hydrogen bond with H285, and previous MD simulations have shown that H285 plays a role in the pH-dependent conformational changes of AcrA.[162] The role of pH may also have influenced the different quenching observed for clorobiocin and SLU-258. The pK_a of an ionizable residue such as histidine can shift due to changes in the microenvironment of the residue.[163] In solution, histidine has a pK_a of ~6 which per the Henderson-Hasselbach equation indicates that ~50% of the molecules in solution are protonated and deprotonated.[105] If histidine is in a more hydrophobic or buried environment, the pK_a may shift to a lower value; thus, a greater percentage of histidine will be neutral and deprotonated.[105] The histidine residue, H285, was predicted by the algorithms PROPKA and the Protonate3d module in MOE 2016 to be ~6 in our AcrA homology model with MexA.[100, 164] Both algorithms rely on different methods of pK_a prediction. Clorobiocin and SLU-258 are predicted to be negatively and positively charged, respectively. Negatively charged

clorobiocin would interact more favorably with a protonated histidine that is positively charged. In contrast, SLU-258 is positively charged and would interact more favorably with a deprotonated and neutral histidine due to a lack of electrostatic repulsion. The protonation state of histidine, clorobiocin, and SLU-258 could be one of the factors that could contribute to different binding poses for both ligands and thus the different quenching behavior observed when potassium iodide was added.

The determination of Site IV as the probable AcrA binding site for the efflux pump inhibitors clorobiocin and SLU-258 provides only a coarse description of ligand binding. The precise binding modes or poses are not able to be discerned by our combination of blind ensemble docking and tryptophan fluorescence. Moreover, standard MD simulations rely on fixed protonation states and thus pH-dependent phenomena pose a challenge for simulation.[165] A specialized computational method referred to as constant-pH MD simulations has been developed to explicitly incorporation protonation state changes and it has recently been applied to sample the O-L transition in the inner membrane transporter AcrB.[165, 166] While constant-pH could be applied to discern binding mode differences for both inhibitors bound to Site IV of AcrA, the binding modes could still not be experimentally verified. To solve this problem in the future, an X-ray co-crystal structure of both inhibitors to the truncated construct of AcrA lacking the MP domain could be solved. The MP domain is unlikely to be solved by X-ray crystallography due to its flexibility.[42, 44] With a crystal structure based on the

orientation of the side chains and nonbonding interactions, the protonation states could be inferred and binding pose differences between the two inhibitors could be reconciled with the fluorescence data. MD simulation could be carried out on the crystallographic poses and further rationalized with the fluorescence data. An enhanced sampling method such as supervised MD, adaptive biasing force, or umbrella sampling could also be implemented on the crystallographic poses to estimate the free energy landscape of both inhibitors and dissect the differences between them.[107, 167] In the absence of crystal structures, multidimensional protein NMR could potentially be carried out on the truncated construct with both inhibitors and distance restraints using NOESY could be derived. The restraints could then be used to determine the protein-ligand complex.[168] A recent NMR method has determined the protein-ligand complex for a ligand with millimolar affinity.[169] All the proposals are options that would extend and continue the work provided here.

Nevertheless, refinement of models of inhibitor binding to Site IV provided here may still form the basis for identifying structure-activity relationships and designing improved inhibitors with greater antibiotic potentiation activity using computer-aided drug design.

CHAPTER III
DISCOVERY OF NEW EFFLUX PUMP INHIBITORS WITH A NOVEL CHEMICAL SCAFFOLD THAT INTERACT WITH THE *ESCHERICHIA COLI* EFFLUX PUMP ADAPTOR ACRA

The results from this chapter are in the process of being prepared for publication. I designed the cheminformatics and docking workflow that predicted the 49 compounds that were subsequently tested by in vivo and in vitro experiments. I also analyzed the results and reconciled the calculations and the experiments to identify a novel chemical scaffold that binds AcrA and potentiates efflux pump substrates. Experiments were carried out by Helen Zgurskaya's lab at the University of Oklahoma.

Abstract

The permeability barrier of the outer membrane and multidrug efflux are two major contributors to antibiotic resistance in Gram-negative bacteria. Previously, a Gram-positive antibiotic obtained broad spectrum activity by addition of an ammonium group and was found to permeate the outer membrane. It was further found that small molecules which are long and planar, rigid, polar, and amphiphilic have a greater tendency to accumulate across the outer membrane. Thus, we have filtered 13 million 3D structures of small molecules available on the ZINC15 database using structural descriptors that identify compounds with characteristics likely to permeate the outer membrane. We then docked 1,427 compounds to four possible binding sites on AcrA and selected the top compounds from all four sites for experimental validation. Seven compounds were found to potentiate the antibiotics and efflux pump substrates novobiocin and erythromycin in *Escherichia coli* and bind AcrA in vitro. All seven compounds have an amino-cyclobutyl pyrimidine scaffold. Lack of this scaffold fails to potentiate antibiotics. However,

the seven compounds did not permeate the outer membrane which implies that additional factors are needed to understand outer membrane permeability. In addition, the seven compounds did not increase the accumulation of the fluorescent probe and efflux pump substrate Hoechst H33342 implying the compounds do not inhibit efflux, but the lack of antibacterial activity and lack of potentiation in efflux-deficient cells for 5 out of the 7 compounds implies that potentiation of novobiocin and erythromycin is efflux related. We propose using electron density docking that the seven compounds likely potentiate by displacement of the antibiotics from their binding site on AcrB.

Introduction

Multidrug antibiotic resistance is a global public health crisis that is leading to the deaths of thousands of people every year.[1] One of the primary causes of resistance in Gram-negative bacteria such as *Escherichia coli* and *Pseudomonas aeruginosa* is the overexpression of multicomponent molecular machines referred to as efflux pumps.[64] In *E. coli,* the efflux pump is a tripartite assembly called AcrAB-TolC and its homolog in *P. aeruginosa* is MexAB-OprM.[35]

Models of the assembled complexes of MexAB-OprM and AcrAB-TolC have been obtained using cryo-EM structures of AcrAB-TolC.[29, 170] The pumps contribute to multidrug resistance through a long-range allosteric transport mechanism.[39] An antibiotic traverses the outer membrane and first interacts with the access pocket of AcrB in the periplasm.[18] AcrB is a trimeric protein with transmembrane domains embedded in the inner membrane and periplasmic

domains that exist in the periplasm.[36] The binding of the antibiotic to the access pocket of AcrB results in a conformational change that reveals a new binding site referred to as the distal binding pocket.[18, 171] Transfer of a proton from the periplasm to Asp407 and Asp408 in the transmembrane domains of AcrB trigger another conformational change that collapses the distal binding pocket and ejects the antibiotic towards TolC for efflux out of the cell.[36, 166] The series of conformational changes in AcrB is referred to as a functional rotation mechanism.[18] Functional rotation of AcrB in the assembled complex results in changes in AcrA and TolC.[39] AcrA exists as a trimer of dimers in the assembled complex that contain spacious gaps between each dimer when no antibiotic is bound to AcrB.[39] These gaps are sealed during antibiotic binding to prevent leakage during efflux.[39] TolC is a trimeric protein composed of coiled-coil domains that form a closed funnel leading out of the cell.[29] The sealing of spacious gaps in AcrA leads to the opening of the funnel in TolC allowing the antibiotic to exit the cell.[39]

Drugs that potentiate antibiotics and inhibit efflux by AcrAB-TolC have been identified that interact with AcrA or AcrB.[66, 69] MBX2319 is one example of an inhibitor with a pyranopyridine scaffold that potentiates the antibiotics levofloxacin and minocycline across a spectrum of clinically relevant Gram-negative bacteria such as *Escherichia coli, Salmonella enterica,* and *Klebsiella pneumoniae*.[66] MBX2319 was found using X-ray crystallography to bind the distal pocket of AcrB.[66] A series of analogs were derived from MBX2319 that exhibited improved potentiation of levofloxacin.[65, 66] The analogs prevent efflux through AcrB and

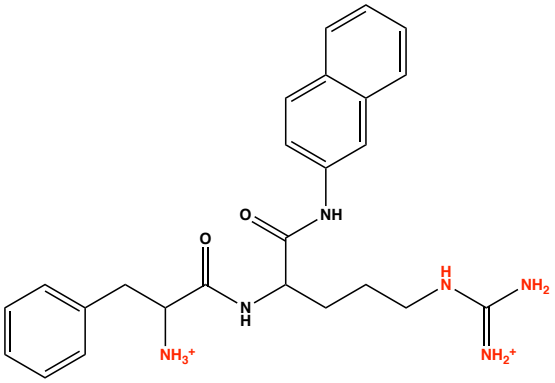
compete for the distal binding pocket with an antibiotic.[66] In contrast, inhibitors such as NSC60339 were found to inhibit efflux and change the structure of AcrA in vivo.[69] A combination of site-directed mutagenesis and fluorescence quenching identified the probable binding site of NSC60339 to AcrA.[172] Based on the binding site, NSC60339 could inhibit efflux through disruption of AcrAB-TolC assembly. Several analogs were derived from NSC60339 and found to have improved characteristics of an EPI (**Table 5**).[173]

Despite advances in the identification of inhibitors that inhibit multidrug efflux in Gram-negative bacteria, the ability to discover new antibiotics and inhibitors that function in Gram-negative bacteria is still limited.[10, 76] One limitation is the Gram-negative outer membrane that provides a permeability barrier to many compounds.[10] The outer membrane (OM) consists of an asymmetric hydrophobic lipid bilayer combined with polysaccharide groups that are cross-linked by divalent cations to create a charged external environment.[17, 174] The lipid bilayer of the OM contains outer membrane porins (OMP) such as OmpF and OmpC in *E. coli* that provide a selective barrier for compounds to enter the cell.[13] Recently, physico-chemical molecular descriptors have been identified for compounds that permeate the OM in *E. coli* and *P. aeruginosa*.[146, 175] One of those descriptors is the presence of an ammonium group.[146] The addition of ammonium was able to provide a Gram-positive antibiotic with broad-spectrum activity.[146] Other descriptors include rigidity (number of rotatable bonds), low globularity (long and planar), amphiphilicity, and polarity (high dipole moment).[146, 175] Long, rigid, amphiphilic, and polar molecules

with ammonium groups tend to be successful at bypassing the permeability barrier in Gram-negative bacteria.

MC-207,110 is one efflux pump inhibitor against *E. coli* and *P. aeruginosa* that exhibits many of the physicochemical properties mentioned above.[35] MC-207,110 potentiates the activity of levofloxacin by non-competitive inhibition of AcrAB-TolC unlike MBX2319.[62] Previous computational models suggested that MC-207,110 binds at a region called the G-loop on AcrB that separates the access and distal binding pockets.[40] The mutation of residues in the G-loop impairs efflux.[40] Surface plasmon resonance (SPR) experiments have also shown that MC-207,110 can bind AcrA with micromolar affinity.[69] In efflux-deficient cells, MC-207,110 can disrupt the structural integrity of the OM and increase the accumulation of levofloxacin.[35] MC-207,110 is predicted to be di-cationic at pH 7.4 according to ZINC15[75] and contains ammonium, two primary amines, and one secondary amine (**Figure 50**). The structure has a polar character (dipole moment > 8), low globularity (< 0.04), and is amphiphilic (amphiphilic moment > 4). These molecular descriptors are all indicative of a molecule that can permeate the OM in *E. coli*. One difference is that MC-207,110 is conformationally flexible with 10 rotatable bonds. Nevertheless, the high polarity and net positive charge from the ammonium and primary amines may have contributed to MC-207,110

A



B

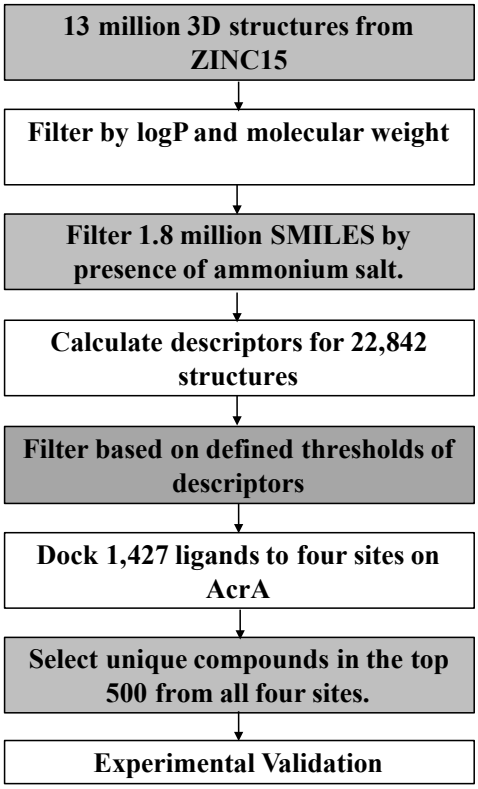
Globularity	**0.04**
Number of single rotatable bonds	**10**
Dipole moment	**8.15**
Amphiphilic moment	**4.87**

Figure 50. (A) Chemical structure of MC-207,110 with amines shown in red. (B) Molecular descriptors for MC-207,110 calculated with MOE 2016.

being able to permeate the OM. An antibiotic, gentamicin, contains 3 primary amines and can permeate the OM in WT and efflux-deficient cells.[142] The polarity and charge of MC-207,110 may prevent binding to the distal pocket which is lined with hydrophobic phenylalanine residues.[170] It may also help binding to AcrA. Inhibitors that bind AcrA such as NSC60339 exhibit similar physicochemical properties as MC-207,110: net positive charge, amphiphilic, low globularity, and the presence of an amine (**Table 7**).[173]

In this work, we aim to identify new inhibitors that can permeate the OM in *E. coli,* inhibit efflux, and interact with AcrA. We filtered 13 million 3D structures from the ZINC15 database by log P, the presence of an ammonium group, rigidity, globularity, dipole moment, and amphiphilic moment. We then docked the compounds to an ensemble of conformations of AcrA from molecular dynamics (MD) simulations to 4 possible binding sites: the probable binding site of NSC60339 and three other possible sites that lowered the MIC of erythromycin when residues at those sites were previously mutated (**Table 8**).[172] Traditional docking algorithms do not incorporate receptor flexibility into their calculations[126], but ensemble docking uses an ensemble of representative conformations of a protein and docks a small molecule to all conformations to mimic a conformational selection mechanism.[126] We selected the unique compounds identified in the top 500 of all docking poses from all four binding sites for experimental validation (**Table 10**).

Table 10. Compound Selection Workflow



Generation of small molecule library

The ZINC15 database contained 13,732,880 3D structures of small molecules as of November 26, 2018, in their dominant protonation state(s) at pH 7.4.[75] Antibiotics tend to have a higher molecular weight and a lower log P value than other classes of drugs[76]; therefore, we removed compounds with a log P calculated by ZINC15 greater than 3 resulting in 1,832,894 small molecules. We selected only the small molecules with an ammonium group by identifying the SMILES tag [NH3+]. This selection was chosen because previous work has shown that antibiotics with an ammonium group bypass the OM better than other functional groups.[146] We then computed the molecular globularity, number of single rotatable bonds, dipole moment, and amphiphilic moment for 22,842 small molecules using MOE 2016.[100] Alternative protonation and tautomeric states at pH 7.4 for each molecule were included.

Filtering by molecular descriptors

The molecular globularity, glob, defines the deviation of the molecular shape of the compound from a perfect sphere.[146] The dipole moment is an estimate of the degree of partial charge separation.[105] The dipole moment is estimated using the PEOE method which estimates electrostatic properties from the molecular topology.[175] The number of rotatable single bonds, b_1rotN, is the number of bonds not found in ring systems and consisting only of single bonds.[100] The amphiphilic moment, vsurf_A is a vector that points from the center of the hydrophobic to the hydrophilic domain of a molecule.[146]The length of the vector is

the strength of the amphiphilic moment.[146] Small molecules that permeate the OM should have a low globularity (glob<=0.14), be rigid (b_1rotN <= 4), polar (dipole >= 5.5), and amphiphilic (vsurf_A >= 4.0). The threshold for all four values was chosen by previous work.[146, 175] A total of 1,427 compounds satisfied all four thresholds.

Ensemble docking

We built a homology model of AcrA using a previously published protocol.[172] We ran a 50 nanosecond MD simulation of the model and extracted 29 conformations using RMSD clustering.[172] The simulation methodology is available from previously published work and described in the previous chapter.[172] We docked 1,427 compounds to all 29 conformations of AcrA using Autodock VinaMPI.[138] Partial charges calculated from AMSOL by the ZINC15 database were used for each compound.[75] All compounds were docked to 4 binding sites. All four sites were shown previously to be possible binding sites on AcrA for small molecules.[172] The docking search space for each site was specified by the center-of-geometry of a single residue at the center. The dimensions for each space was 25 Å x 25 Å x 25 Å with exhaustiveness of 10. For the site I, site II, site III, and site IV, the following residues were selected, respectively: E67, K241, I343 and I252, and F81 and F254. All residues were selected based on previously published work and described in the previous chapter.[172] For each site, we sorted the top 500 poses by their docking score, an estimate of the binding free energy.[130] We then selected only the unique compounds that were in the top 500 poses of all four

sites. A total of 49 compounds were suggested for experimental validation, but only 34 were tested due to commercial availability.

Electron density docking

To test whether the six compounds that potentiate erythromycin could inhibit efflux by competitive inhibition, we performed electron density docking with MOE 2016.[100] The 11839473 was not docked to AcrB since the modeled structure from ZINC15 is identical to 65071797 (**Figure 51**). Erythromycin was determined to bind the access binding pocket of AcrB by X-ray crystallography (PDB 3AOC).[38] The residues of the access binding pocket that surround erythromycin include S79, T91, S135, F136, M573, M575, F615, G616, F617, A618, G619, I626, F666, E673, L674, D681, E683, G826, G861, and M862. We placed the six compounds into the access binding pocket defined by the residues mentioned previously using the crystal structure of AcrB bound to erythromycin. Erythromycin was removed and docked with the same procedure. The compounds were placed using the electron density of the crystal structure and assigned an energy score to define the agreement between the simulated density of the docked compound and the experimental electron density. The more favorable, lower the energy, the better the agreement between the densities. The better the agreement of the densities, we predict a greater likelihood that the compound could inhibit by competitive inhibition through the access binding pocket. Docking of erythromycin had the lowest score (**Table 11**). After placement, the compounds were refined using an induced fit protocol that adjusts the ligand pose by the inclusion of side chain

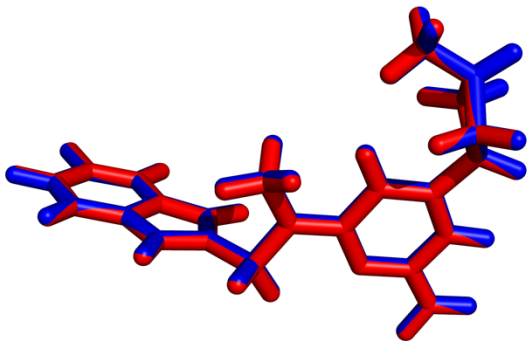


Figure 51. Alignment of the modeled structures from ZINC15 for 65071797 (blue) and 11839473 (red).

Table 11. Electron Density Placement Scores for erythromycin (ERY) and the six compounds.

Compound	Placement score (kcal/mol)
ERY	-98.7
56871955	-94.0
985577577	-88.0
65071797	-86.5
24123034	-86.0
36287038	-83.7
58997260	-77.9

flexibility in the binding pocket. Refinement by induced fit produced 5 poses scored using the GBVI scoring function in MOE 2016.[176] The selected pose for each compound had the lowest placement score. Structures for each compound with a protonated/deprotonated nitrogen in the pyrimidine ring were docked. Both structures were taken from the ZINC15 database.[75] Two protonation states were included for erythromycin and built using MOE 2016.[100] Docking was carried out with the AMBER10-EHT force field in MOE 2016 with AM1-BCC partial charges assigned for the ligands.[177]

7 compounds potentiate novobiocin and erythromycin, bind AcrA, but do not permeate the outer membrane

Out of 34 compounds tested, we identified seven compounds that potentiate the antibiotics and the efflux pump substrates novobiocin and erythromycin in WT-Pore cells (**Table 12**). WT-Pore cells have ~2.4 nm size pores in the outer membrane (OM) that allow small molecules to artificially overcome the permeability barrier without affecting efflux.[142] Despite filtering the ZINC15 database by structural descriptors that correlate with OM accumulation, no or minimal potentiation of novobiocin and erythromycin was observed in WT cells compared to WT-Pore (**Table 13**). A lack of potentiation indicates that the compounds are impermeable to the outer membrane. Additional structural descriptors may still be needed to adequately predict outer membrane permeability.

Potentiation is quantified by a quantity referred to as the minimal

Table 12. Antibiotic Susceptibility and Potentiation of Top Hits in WT-Pore Cells.

Compounds	MIC WT-Pore μM	MIC ΔTolC-Pore μM	MPC_4 WT-Pore NOV μM	MPC_4 WT-Pore ERY μM	MPC_4 ΔTolC-Pore NOV μM	MPC_4 ΔTolC-Pore ERY μM	AcrA Binder?
24123034	≥200	50	25	12.5	100	100	yes
58997260	≥200	100	50	12.5	50	50	yes
36287038	≥200	200	50-100	25	>200	50	yes
56871955	≥200	200	50	50	200	100	yes
11839473	≥200	100	50-100	25	100	100	yes
65071797	≥200	200	25	25	100	100	yes
98577577	≥200	200	50	50	200	100	yes

Table 13. Potentiation of Top Hits in WT Cells

Compounds	MIC WT μM	MPC_4 WT NOV μM	MPC_4 WT ERY μM
24123034	≥200	200	200
58997260	≥200	>200	200
36287038	≥200	200	NA
56871955	≥200	>200	200
11839473	≥200	100	100
65071797	≥200	200	100
98577577	≥200	200	200

potentiating concentration (MPC).[61] We found that the seven compounds potentiate novobiocin and erythromycin by at least 4-fold; thus, the quantity is referred to as MPC_4. Novobiocin and erythromycin have minimal inhibitory concentrations (MIC) of 32 μg/mL and 16 μg/mL, respectively.[69] At concentrations of 8 μg/mL and 4 μg/mL for novobiocin and erythromycin with a specific concentration of one of the seven compounds, *E. coli* growth is inhibited indicative of potentiation by the compounds. The lower the MPC_4 value, the greater the potency of the compound. The compounds 24123034 and 65071797 are the most potent against novobiocin with concentrations of 25 μM (**Table 12**). 24123034, in addition to 58997260, is also the most potent against erythromycin with concentrations of 12.5 μM; however, 58997260 has an MPC_4 value of 50 μM in ΔTolC cells which is identical to the MPC_4 in WT-Pore cells with novobiocin (**Table 12**). 58997260 potentiates novobiocin in efflux-deficient, ΔTolC, indicative that the potentiation may not be due to interaction with AcrAB-TolC. None of the other compounds potentiate in efflux-deficient cells, which indicates that the potentiation of the remaining compounds is related to efflux inhibition.

All seven compounds not only potentiate novobiocin and erythromycin but also bind AcrA using surface plasmon resonance (SPR) (**Figure 52**). AcrA binding with SPR confirms the docking predictions that the compounds could bind AcrA, but cannot provide details about the binding site(s) of the compounds. AcrA binding also implies that potentiation could be due to efflux inhibition by disrupting the assembly of the pump similar to NSC60339 discovered previously (**Figure 26**).

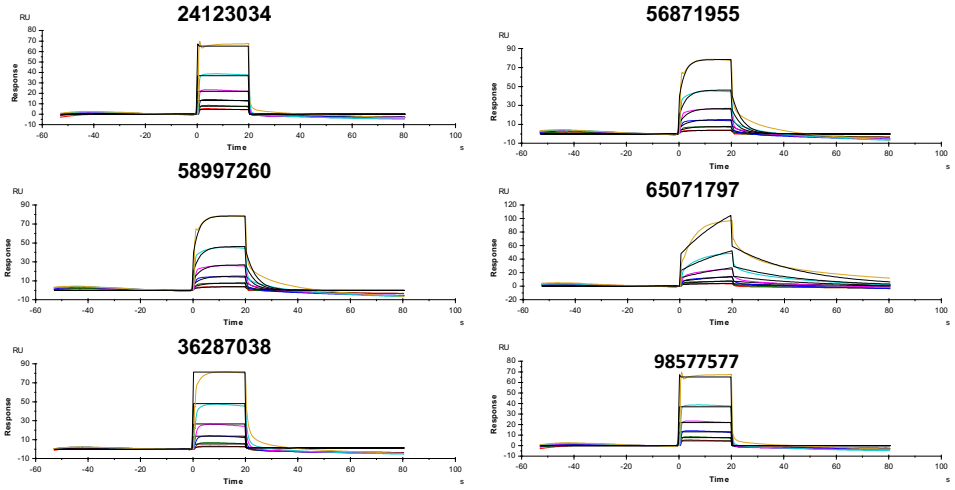


Figure 52. SPR curves for the six compounds that bind AcrA. Compound 11839473 is identical to 65071797**.**

The lack of intrinsic antibacterial activity also implies that potentiation is likely not disrupting the proton gradient across the inner membrane. Disruption of the proton gradient would indicate that a compound would have off-target effects a part from AcrAB-TolC inhibition. The potentiation of novobiocin and erythromycin and AcrA binding by the seven compounds thus appears to correlate with efflux inhibition. Efflux inhibition for most efflux pump inhibitors (EPIs) is monitored by the accumulation or increase in fluorescence of a dye referred to as Hoechst H33342.[62] Hoechst H33342 is an AcrAB-TolC substrate that enters the cell and intercalates with DNA increasing fluorescence.[62] WT cells with active efflux eject the dye from the cell; thus, a decrease in fluorescence is observed. The addition of a potential EPI in increasing concentrations should lead to an increase in fluorescence if the compound inhibits AcrAB-TolC. The increase in fluorescence indicates that more of the dye can remain in the cell to intercalate with DNA. For all seven compounds, none increased the fluorescence of the dye indicative that the efflux of the dye is not disrupted by the addition of each compound (**Figure 53**).

7 compounds may inhibit efflux competitively through interaction with AcrB in the access binding pocket

The ability of the compounds to potentiate known efflux pump substrates, lack of intrinsic antibacterial activity, and binding AcrA imply that the compounds possess some EPI-like characteristics despite the lack of accumulation of Hoechst H33342. One plausible explanation is that the compounds do not inhibit the



Figure 53. Lack of accumulation of the fluorescent probe Hoechst H33342 for the six compounds that bind AcrA. Compound 11839473 is identical to 65071797.

assembly of the pump through binding AcrA analogous to NSC60339, but prevent novobiocin and erythromycin from being effluxed through competitive inhibition. The compounds could bind at the same binding pocket on AcrB as novobiocin and erythromycin; thus, displacing the antibiotics and allowing them to remain in the cell without impairing efflux. Currently, no crystal structure of AcrB with novobiocin exists, but erythromycin has been shown to bind the access binding pocket of AcrB.[38]

To predict whether six of the seven compounds could occupy the binding pocket of AcrB, docking of the six compounds was conducted by placement and scoring of the compounds into the access binding pocket using the available electron density map from the AcrB crystal structure with erythromycin (ERY) bound using MOE 2016. 11839473 was not docked since the modeled structure from ZINC15 was identical to 65071797 (**Figure 51**). ERY was removed from the binding pocket and subsequently docked and scored. Unsurprisingly, the placement score of ERY into the electron density of the access pocket of AcrB was the lowest energy compared to the other compounds; thus, serving as a reference for our calculations. The agreement between the crystallographic and docking pose of ERY had an RMSD of 1.6 Å (**Figure 54**). The disagreement between the poses may due to the large size and flexibility of the molecule. 56871955 has the lowest placement score of all six compounds and is predicted to bind the access pocket by hydrogen bonding interaction with E673 and in proximity to F664 and F666 (**Table 11**). 98577577 and 24123034 were also predicted to form a hydrogen

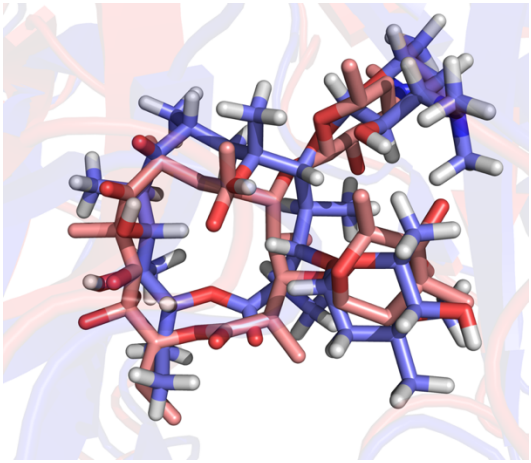


Figure 54. Alignment of the crystallographic pose of erythromycin (pink) with the best-scoring docked pose (blue). The RMSD of the alignment was 1.6 Å.

bond with E673 and reside near F664 and F666 (**Figure 55**). E673, F664, and F666 are functionally relevant for efflux in that previous mutagenesis to alanine resulted in increased antibiotic susceptibility and disruption of efflux.[178] The ability of 56871955, 98577577, and 24123034 to form interactions and reside near these three residues analogous to ERY indicates that these three compounds could bind the access binding pocket and displace ERY to potentiate its activity. 65071797, 36287038, and 58997260 are predicted to interact above E673, F664, and F666 and bind in between the residues F615 and R620 (**Figure 55**). The residues in between F615 and R620 include residues F617 and G619. These residues correspond to a region on AcrB referred to as the G-loop or switch-loop.[38, 40] The G-loop acts as a gate between the access and distal binding pockets.[40, 179] Mutations of F615 and F617 into alanine have been shown to impair efflux and increase antibiotic susceptibility.[180] Moreover, a G616N mutation has been shown to impair the efflux and transport of large drugs including erythromycin.[181]

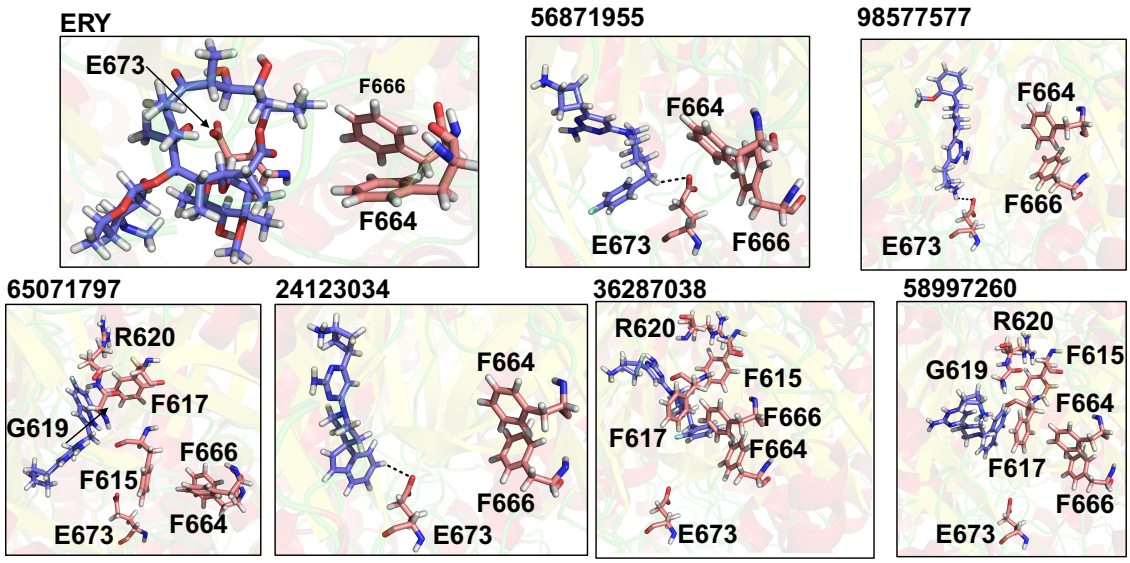


Figure 55. The six compounds that bind AcrA may bind AcrB and reside near functionally important residues of the access binding pocket (E673+F664+F666) or residues of the G-loop (F615+F617+G619+R620). All residues listed except R620, to the best of my knowledge, have been shown previously to affect drug transport and efflux.

The predicted binding of the six compounds by docking to the access pocket using the electron density map reveals that the compounds could interact with key functional residues at the access pocket and the G-loop (**Figure 55**). The results provide molecular details of how the compounds could potentiate erythromycin by displacement from its binding site without increasing fluorescence accumulation. The compounds don't displace Hoechst H33342, but novobiocin and erythromycin. We expect that these results are also applicable to novobiocin despite the absence of an AcrB crystal structure with novobiocin bound. Novobiocin is known to bind AcrB.[42] A molecule that enters the periplasm to bind AcrA can only interact with AcrB through two known channels that both result in binding the access binding pocket before efflux.[37] Thus, if the compounds can displace erythromycin by interacting with residues in the access pocket or hinder efflux by binding at the G-loop, then it can do the same for novobiocin.

Aminocyclobutyl pyrimidine scaffold is required for potentiation of novobiocin and erythromycin

An interesting feature of these 7 compounds that potentiate antibiotics and bind AcrA is that they all contain the same core scaffold (**Figure 56**). All the compounds contain an aminocyclobutyl pyrimidine scaffold (**Table 14**). The scaffold appears to be required for antibiotic potentiation, but not for binding AcrA. Compounds such as 36579393 potentiate novobiocin and erythromycin with MPC_4 values of 50 μM.

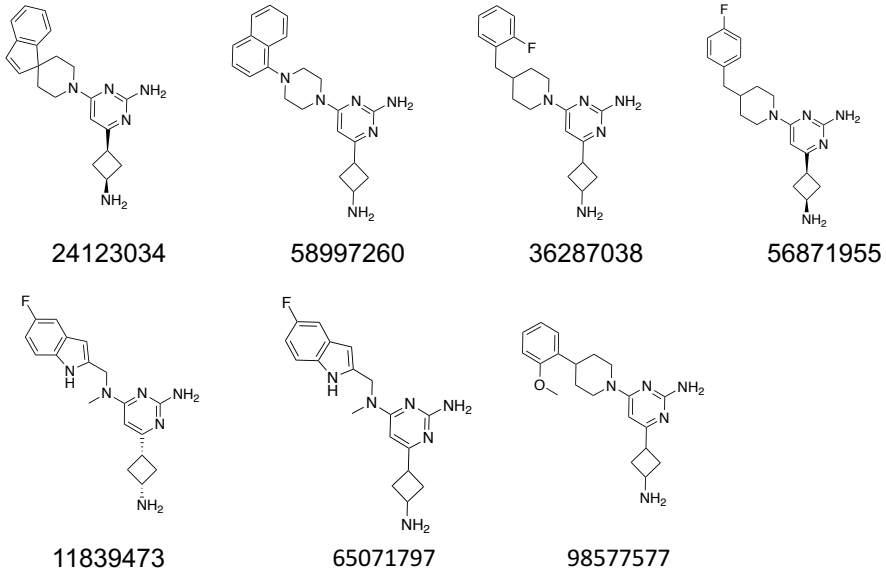
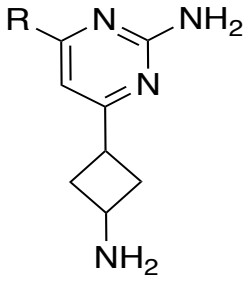
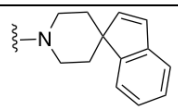
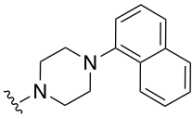
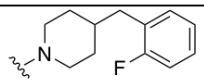
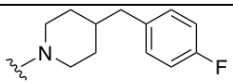
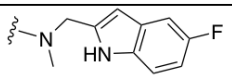
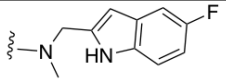
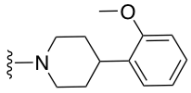


Figure 56. Chemical structures of compounds that potentiate novobiocin and erythromycin and bind AcrA.

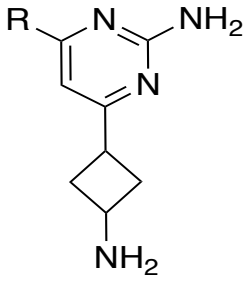
Table 14. Structure-activity relationship (SAR) of compounds that bind AcrA.



R	WT-Pore MPC_4 (μM) NOV	WT-Pore MPC_4 (μM) ERY
 24123034	25	12.5
 58997260	50	12.5
 36287038	50-100	25
 56871955	50	50
 11839473	50-100	25
 65071797	25	25
 98577577	50	50

Compounds such as 36579393 potentiate novobiocin and erythromycin with MPC_4 values of 50 μM and 25 μM, respectively, but do not bind AcrA (**Table 15**). When this scaffold is removed such as in 55628364, no potentiation of novobiocin or erythromycin is observed (**Table 16**). When the scaffold is modified such as alteration of the six-membered pyrimidine ring in 81717872 to a five-membered ring, no potentiation is observed (**Table 16**). In 80737104, the primary amine is removed from the pyrimidine ring and no potentiation is observed for novobiocin (**Table 16**). The conservation of the aminocyclobutyl group for AcrA binding and antibiotic potentiation appears to at least be qualitatively consistent with docking predictions. As a representative example, we selected the best-scoring compound, 56871955, from AcrB docking to the access binding pocket to observe how this same compound could interact with one of the four possible binding sites on AcrA (**Table 11**). We observed that the hydrogen bonding interactions appear to be localized to the aminocyclobutyl scaffold in all four sites (**Figure 57**). We see a similar trend when 56871955 binds the access pocket of AcrB (**Figure 58**). For AcrA and AcrB, the fluorine group appears to be exposed to solvent and/or uninvolved in the formation of interactions necessary for binding; thus, modification of this group may be an initial step towards developing new analogs with an aminocyclobutyl pyrimidine scaffold that potentiates antibiotics. A continued structure-activity relationship to further explore this scaffold could lead to new inhibitors that potentiate antibiotics through competitive or allosteric inhibition with AcrB or AcrA, respectively.

Table 15. Structures with the aminocyclobutyl pyrimidine scaffold that do not bind AcrA



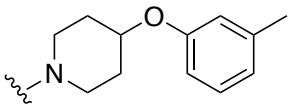
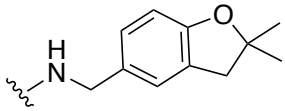
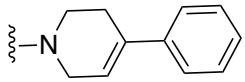
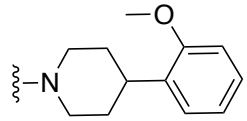
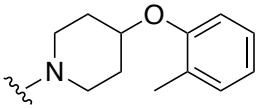
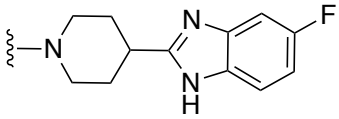
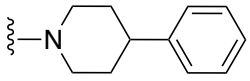
R	WT-Pore MPC_4 (μM) NOV	WT-Pore MPC_4 (μM) ERY
 83745449	100	50
 2158002	200	100
 24695708	100	100
 90425405	200	100
 40735676	100	100
 99815217	>200	>200
 87676550	200	200

Table 15. Continued.

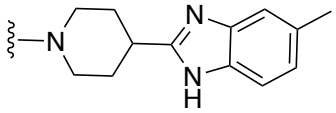
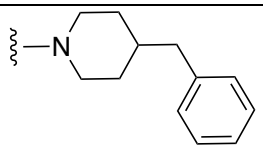
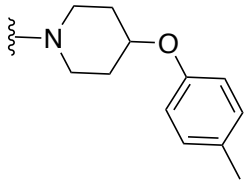
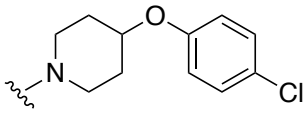
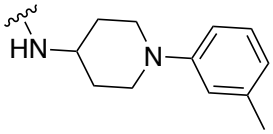
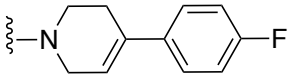
R	WT-Pore MPC_4 (μM) NOV	WT-Pore MPC_4 (μM) ERY
 41326066	100	200
 58871939	50	100
 88098678	50-100	200
 36579393	50	25
 45271910	100	100
 23380367	50	100

Table 16. Structures of compounds that do not bind AcrA or potentiate antibiotics

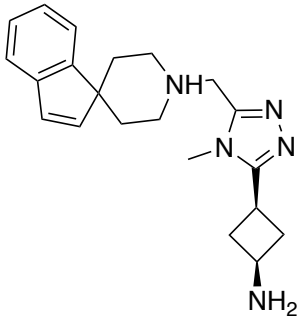
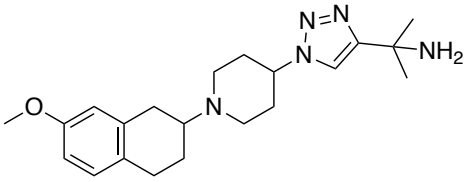
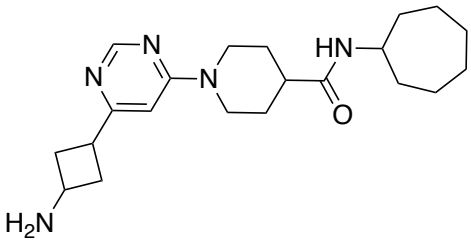
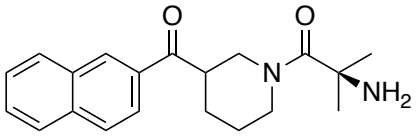
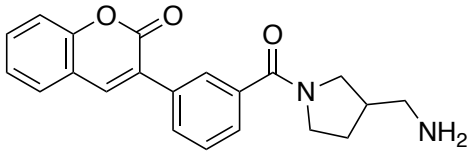
Compound	WT-Pore MPC_4 NOV (μM)	WT-Pore MPC_4 ERY (μM)	AcrA Binder
 81717872	200	NA	no
 47736881	>200	NA	no
 80737104	>200	NA	no
 65836564	>200	NA	no
 48466971	>200	NA	no

Table 16. Continued.

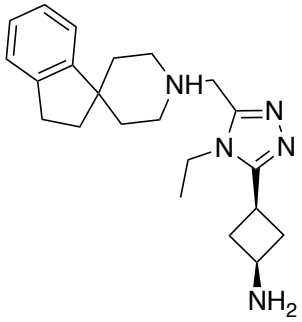
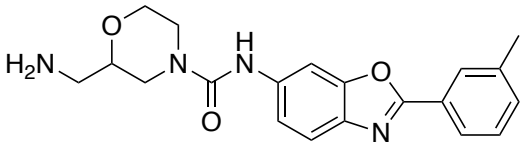
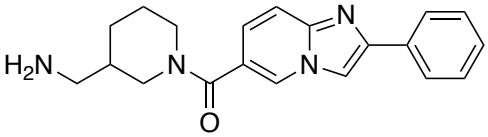
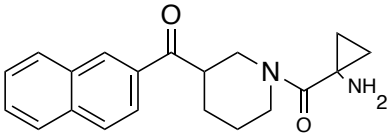
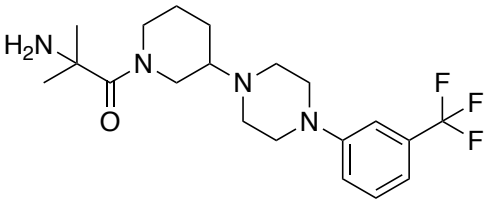
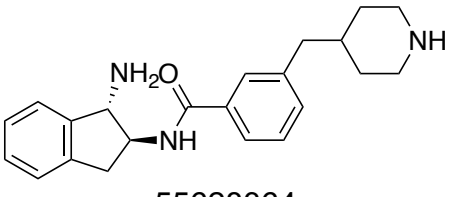
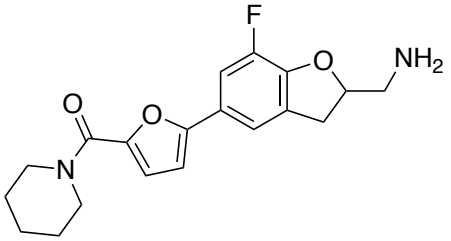
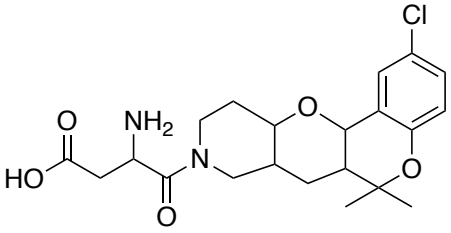
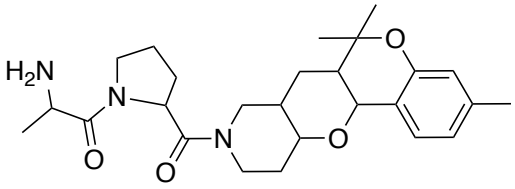
Compound	WT-Pore MPC_4 (μM) NOV	WT-Pore MPC_4 (μM) ERY	AcrA Binder
 29404228	>200	NA	no
 53100585	>200	NA	no
 33910334	>200	NA	no
 84453338	>200	NA	no
 65790289	>200	NA	no
 55628364	>200	>200	no

Table 16. Continued.

Compound	WT-Pore MPC_4 (μM) NOV	WT-Pore MPC_4 (μM) ERY	AcrA Binder
 84049996	>200	NA	no
 BDG33905166	NA	>200	NA
 BDG33905331	NA	>200	NA

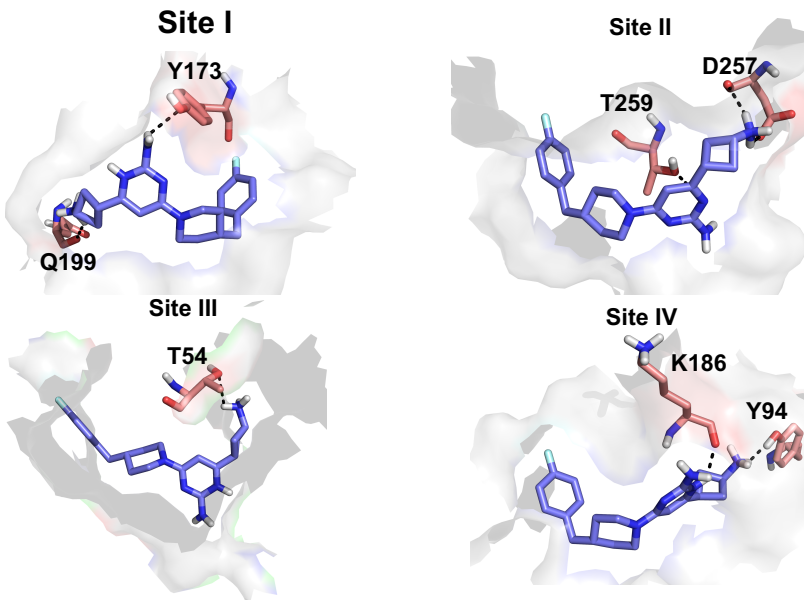


Figure 57. Best-scoring docking poses for 56871955 bound to AcrA at Site I, II, III, and IV.

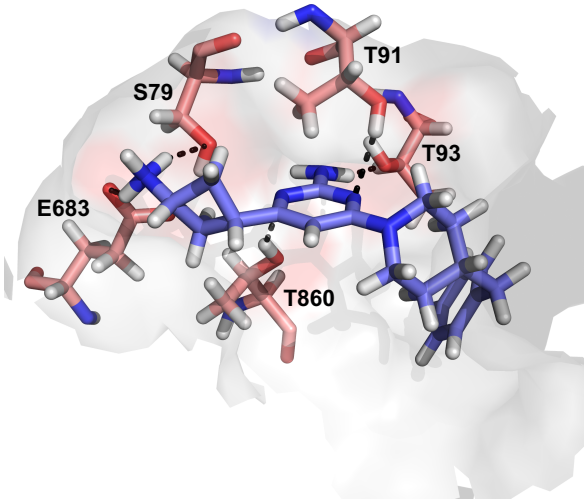


Figure 58. Contacts between 56871955 and AcrB are extensive for the aminocyclobutyl pyrimidine scaffold. The fluorine group attached to the phenyl ring appears to be unimportant for binding to AcrB.

CONCLUSIONS, SIGNIFICANCE, AND FUTURE DIRECTIONS

We have for the first time identified efflux pump inhibitors that interact with the periplasmic component AcrA of the AcrAB-TolC efflux pump in *Escherichia coli*. We have identified inhibitors using a combination of virtual screening, antibiotic potentiation, binding, and fluorescence accumulation assays. We found that one of the inhibitors, NSC60339, can change the structure of AcrA in vivo using trypsin proteolysis. No previous inhibitor shares this mechanism of inhibition of AcrAB-TolC. Regardless, NSC60339 was still unable to bypass the outer membrane (OM) of *E. coli* in wild-type cells.

Further development of a structure-activity relationship of NSC60339 identified at least four analogs with improved OM permeability and equal or improved potency against novobiocin and erythromycin. However, the binding site(s) on AcrA was not experimentally validated for NSC60339 or any of the analogs. We thus performed blind docking calculations using multiple conformations of an improved AcrA homology model in parallel with site-directed mutagenesis and tryptophan fluorescence spectroscopy. We deduced that the likely binding site for at least two of the discovered inhibitors, NSC60339 and NSC227186, was located between the β-barrel and lipoyl domains of AcrA. We further identified three other binding sites with residues that impair efflux upon mutagenesis. The disruption of efflux by mutagenesis implies that these residues are functionally relevant and thus could be targeted by new inhibitors to bind AcrA and disrupt efflux.

The four analogs derived from NSC60339 with improved OM permeability contain structural traits consistent with accumulation across the outer membrane. A previous study had found that small molecules which were long, planar, rigid, polar, and amphiphilic, and contained an ammonium group were more likely to bypass the outer membrane.[146] The four analogs contained these traits except for the ammonium group. To further discover new chemical scaffolds that bind AcrA, we filtered 13 million structures from the ZINC15 database for compounds that possessed these specific criteria. A total of 1,427 compounds were then docked to the four possible binding sites on AcrA and the top compounds that were predicted to bind all four sites were suggested for experimental validation. Seven compounds with an amino-cyclobutyl pyrimidine scaffold were found to bind AcrA and potentiate novobiocin and erythromycin. The compounds were not able to bypass the OM permeability barrier indicative that more information is needed to understand the structure-activity relationship of OM permeation. In addition, the compounds lacked antibacterial activity and five of the compounds lacked potentiation in efflux-deficient cells. The compounds also failed to increase the accumulation of Hoechst H33342 implying that the compounds do not inhibit efflux. However, since the compounds lack antibacterial activity and potentiation in efflux-deficient cells, it seems that the potentiation of novobiocin and erythromycin is efflux-dependent. We thus propose that the compounds bind the erythromycin binding pocket on AcrB and displace the antibiotic from the pump. The compounds then do not displace the binding of Hoechst H33342.

In this work, we have improved upon the modeling of AcrA using a multi-template approach that uses both the AcrA crystal structure and MP domain from the homologous MexA in *Pseudomonas aeruginosa*. AcrA has been shown to form a partially functionally complex with MexB; thus, AcrA and MexA are structurally and functionally similar.[182] The AcrA structure from cryo-EM determined after our modeling efforts used the MexA MP domain to fit into the cryo-EM density of AcrAB-TolC.[39]

Further significance of this work is that not only have we shown, for the first time, that efflux pump inhibitors can be identified to interact with AcrA, but they can be identified with computational methods specifically ensemble-based virtual screening and physicochemical descriptors. The previous two efflux pump inhibitors discussed here, MC-207,110 and MBX2319 were discovered by whole-cell high-throughput screens.[35, 62] With our approach, novel compounds can be initially identified in a less time-consuming and resource-intensive manner. In addition, the computational methods used were successful because of a novel experimental protocol that engineered *E. coli* cells to create 2.4 nm pores to allow for more diverse compounds to enter the periplasm.[142]

In early-stage drug discovery, the two initial stages are referred to as hit identification and lead optimization.[76] In hit identification, potential drug candidates are identified that function on your intended target. Afterwards, in lead optimization, the candidates can be modified to improve the binding and/or potency to the intended target to design a drug. Ultimately, our approach of utilizing comparative

modeling, ensemble-based virtual screening, and physico-chemical descriptors in combination with WT-Pore cells will help to accelerate the first phase of early-stage drug discovery in bacterial cells: hit identification and take advantage of the new regions and probable binding site identified on AcrA.

Further work still needs to be carried out to improve the potency for the lead optimization of the inhibitors with the aminocyclobutyl scaffold and analogs derived from NSC60339. To best achieve that goal, I propose that more extensive binding site characterization on AcrA and knowledge of outer membrane permeability is needed. The probable binding site on AcrA was indirectly inferred by tryptophan fluorescence spectroscopy, a non-atomic resolution experimental method. The method could not even distinguish the differences in the quenching of NSC60339 and NSC227186 when potassium iodide was added. The method could identify the likely site or region, but not the specific poses of the inhibitors. The differences in the poses could only be inferred by docking calculations. An X-ray or NMR structure could further reconcile the docking calculations with the tryptophan fluorescence spectroscopy data by providing atomic resolution. The biolayer interferometry experiment showed that an analog of NSC60339 could bind AcrA without the flexible MP domain. The MP domain was not determined in the X-ray structure of AcrA due to its intrinsic flexibility.[78] NSC60339 and NSC227186 could be potentially crystallized with the truncated construct of AcrA and the differences in the binding poses could be assessed.

Currently, the most potent efflux pump inhibitors to date, the pyranopyridines, have achieved their high potency in part due to the availability of co-crystal structures.[61] Thus, the determination of AcrA co-crystal structures could further improve the lead optimization process. With co-crystal structures, predicted relative free energies could be estimated using free energy perturbation (FEP) with finite-size corrections due to the ligands being charged.[183] Alternatively, application of the attach-pull-release (APR) method could be used to assess the absolute binding free energy.[184] FEP or APR in conjunction with co-crystal structures could propose new compounds with improved potency and potentially accelerate the lead optimization process, but the outer membrane permeation remains in question.

Since none of the seven compounds bypass the outer membrane even by filtering the ZINC15 database for optimal physicochemical descriptors, more knowledge is needed to explain the permeability of our inhibitors at the atomic level. Previously, metadynamics simulations have been used to estimate two-dimensional free energy profiles from a single pass through the outer membrane porin OmpF in *E. coli*, but these simulations were carried out in homogenous model membranes.[185] The web server CHARMM-GUI allows for the automated construction of native outer membranes in bacteria with proteins embedded.[186, 187] Classical MD simulations have already been carried out with OmpF embedded in a native outer membrane.[17] Two-dimensional metadynamics could thus be carried out to estimate the free energy of translocating our inhibitors across the highly

charged outer leaflet and OmpF porin. Modifications could then be proposed and assessed to observe if they lower the energetic barrier through the porin. A combination of metadynamics with relative binding free energies using X-ray co-crystal structures of AcrA could lead to new analogs with improved potency that bypass the outer membrane, potentiate antibiotics, and inhibit multidrug resistance.

REFERENCES

1. Levy, S. B.; Marshall, B., Antibacterial resistance worldwide: causes, challenges and responses. *Nat Med* **2004,** *10* (12 Suppl), S122-9.
2. Kohanski, M. A.; Dwyer, D. J.; Collins, J. J., How antibiotics kill bacteria: from targets to networks.(Report). *Nature Reviews Microbiology* **2010,** *8* (6), 423.
3. Phoenix, D. A., *Novel Antimicrobial Agents and Strategies*. 1st ed.. ed.; Weinheim : John Wiley & Sons, Incorporated: 2014.
4. Fleming, A., Penicillin, its practical application. Philadelphia, Blakiston: Philadelphia, 1946.
5. Lipsitch, M.; Singer, R. S.; Levin, B. R., Antibiotics in Agriculture: When Is It Time to Close the Barn Door? *Proceedings of the National Academy of Sciences of the United States of America* **2002,** *99* (9), 5752-5754.
6. Darwin, C., On the origin of species, 1859. Washington Square, N.Y. : New York University Press: Washington Square, N.Y., 1988.
7. Heather, K. A.; Justin, D.; Helena Huimi, W.; Karen, A. C.-H.; Julian, D.; Jo, H., Call of the wild: antibiotic resistance genes in natural environments. *Nature Reviews Microbiology* **2010,** *8* (4), 251.
8. Ruiz, J., Mechanisms of resistance to quinolones: target alterations, decreased accumulation and DNA gyrase protection. *Journal of Antimicrobial Chemotherapy* **2003,** *51* (5), 1109-1117.
9. Frere, J., BETA-LACTAMASES AND BACTERIAL-RESISTANCE TO ANTIBIOTICS. *Mol. Microbiol.* **1995,** *16* (3), 385-395.
10. Zgurskaya, H.; Lopez, C.; Gnanakaran, S., Permeability Barrier of Gram-Negative Cell Envelopes and Approaches To Bypass It. *ACS infectious diseases* **2015,** *1* (11), 512-522.
11. Bolla, J. M.; Alibert-Franco, S.; Handzlik, J.; Chevalier, J.; Mahamoud, A.; Boyer, G.; Kiec-Kononowicz, K.; Pages, J. M., Strategies for bypassing the membrane barrier in multidrug resistant Gram-negative bacteria. *FEBS letters* **2011,** *585* (11), 1682-90.
12. Du, D.; van Veen, H. W.; Luisi, B. F., Assembly and operation of bacterial tripartite multidrug efflux pumps. *Trends Microbiol* **2015,** *23* (5), 311-9.
13. Pages, J. M.; James, C. E.; Winterhalter, M., The porin and the permeating antibiotic: a selective diffusion barrier in Gram-negative bacteria. *Nature reviews. Microbiology* **2008,** *6* (12), 893-903.
14. Botos, I.; Majdalani, N.; Mayclin, Stephen j.; McCarthy, Jennifer g.; Lundquist, K.; Wojtowicz, D.; Barnard, Travis j.; Gumbart, James c.; Buchanan, Susan k., Structural and Functional Characterization of the LPS Transporter LptDE from Gram-Negative Pathogens. *Structure* **2016,** *24* (6), 965-976.
15. Snyder, D. S.; McIntosh, T. J., The Lipopolysaccaride Barrier: Correlation of Antibiotic Susceptibility with Antibiotic Permeability and Fluorescent Probe Binding Kinetics. *Biochemistry* **2000,** (39), 11777-11787.
16. Balusek, C.; Gumbart, J. C., Role of the Native Outer-Membrane Environment on the Transporter BtuB. *Biophysical journal* **2016,** *111* (7), 1409-1417.

17. Patel, D. S.; Re, S.; Wu, E. L.; Qi, Y.; Klebba, P. E.; Widmalm, G.; Yeom, M. S.; Sugita, Y.; Im, W., Dynamics and Interactions of OmpF and LPS: Influence on Pore Accessibility and Ion Permeability. *Biophysical journal* **2016,** *110* (4), 930-8.
18. Pos, K. M., Drug transport mechanism of the AcrB efflux pump. *Biochimica et biophysica acta* **2009,** *1794* (5), 782-93.
19. Silver, L., Challenges of Antibacterial Discovery. *Clinical Microbiology Reviews* **2011,** *24* (1), 71.
20. Du, D.; Wang-Kan, X.; Neuberger, A.; van Veen, H.; Pos, K.; Piddock, L.; Luisi, B., Multidrug efflux pumps: structure, function and regulation. *Nature reviews. Microbiology* **2018,** *16* (9), 523-539.
21. Viale, P.; Giannella, M.; Tedeschi, S.; Lewis, R., Treatment of MDR-Gram negative infections in the 21st century: a never ending threat for clinicians. *Current Opinion in Pharmacology* **2015,** *24*, 30-37.
22. Fraimow, H. S.; Tsigrelis, C., Antimicrobial resistance in the intensive care unit: mechanisms, epidemiology, and management of specific resistant pathogens. *Critical care clinics* **2011,** *27* (1), 163.
23. Gould, D., Escherichia coli recognition and prevention. *Primary Health Care (through 2013)* **2011,** *21* (8), 32-39.
24. E.coli outbreak traced to undercooked beef.(Brief Article). *Nation's Restaurant News* **2000,** *34* (16), 18.
25. Kaye, D., Multistate Outbreak of E.coli O157:H7 Infections Linked to Romaine Lettuce. *Clin. Infect. Dis.* **2018,** *67* (7), I-II.
26. João, E.; Matthew, P. M.; Seamus, E.; Marta, E., The Ins and Outs of RND Efflux Pumps in Escherichia coli. *Frontiers in microbiology* **2015,** *6*.
27. Merritt, M. E.; Donaldson, Jr., Effect of bile salts on the DNA and membrane integrity of enteric bacteria. *J. Med. Microbiol.* **2009,** *58* (12), 1533-1541.
28. Rosenberg, E. Y.; Bertenthal, D.; Nilles, M. L.; Bertrand, K. P.; Nikaido, H., Bile salts and fatty acids induce the expression of Escherichia coli AcrAB multidrug efflux pump through their interaction with Rob regulatory protein. *Molecular Microbiology* **2003,** *48* (6), 1609-1619.
29. Du, D.; Wang, Z.; James, N. R.; Voss, J. E.; Klimont, E.; Ohene-Agyei, T.; Venter, H.; Chiu, W.; Luisi, B. F., Structure of the AcrAB-TolC multidrug efflux pump. *Nature* **2014,** *509* (7501), 512-5.
30. Murakami, S.; Nakashima, R.; Yamashita, E.; Matsumoto, T.; Yamaguchi, A., Crystal structures of a multidrug transporter reveal a functionally rotating mechanism. *Nature* **2006,** *443* (7108), 173-179.
31. Nikaido, H.; Takatsuka, Y., Mechanisms of RND multidrug efflux pumps. *BBA - Proteins and Proteomics* **2009,** *1794* (5), 769-781.
32. Maxwell, A., The interaction between coumarin drugs and DNA gyrase. *Molecular Microbiology* **1993,** *9* (4), 681-686.
33. Pavlova, A.; Gumbart, J. C., Parametrization of macrolide antibiotics using the force field toolkit. *Journal of computational chemistry* **2015,** *36* (27), 2052-63.

34. Danelon, C.; Nestorovich, E. M.; Winterhalter, M.; Ceccarelli, M.; Bezrukov, S. M., Interaction of zwitterionic penicillins with the OmpF channel facilitates their translocation. *Biophysical journal* **2006,** *90* (5), 1617-27.
35. Lomovskaya, O.; Warren, M. S.; Lee, A.; Galazzo, J.; Fronko, R.; Lee, M.; Blais, J.; Cho, D.; Chamberland, S.; Renau, T.; Leger, R.; Hecker, S.; Watkins, W.; Hoshino, K.; Ishida, H.; Lee, V. J., Identification and characterization of inhibitors of multidrug resistance efflux pumps in Pseudomonas aeruginosa: novel agents for combination therapy. *Antimicrobial agents and chemotherapy* **2001,** *45* (1), 105-16.
36. Seeger, M. A.; Schiefner, A.; Eicher, T.; Verrey, F.; Diederichs, K.; Pos, K. M., Structural asymmetry of AcrB trimer suggests a peristaltic pump mechanism. *Science* **2006,** *313* (5791), 1295-8.
37. Zwama, M.; Yamasaki, S.; Nakashima, R.; Sakurai, K.; Nishino, K.; Yamaguchi, A., Multiple entry pathways within the efflux transporter AcrB contribute to multidrug recognition. *Nature communications* **2018,** *9* (1), 124-124.
38. Eicher, T.; Cha, H.-J.; Seeger, M. A.; Brandstätter, L.; El-Delik, J.; Bohnert, J. A.; Kern, W. V.; Verrey, F.; Grütter, M. G.; Diederichs, K.; Pos, K. M., Transport of drugs by the multidrug transporter AcrB involves an access and a deep binding pocket that are separated by a switch-loop. *Proceedings of the National Academy of Sciences of the United States of America* **2012,** *109* (15), 5687.
39. Wang, Z.; Fan, G.; Hryc, C. F.; Blaza, J. N.; Serysheva, II; Schmid, M. F.; Chiu, W.; Luisi, B. F.; Du, D., An allosteric transport mechanism for the AcrAB-TolC multidrug efflux pump. *Elife* **2017,** *6*.
40. Vargiu, A. V.; Nikaido, H., Multidrug binding properties of the AcrB efflux pump characterized by molecular dynamics simulations. *PNAS* **2012,** *109* (50), 20637-20642.
41. Eicher, T.; Seeger, M. A.; Anselmi, C.; Zhou, W.; Brandstätter, L.; Verrey, F.; Diederichs, K.; Faraldo-Gómez, J. D.; Pos, K. M., Coupling of remote alternating-access transport mechanisms for protons and substrates in the multidrug efflux pump AcrB. *eLife* **2014,** *3*, e03145.
42. Tikhonova, E. B.; Yamada, Y.; Zgurskaya, H. I., Sequential mechanism of assembly of multidrug efflux pump AcrAB-TolC. *Chemistry & biology* **2011,** *18* (4), 454-63.
43. Zgurskaya, H. I.; Yamada, Y.; Tikhonova, E. B.; Ge, Q.; Krishnamoorthy, G., Structural and functional diversity of bacterial membrane fusion proteins. *BBA - Proteins and Proteomics* **2009,** *1794* (5), 794-807.
44. Symmons, M. F.; Bokma, E.; Koronakis, E.; Hughes, C.; Koronakis, V., The assembled structure of a complete tripartite bacterial multidrug efflux pump. *Proceedings of the National Academy of Sciences of the United States of America* **2009,** *106* (17), 7173-8.
45. Kim, J. S.; Jeong, H.; Song, S.; Kim, H. Y.; Lee, K.; Hyun, J.; Ha, N. C., Structure of the tripartite multidrug efflux pump AcrAB-TolC suggests an alternative assembly mode. *Mol Cells* **2015,** *38* (2), 180-6.

46. Vassilis, K.; Andrew, S.; Eva, K.; Ben, L.; Colin, H., Crystal structure of the bacterial membrane protein TolC central to multidrug efflux and protein export. *Nature* **2000,** *405* (6789), 914.
47. Zgurskaya, H.; Nikaido, H., Cross-Linked Complex between Oligomeric Periplasmic Lipoprotein AcrA and the Inner-Membrane-Associated Multidrug Efflux Pump AcrB from Escherichia coli. *Journal of Bacteriology* **2000,** *182* (15), 4264-4267.
48. Zgurskaya, H. I.; Nikaido, H., AcrA is a highly asymmetric protein capable of spanning the periplasm. *Journal of Molecular Biology* **1999,** *285* (1), 409-420.
49. Xu, Y.; Lee, M.; Moeller, A.; Song, S.; Yoon, B. Y.; Kim, H. M.; Jun, S. Y.; Lee, K.; Ha, N. C., Funnel-like hexameric assembly of the periplasmic adapter protein in the tripartite multidrug efflux pump in gram-negative bacteria. *J Biol Chem* **2011,** *286* (20), 17910-20.
50. Xiaodong, S.; Muyuan, C.; Zhili, Y.; James, M. B.; Hans, W.; Isaac, F.; Heather, V.; Joanita, J.; Dijun, D.; Ben, F. L.; Steven, J. L.; Zhao, W., In situ structure and assembly of the multidrug efflux pump AcrAB-TolC. *Nature communications* **2019,** *10* (1), 1-6.
51. Tamura, N.; Murakami, S.; Oyama, Y.; Ishiguro, M.; Yamaguchi, A., Direct interaction of multidrug efflux transporter AcrB and outer membrane channel TolC detected via site-directed disulfide cross-linking. *Biochemistry* **2005,** *44* (33), 11115-11121.
52. Tsutsumi, K.; Yonehara, R.; Ishizaka-Ikeda, E.; Miyazaki, N.; Maeda, S.; Iwasaki, K.; Nakagawa, A.; Yamashita, E., Structures of the wild-type MexAB–OprM tripartite pump reveal its complex formation and drug efflux mechanism. *Nature communications* **2019,** *10* (1), <xocs:firstpage xmlns:xocs=""/>.
53. Anthony, W. P. F.; Salomé, L.; Arthur, N.; James, N. B.; Xiao-Chen, B.; Ui, O.; Satoshi, M.; Hendrik, W. V. V.; Ulrich, Z.; Sjors, H. W. S.; Ben, F. L.; Dijun, D., Structure of the MacAB–TolC ABC-type tripartite multidrug efflux pump. *Nature Microbiology* **2017,** *2* (7).
54. Song, S.; Kim, J.-S.; Lee, K.; Ha, N.-C., Molecular architecture of the bacterial tripartite multidrug efflux pump focusing on the adaptor bridging model. *Journal of Microbiology* **2015,** *53* (6), 355-364.
55. Krishnamoorthy, G.; Tikhonova, E. B.; Dhamdhere, G.; Zgurskaya, H. I., On the role of TolC in multidrug efflux: the function and assembly of AcrAB – TolC tolerate significant depletion of intracellular TolC protein. *Molecular Microbiology* **2013,** *87* (5), 982-997.
56. Lomovskaya, O.; Watkins, W., Inhibition of Efflux Pumps as a Novel Approach to Combat Drug Resistance in Bacteria. *J.Mol.Microbiol.Biotechnol* **2001,** *3* (2), 225-236.
57. Lomovskaya, O.; Bostian, K. A., Practical applications and feasibility of efflux pump inhibitors in the clinic—A vision for applied use. *Biochemical Pharmacology* **2006,** *71* (7), 910-918.

58. Wright, G. D., Resisting resistance: new chemical strategies for battling superbugs. *Chemistry & biology* **2000,** *7* (6), R127-R132.
59. Lomovskaya, O.; Lee, A.; Hoshino, K.; Ishida, H.; Mistry, A.; Warren, M. S.; Boyer, E.; Chamberland, S.; Lee, V. J., Use of a Genetic Approach To Evaluate the Consequences of Inhibition of Efflux Pumps in Pseudomonas aeruginosa. *Antimicrobial agents and chemotherapy* **1999,** *43* (6), 1340.
60. El Meouche, I.; Dunlop, M. J., Heterogeneity in efflux pump expression predisposes antibiotic-resistant cells to mutation. *Science (New York, N.Y.)* **2018,** *362* (6415), 686-690.
61. Lamut, A.; Peterlin Mašič, L.; Kikelj, D.; Tomašič, T., Efflux pump inhibitors of clinically relevant multidrug resistant bacteria. *Medicinal research reviews* **2019**.
62. Opperman, T. J.; Kwasny, S. M.; Kim, H. S.; Nguyen, S. T.; Houseweart, C.; D'Souza, S.; Walker, G. C.; Peet, N. P.; Nikaido, H.; Bowlin, T. L., Characterization of a Novel Pyranopyridine Inhibitior of the AcrAB Efflux Pump of Escherichia coli *Antimicrobial agents and chemotherapy* **2014,** *58* (2), 722-733.
63. Coldham, N.; Webber, M.; Woodward, M.; Piddock, L., A 96-well plate fluorescence assay for assessment of cellular permeability and active efflux in Salmonella enterica serovar Typhimurium and Escherichia coli. *The Journal of Antimicrobial Chemotherapy* **2010,** *65* (8), 1655.
64. Opperman, T. J.; Nguyen, S. T., Recent advances toward a molecular mechanism of efflux pump inhibition. *Frontiers in microbiology* **2015,** *6*, 421.
65. Nguyen, S. T.; Kwasny, S. M.; Ding, X.; Cardinale, S. C.; McCarthy, C. T.; Kim, H. S.; Nikaido, H.; Peet, N. P.; Williams, J. D.; Bowlin, T. L.; Opperman, T. J., Structure-activity relationships of a novel pyranopyridine series of Gram-negative bacterial efflux pump inhibitors. *Bioorganic & medicinal chemistry* **2015,** *23* (9), 2024-34.
66. Sjuts, H.; Vargiu, A. V.; Kwasny, S. M.; Nguyen, S. T.; Kim, H. S.; Ding, X.; Ornik, A. R.; Ruggerone, P.; Bowlin, T. L.; Nikaido, H.; Pos, K. M.; Opperman, T. J., Molecular basis for inhibition of AcrB multidrug efflux pump by novel and powerful pyranopyridine derivatives. *Proceedings of the National Academy of Sciences of the United States of America* **2016,** *113* (13), 3509-14.
67. Vargiu, A. V.; Ruggerone, P.; Opperman, T. J.; Nguyen, S. T.; Nikaido, H., Molecular Mechanism of MBX2319 Inhibition of Escherichia coli AcrB Multidrug Efflux Pump and Comparison with Other Inhibitors. *Antimicrobial agents and chemotherapy* **2014,** *58* (10), 6224-6234.
68. Takatsuka, Y.; Chen, C.; Nikaido, H., Mechanism of recognition of compounds of diverse structures by the multidrug efflux pump AcrB of Escherichia coli. *Proceedings of the National Academy of Sciences of the United States of America* **2010,** *107* (15), 6559-65.
69. Abdali, N.; Parks, J. M.; Haynes, K. M.; Chaney, J. L.; Green, A. T.; Wolloscheck, D.; Walker, J. K.; Rybenkov, V. V.; Baudry, J.; Smith, J. C.; Zgurskaya, H., Reviving Antibiotics: Efflux Pump Inhibitors That Interact with

AcrA, a Membrane Fusion Protein of the AcrAB-TolC Multidrug Efflux Pump *ACS infectious diseases* **2016,** *3*, 89-98.
70. Higgins, M. K.; Eswaran, J.; Edwards, P.; Schertler, G. F. X.; Hughes, C.; Koronakis, V., Structure of the Ligand-blocked Periplasmic Entrance of the Bacterial Multidrug Efflux Protein TolC. *Journal of Molecular Biology* **2004,** *342* (3), 697-702.
71. Gilardi, A. Novel approaches to identify small molecules modulating E. coli TolC protein function. PhD, Jacobs University Bremen, 2017.
72. Hirakawa, H.; Takumi-Kobayashi, A.; Theisen, U.; Hirata, T.; Nishino, K.; Yamaguchi, A., AcrS/EnvR represses expression of the acrAB multidrug efflux genes in Escherichia coli. *Journal of bacteriology* **2008,** *190* (18), 6276.
73. Eric, D. B.; Gerard, D. W., Antibacterial drug discovery in the resistance era. *Nature* **2016,** *529* (7586), 336.
74. Weist, S.; Süssmuth, R., Mutational biosynthesis—a tool for the generation of structural diversity in the biosynthesis of antibiotics. *Applied Microbiology and Biotechnology* **2005,** *68* (2), 141-150.
75. Sterling, T.; Irwin, J. J., ZINC 15--Ligand Discovery for Everyone. *Journal of chemical information and modeling* **2015,** *55* (11), 2324-37.
76. Payne, D. J.; Gwynn, M. N.; Holmes, D. J.; Pompliano, D. L., Drugs for bad bugs: confronting the challenges of antibacterial discovery. *Nature reviews. Drug discovery* **2007,** *6* (1), 29-40.
77. Marrone, T. J.; Briggs, a. J. M.; McCammon, J. A., STRUCTURE-BASED DRUG DESIGN:Computational Advances. *Annu. Rev. Pharmacol. Toxicol.* **1997,** *37* (1), 71-90.
78. Mikolosko, J.; Bobyk, K.; Zgurskaya, H. I.; Ghosh, P., Conformational flexibility in the multidrug efflux system protein AcrA. *Structure* **2006,** *14* (3), 577-87.
79. Boehr, D. D.; Nussinov, R.; Wright, P. E., The role of dynamic conformational ensembles in biomolecular recognition. *Nat Chem Biol* **2009,** *5* (11), 789-96.
80. Halperin, I.; Ma, B.; Wolfson, H.; Nussinov, R., Principles of docking: An overview of search algorithms and a guide to scoring functions. *Proteins: Structure, Function, and Genetics* **2002,** *47* (4), 409-443.
81. Fischer, E., Einfluss der Configuration auf die Wirkung der Enzyme. *Berichte der deutschen chemischen Gesellschaft* **1894,** *27* (3), 2985-2993.
82. Mobley, D. L.; Dill, K. A., Binding of Small-Molecule Ligands to Proteins: "What You See" Is Not Always "What You Get". *Structure* **2009,** *17* (4), 489-498.
83. Dill, K.; Bromberg, S., *Molecular Driving Forces: Statistical Thermodynamics in Chemistry and Biology*. Garland Science New York 2003.
84. Levinthal, C., Are there pathways for protein folding? . *Extrait du Journal de Chimie Physique* **1968,** *65*, 44-45.
85. Zwanzig, R.; Szabo, A.; Bagchi, B., Levinthal's paradox. *Proceedings of the National Academy of Sciences of the United States of America* **1992,** *89* (1), 20.

86. Bryngelson, J. D.; Onuchic, J. N.; Socci, N. D.; Wolynes, P. G., Funnels, pathways, and the energy landscape of protein folding: A synthesis. *Proteins: Structure, Function, and Bioinformatics* **1995,** *21* (3), 167-195.
87. Koshland, D. E., Application of a Theory of Enzyme Specificity to Protein Synthesis. *Proceedings of the National Academy of Sciences of the United States of America* **1958,** *44* (2), 98-104.
88. Dill, K. A.; Maccallum, J. L., The protein-folding problem, 50 years on. *Science (New York, N.Y.)* **2012,** *338* (6110), 1042.
89. Amaro, R. E.; Baudry, J.; Chodera, J.; Demir, Ö.; McCammon, J. A.; Miao, Y.; Smith, J. C., Ensemble Docking in Drug Discovery. *Biophysical journal* **2018**.
90. Sandak, B.; Wolfson, H. J.; Nussinov, R., Flexible docking allowing induced fit in proteins: insights from an open to closed conformational isomers. *Proteins* **1998,** *32* (2), 159.
91. Muhammed, M. T.; Aki-Yalcin, E., Homology modeling in drug discovery: Overview, current applications, and future perspectives. *Chemical biology & drug design* **2019,** *93* (1), 12.
92. Baker, D.; Sali, A., Protein Structure Prediction and Structural Genomics. *Science* **2001,** *294* (5540), 93-96.
93. Bradley, P.; Misura, K. M. S.; Baker, D., Toward high-resolution de novo structure prediction for small proteins. *Science (New York, N.Y.)* **2005,** *309* (5742), 1868.
94. MacKerell, A. D., Jr.; Bashford, D.; Bellot, M.; Dunbrack, R. L. J.; Evanseck, J. D.; Field, M. J.; Fischer, S.; Gao, J.; Guo, H.; Ha, S.; McCarthy, D. J.; Kuchnir, L.; Kuczera, K.; Lau, F. T. K.; Mattos, C.; Michnick, S.; Ngo, T.; Nguyen, D. T.; Prodham, B.; Reiher, W. E. I.; Roux, B.; Schlenkrich, M.; Smith, J. C.; Stote, R.; Straub, J.; Watanabe, M.; Wiorkiewicz-Kuczera, J.; Yin, D.; Karplus, M., All-Atom Empirical Potential for Molecular Modeling and Dynamics Studies of Proteins. *J. Phys. Chem. B* **1998,** *102*, 3586-3616.
95. Kaufmann, K. W.; Lemmon, G. H.; DeLuca, S. L.; Sheehan, J. H.; Meiler, J., Practically Useful: What the R osetta Protein Modeling Suite Can Do for You. *Biochemistry* **2010,** *49* (14), 2987-2998.
96. Ovchinnikov, S.; Park, H.; Varghese, N.; Huang, P.-S.; Pavlopoulos, G. A.; Kim, D. E.; Kamisetty, H.; Kyrpides, N. C.; Baker, D., Protein structure determination using metagenome sequence data. *Science (New York, N.Y.)* **2017,** *355* (6322), 294.
97. Hetunandan, K.; Baker, D., Robust and accurate prediction of residue–residue interactions across protein interfaces using evolutionary information. *eLife* **2014,** *3* (3).
98. Zimmermann, L.; Stephens, A.; Nam, S.-Z.; Rau, D.; Kübler, J.; Lozajic, M.; Gabler, F.; Söding, J.; Lupas, A. N.; Alva, V., A Completely Reimplemented MPI Bioinformatics Toolkit with a New HHpred Server at its Core. *Journal of Molecular Biology* **2018,** *430* (15), 2237-2243.

99. Sali, A.; Blundell, T. L., Comparative protein modelling by satisfaction of spatial restraints. *J Mol Biol* **1993,** *234* (3), 779-815.
100. *Molecular Operating Environment (MOE)* 2016; Chemical Computing Group Inc: 1010 Sherbooke St. West, Suite #910, Montreal, QC, Canada, H3A 2R7, 2013.08.
101. De Angelis, F.; Lee, J. K.; O'Connell, J. D.; Miercke, L. J. W.; Verschueren, K. H.; Srinivasan, V.; Bauvois, C.; Govaerts, C.; Robbins, R. A.; Ruysschaert, J.-M.; Stroud, R. M.; Vandenbussche, G., Metal-induced conformational changes in ZneB suggest an active role of membrane fusion proteins in efflux resistance systems. *Proceedings of the National Academy of Sciences of the United States of America* **2010,** *107* (24), 11038.
102. Chih-Chia, S.; Feng, L.; Michael, T. Z.; Kanagalaghatta, R. R.; Robert, L. J.; Edward, W. Y., Crystal structure of the CusBA heavy-metal efflux complex of Escherichia coli. *Nature* **2011,** *470* (7335), 558.
103. Larsson, P.; Wallner, B.; Lindahl, E.; Elofsson, A., Using multiple templates to improve quality of homology models in automated homology modeling. *Protein Science* **2008,** *17* (6), 990-1002.
104. Fan, H.; Mark, A. E., Refinement of homology-based protein structures by molecular dynamics simulation techniques. *Protein Science* **2004,** *13* (1), 211-220.
105. Nelson, D. L.; Cox, M. M., *Lehninger Principles of Biochemistry*. 6th ed.; W.H. Freeman: 2012.
106. Soto, C. S.; Fasnacht, M.; Zhu, J.; Forrest, L.; Honig, B., Loop modeling: Sampling, filtering, and scoring. *Proteins: Structure, Function, and Bioinformatics* **2008,** *70* (3), 834-843.
107. Salmaso, V.; Moro, S., Bridging Molecular Docking to Molecular Dynamics in Exploring Ligand-Protein Recognition Process: An Overview.(Report)(Brief article). *Frontiers in Pharmacology* **2018,** *9*.
108. Leuchter, J. D.; Green, A. T.; Gilyard, J.; Rambarat, C. G.; Cho, S. S., Coarse-Grained and Atomistic MD Simulations of RNA and DNA Folding. *Israel Journal of Chemistry* **2014,** *54* (8-9), 1152-1164.
109. Abraham, M.; Hess, B.; Spoel, D. V. D.; Lindahl, E., *GROMACS Reference Manual*. 5.1 ed.
110. Van Der Spoel, D.; Lindahl, E.; Hess, B.; Groenhof, G.; Mark, A. E.; Berendsen, H. J., GROMACS: fast, flexible, and free. *Journal of computational chemistry* **2005,** *26* (16), 1701-18.
111. Toxvaerd, S., Algorithms for canonical molecular dynamics simulations. *Molecular Physics* **1991,** *72* (1), 159-168.
112. Lewars, E. G., *Computational Chemistry : Introduction to the Theory and Applications of Molecular and Quantum Mechanics*. Dordrecht : Springer Science+Business Media B.V.: Dordrecht, 2011.
113. Huang, J.; MacKerell, A. D., Jr., CHARMM36 all-atom additive protein force field: validation based on comparison to NMR data. *Journal of computational chemistry* **2013,** *34* (25), 2135-45.

114. Jorgensen, W. L.; Chandrasekhar, J.; Madura, J. D.; Impey, R. W.; Klein, M. L., Comparison of simple potential functions for simulating liquid water. *Journal of Chemical Physics* **1983,** *79* (2).
115. Glättli, A.; Daura, X.; van Gunsteren, W. F., Derivation of an improved simple point charge model for liquid water: SPC/A and SPC/L. *The Journal of Chemical Physics* **2002,** *116* (22), 9811-9828.
116. Miyamoto, S.; Kollman, P. A., Settle: An analytical version of the SHAKE and RATTLE algorithm for rigid water models. *Journal of computational chemistry* **1992,** *13* (8), 952-962.
117. Lemkul, J. A.; Huang, J.; Roux, B.; MacKerell, A. D., Jr., An Empirical Polarizable Force Field Based on the Classical Drude Oscillator Model: Development History and Recent Applications. *Chemical reviews* **2016,** *116* (9), 4983-5013.
118. Mobley, D. L.; Dumont, É.; Chodera, J. D.; Dill, K. A., Comparison of Charge Models for Fixed-Charge Force Fields: Small Molecule Hydration Free Energies in Explicit Solvent. *The Journal of Physical Chemistry B* **2011,** *115* (5), 1329-1332.
119. Shirts, M. R.; Mobley, D. L.; Chodera, J. D.; Pande, V. S., Accurate and efficient corrections for missing dispersion interactions in molecular simulations. *The journal of physical chemistry. B* **2007,** *111* (45), 13052.
120. Phillips, J. C.; Braun, R.; Wang, W.; Gumbart, J.; Tajkhorshid, E.; Villa, E.; Chipot, C.; Skeel, R. D.; Kale, L.; Schulten, K., Scalable molecular dynamics with NAMD. *Journal of computational chemistry* **2005,** *26* (16), 1781-802.
121. Price, D. J.; Brooks, C. L., A modified TIP3P water potential for simulation with Ewald summation. *The Journal of Chemical Physics* **2004,** *121* (20), 10096-10103.
122. Darden, T.; York, D.; Pedersen, L., Particle mesh Ewald: An N·log(N) method for Ewald sums in large systems. *Journal of Chemical Physics* **1993,** *98* (12).
123. Shirts, M. R.; Pande, V. S., Solvation free energies of amino acid side chain analogs for common molecular mechanics water models. *The Journal of Chemical Physics* **2005,** *122* (13).
124. Yin, S.; Ding, F.; Dokholyan, N. V., Modeling Backbone Flexibility Improves Protein Stability Estimation. *Structure* **2007,** *15* (12), 1567-1576.
125. Vaccaro, L.; Koronakis, V.; Sansom, M. S. P., Flexibility in a Drug Transport Accessory Protein: Molecular Dynamics Simulations of MexA. *Biophysical journal* **2006,** *91* (2), 558-564.
126. Ellingson, S. R.; Miao, Y.; Baudry, J.; Smith, J. C., Multi-Conformer Ensemble Docking to Difficult Protein Targets. *The Journal of Physical Chemistry B* **2015,** *119* (3), 1026-1034.
127. Daura, X.; Gademann, K.; Jaun, B.; Seebach, D.; Van Gunsteren, W. F.; Mark, A. E., Peptide Folding: When Simulation Meets Experiment. *Angewandte Chemie International Edition* **1999,** *38* (1-2), 236-240.

128. Chen, Y.-C., Beware of docking! *Trends in Pharmacological Sciences* **2015,** *36* (2), 78-95.
129. Gaillard, T., Evaluation of AutoDock and AutoDock Vina on the CASF-2013 Benchmark. *Journal of chemical information and modeling* **2018,** *58* (8), 1697.
130. Trott, O.; Olson, A. J., AutoDock Vina: improving the speed and accuracy of docking with a new scoring function, efficient optimization, and multithreading. *Journal of computational chemistry* **2010,** *31* (2), 455-61.
131. Morris, G. M.; Goodsell, D. S.; Halliday, R. S.; Huey, R.; Hart, W. E.; Belew, R. K.; Olson, A. J., Automated Docking Using a Lamarckian Genetic Algorithm and an Empirical Free Energy Function. *Journal of computational chemistry* **1998,** *19* (14), 1639-1662.
132. Abagyan, R.; Totrov, M.; Kuznetsov, D., ICM—A new method for protein modeling and design: Applications to docking and structure prediction from the distorted native conformation. *Journal of computational chemistry* **1994,** *15* (5), 488-506.
133. Li, Z.; Scheraga, H. A., Monte Carlo-Minimization Approach to the Multiple-Minima Problem in Protein Folding. *Proceedings of the National Academy of Sciences of the United States of America* **1987,** *84* (19), 6611-6615.
134. Stefano, F.; Ruth, H.; Michael, E. P.; Michel, F. S.; David, S. G.; Arthur, J. O., Computational protein–ligand docking and virtual drug screening with the AutoDock suite. *Nature protocols* **2016,** *11* (5), 905.
135. Huey, R.; Morris, G. M.; Olson, A. J.; Goodsell, D. S., A semiempirical free energy force field with charge-based desolvation. *Journal of computational chemistry* **2007,** *28* (6), 1145-1152.
136. Totrov, M.; Abagyan, R., Flexible ligand docking to multiple receptor conformations: a practical alternative. *Current Opinion in Structural Biology* **2008,** *18* (2), 178-184.
137. Lin, J.-H.; Perryman, A. L.; Schames, J. R.; McCammon, J. A., Computational drug design accommodating receptor flexibility: the relaxed complex scheme. *Journal of the American Chemical Society* **2002,** *124* (20), 5632.
138. Ellingson, S. R.; Smith, J. C.; Baudry, J., VinaMPI: facilitating multiple receptor high-throughput virtual docking on high-performance computers. *Journal of computational chemistry* **2013,** *34* (25), 2212-21.
139. Schames, J. R.; Henchman, R. H.; Siegel, J. S.; Sotriffer, C. A.; Ni, H.; McCammon, J. A., Discovery of a novel binding trench in HIV integrase. *Journal of medicinal chemistry* **2004,** *47* (8), 1879.
140. Katherine, H.-W.; Dorothee, K., Dynamic personalities of proteins. *Nature* **2007,** *450* (7172), 964.
141. Brown, D., Antibiotic resistance breakers: Can repurposed drugs fill the antibiotic discovery void? *Nature Reviews Drug Discovery* **2015,** *14* (12), 821-832.

142. Krishnamoorthy, G.; Wolloscheck, D.; Weeks, J. W.; Croft, C.; Rybenkov, V. V.; Zgurskaya, H. I., Breaking the Permeability Barrier of Escherichia coli by Controlled Hyperporination of the Outer Membrane. *Antimicrobial agents and chemotherapy* **2016,** *60* (12), 7372-7381.
143. Marvin http://www.chemaxon.com/.
144. Claramunt, R. M.; Sanz, D. S.; CatalN, J.; Fabero, F.; Garca, N. A.; Foces-Foces, C. N.; Llamas-Saiz, A. L.; Elguero, J., N-aminoazoles. Part 2. Basicity and protonation site of N-aminoazoles: an experimental (pK a, 13C and 15N NMR spectroscopy and crystallography) and theoretical study. *Journal of the Chemical Society, Perkin Transactions 2* **1993,** (9), 1687.
145. Ahmed, S.; Booth, I. R., The use of valinomycin, nigericin and trichlorocarbanilide in control of the protonmotive force in Escherichia coli cells. *The Biochemical journal* **1983,** *212* (1), 105.
146. Richter, M. F.; Drown, B. S.; Riley, A. P.; Garcia, A.; Shirai, T.; Svec, R. L.; Hergenrother, P. J., Predictive compound accumulation rules yield a broad-spectrum antibiotic. *Nature* **2017,** *545* (7654), 299-304.
147. About Antimicrobial Resistance https://www.cdc.gov/drugresistance/about.html.
148. Lechtenberg, B. C.; Johnson, D. J. D.; Freund, S. M. V.; Huntington, J. A., NMR resonance assignments of thrombin reveal the conformational and dynamic effects of ligation. *Proceedings of the National Academy of Sciences of the United States of America* **2010,** *107* (32), 14087.
149. Maes, M.; Rimon, A.; Kozachkov-Magrisso, L.; Friedler, A.; Padan, E., Revealing the Ligand Binding Site of NhaA Na+/H+ Antiporter and Its pH Dependence. *Journal of Biological Chemistry* **2012,** *287* (45), 38150-38157.
150. Braberg, H.; Webb, B. M.; Tjioe, E.; Pieper, U.; Sali, A.; Madhusudhan, M. S., SALIGN: a web server for alignment of multiple protein sequences and structures. *Bioinformatics* **2012,** *28* (15), 2072-2073.
151. Eswar, N.; Eramian, D.; Webb, B.; Shen, M.-Y.; Sali, A., Protein Structure Modeling with MODELLER. In *Structural Proteomics: High-Throughput Methods*, Kobe, B.; Guss, M.; Huber, T., Eds. Humana Press: Totowa, NJ, 2008; pp 145-159.
152. Shen, M. Y.; Sali, A., Statistical potential for assessment and prediction of protein structures. *Protein Science* **2006,** *15* (11), 2507-2524.
153. Jorgensen, W. L.; Chandrasekhar, J.; Madura, J. D.; Impey, R. W.; Klein, M. L., Comparison of simple potential functions for simulating liquid water. *The Journal of Chemical Physics* **1983,** *79* (2), 926-935.
154. Showalter, S. A.; Bruschweiler, R., Validation of Molecular Dynamics Simulations of Biomolecules Using NMR Spin Relaxation as Benchmarks: Application to the AMBER99SB Force Field. *Journal of chemical theory and computation* **2007,** *3* (3), 961-75.
155. Hess, B., P-LINCS: A Parallel Linear Constraint Solver for Molecular Simulation. *Journal of chemical theory and computation* **2008,** *4* (1), 116-22.

156. Bussi, G.; Donadio, D.; Parrinello, M., Canonical sampling through velocity rescaling. *J Chem Phys* **2007,** *126* (1).
157. Parrinello, M.; Rahman, A., Polymorphic transitions in single crystals: A new molecular dynamics method. *Journal of Applied Physics* **1981,** *52* (12), 7182-7190.
158. Kozakov, D.; Grove, L. E.; Hall, D. R.; Bohnuud, T.; Mottarella, S. E.; Luo, L.; Xia, B.; Beglov, D.; Vajda, S., The FTMap family of web servers for determining and characterizing ligand-binding hot spots of proteins. *Nature protocols* **2015,** *10* (5), 733-55.
159. Michaud-Agrawal, N.; Denning, E. J.; Woolf, T. B.; Beckstein, O., MDAnalysis: a toolkit for the analysis of molecular dynamics simulations. *Journal of computational chemistry* **2011,** *32* (10), 2319-27.
160. van de Weert, M.; Stella, L., Fluorescence quenching and ligand binding: A critical discussion of a popular methodology. *Journal of Molecular Structure* **2011,** *998* (1-3), 144-150.
161. Vivian, J. T.; Callis, P. R., Mechanisms of Tryptophan Fluorescence Shifts in Proteins. *Biophysical journal* **2001,** *80* (5), 2093-2109.
162. Wang, B.; Weng, J.; Fan, K.; Wang, W., Interdomain flexibility and pH-induced conformational changes of AcrA revealed by molecular dynamics simulations. *The journal of physical chemistry. B* **2012,** *116* (10), 3411-20.
163. Wolff, N., Histidine pKa shifts and changes of tautomeric states induced by the binding of gallium-protoporphyrin IX in the hemophore HasASM. *Protein Science* **2002,** *11* (4), 757-765.
164. Olsson, M. H. M.; Søndergaard, C. R.; Rostkowski, M.; Jensen, J. H., PROPKA3: Consistent Treatment of Internal and Surface Residues in Empirical pKa Predictions. *Journal of chemical theory and computation* **2011,** *7* (2), 525.
165. Goh, G. B.; Hulbert, B. S.; Zhou, H.; Brooks, C. L., Constant pH molecular dynamics of proteins in explicit solvent with proton tautomerism. *Proteins: Structure, Function, and Bioinformatics* **2014,** *82* (7), 1319-1331.
166. Yue, Z.; Chen, W.; Zgurskaya, H. I.; Shen, J., Constant pH molecular dynamics reveals how proton release drives the conformational transition of a transmembrane efflux pump. *Journal of chemical theory and computation* **2017,** *13* (12), 6405-6414.
167. De Vivo, M.; Masetti, M.; Bottegoni, G.; Cavalli, A., Role of Molecular Dynamics and Related Methods in Drug Discovery. *Journal of medicinal chemistry* **2016,** *59* (9), 4035-61.
168. Clore, G. M.; Gronenborn, A. M., Structures of larger proteins, protein-ligand and protein-DNA complexes by multidimensional heteronuclear NMR. *Protein Science* **1994,** *3* (3), 372-390.
169. Wälti, M. A.; Riek, R.; Orts, J., Fast NMR-Based Determination of the 3D Structure of the Binding Site of Protein–Ligand Complexes with Weak Affinity Binders. *Angewandte Chemie International Edition* **2017,** *56* (19), 5208-5211.

170. Nakashima, R.; Sakurai, K.; Yamasaki, S.; Hayashi, K.; Nagata, C.; Hoshino, K.; Onodera, Y.; Nishino, K.; Yamaguchi, A., Structural basis for the inhibition of bacterial multidrug exporters. *Nature* **2013,** *500* (7460), 102-6.
171. Zuo, Z.; Wang, B.; Weng, J.; Wang, W., Stepwise substrate translocation mechanism revealed by free energy calculations of doxorubicin in the multidrug transporter AcrB. *Scientific reports* **2015,** *5*, 13905.
172. Darzynkiewicz, Z. M.; Green, A. T.; Abdali, N.; Hazel, A.; Fulton, R. L.; Kimball, J.; Gryczynski, Z.; Gumbart, J. C.; Parks, J. M.; Smith, J. C.; Zgurskaya, H. I., Identification of Binding Sites for Efflux Pump Inhibitors of the AcrAB-TolC Component AcrA. *Biophysical journal* **2019,** *116* (4), 648-658.
173. Haynes, K. M.; Abdali, N.; Jhawar, V.; Zgurskaya, H. I.; Parks, J. M.; Green, A. T.; Baudry, J.; Rybenkov, V. V.; Smith, J. C.; Walker, J. K., Identification and Structure-Activity Relationships of Novel Compounds that Potentiate the Activities of Antibiotics in Escherichia coli. *Journal of medicinal chemistry* **2017,** *60* (14), 6205-6219.
174. Raetz, C. R. H., Biochemistry of Endotoxins. *Annu.Rev.Biochem* **1990,** (59), 129-170.
175. Cooper, S. J.; Krishnamoorthy, G.; Wolloscheck, D.; Walker, J. K.; Rybenkov, V. V.; Parks, J. M.; Zgurskaya, H. I., Molecular Properties That Define the Activities of Antibiotics in Escherichia coli and Pseudomonas aeruginosa. *ACS infectious diseases* **2018,** *4* (8), 1223-1234.
176. Labute, P., The generalized Born/volume integral implicit solvent model: Estimation of the free energy of hydration using London dispersion instead of atomic surface area. *Journal of computational chemistry* **2008,** *29* (10), 1693-1698.
177. Jakalian, A.; Jack, D. B.; Bayly, C. I., Fast, efficient generation of high-quality atomic charges. AM1-BCC model: II. Parameterization and validation. *Journal of computational chemistry* **2002,** *23* (16), 1623-41.
178. Yu, E. W.; Aires, J. R.; McDermott, G.; Nikaido, H., A Periplasmic Drug-Binding Site of the AcrB Multidrug Efflux Pump: a Crystallographic and Site-Directed Mutagenesis Study. *The Journal of Bacteriology* **2005,** *187* (19), 6804.
179. Ababou, A.; Koronakis, V., Structures of Gate Loop Variants of the AcrB Drug Efflux Pump Bound by Erythromycin Substrate.(Report). **2016,** *11* (7).
180. Bohnert, J. A.; Schuster, S.; Seeger, M. A.; Fahnrich, E.; Pos, K. M.; Kern, W. V., Site-directed mutagenesis reveals putative substrate binding residues in the Escherichia coli RND efflux pump AcrB. *J Bacteriol* **2008,** *190* (24), 8225-9.
181. Cha, H.-J.; Müller, R. T.; Pos, K. M., Switch-loop flexibility affects transport of large drugs by the promiscuous AcrB multidrug efflux transporter. *Antimicrobial agents and chemotherapy* **2014,** *58* (8), 4767.
182. Krishnamoorthy, G.; Tikhonova, E. B.; Zgurskaya, H. I., Fitting periplasmic membrane fusion proteins to inner membrane transporters: mutations that enable Escherichia coli AcrA to function with Pseudomonas aeruginosa MexB. *J Bacteriol* **2008,** *190* (2), 691-8.

183. Rocklin, G. J.; Mobley, D. L.; Dill, K. A.; Hünenberger, P. H., Calculating the binding free energies of charged species based on explicit-solvent simulations employing lattice-sum methods: An accurate correction scheme for electrostatic finite-size effects. *The Journal of Chemical Physics* **2013,** *139* (18).
184. Heinzelmann, G.; Henriksen, N. M.; Gilson, M. K., Attach-Pull-Release Calculations of Ligand Binding and Conformational Changes on the First BRD4 Bromodomain. *Journal of chemical theory and computation* **2017,** *13* (7), 3260.
185. Ceccarelli, M.; Danelon, C.; Laio, A.; Parrinello, M., Microscopic Mechanism of Antibiotics Translocation through a Porin. *Biophysical journal* **2004,** *87* (1), 58-64.
186. Jo, S.; Kim, T.; Iyer, V. G.; Im, W., CHARMM-GUI: a web-based graphical user interface for CHARMM. *Journal of computational chemistry* **2008,** *29* (11), 1859-65.
187. Wu, E. L.; Cheng, X.; Jo, S.; Rui, H.; Song, K. C.; Davila-Contreras, E. M.; Qi, Y.; Lee, J.; Monje-Galvan, V.; Venable, R. M.; Klauda, J. B.; Im, W., CHARMM-GUI Membrane Builder toward realistic biological membrane simulations. *Journal of computational chemistry* **2014,** *35* (27), 1997-2004.

VITA

Adam Green began his scientific career at Wake Forest University in the computational biophysics group of Samuel Cho in the Department of Physics and Computer Science. At Wake Forest, Adam built homology models and conducted all-atom molecular dynamics simulations of DNA and RNA G-Quadruplexes with and without putative chemotherapeutics bound. Adam graduated from Wake Forest with a bachelor of science in biology and a minor in chemistry in 2014. He subsequently enrolled in the PhD program at the University of Tennessee-Knoxville where he began working with Dr. Jeremy C. Smith, Dr. Jerry M. Parks, and Dr. Jerome Baudry at the University of Tennessee/Oak Ridge National Lab Center for Molecular Biophysics. Afterwards, Adam will be a pre-sales computational biology solutions scientist at Dassault Systemes BIOVIA in Waltham, MA.